Title
Eddy-covariance observations of the atmosphere-biosphere exchange of nitrogen oxides

Author
Min, Kyung-Eun

Publication Date
2012

Peer reviewed|Thesis/dissertation

Eddy-covariance observations of the atmosphere-biosphere exchange of nitrogen oxides

By

Kyung-Eun Min

A dissertation submitted in partial satisfaction of the

requirements for the degree of

Doctor of Philosophy

in

Earth and Planetary Science

in the

Graduate Division

of the

University of California, Berkeley

Committee in charge:

Professor Ronald C. Cohen, Chair

Professor Inez Fung

Professor Allen H. Goldstein

Spring 2012

Eddy-covariance observations of the atmosphere-biosphere exchange of nitrogen oxides

Abstract

Eddy-covariance observations of the atmosphere-biosphere exchange of nitrogen oxides

by

Kyung-Eun Min

Doctor of Philosophy in Earth and Planetary Science

University of California, Berkeley

Professor Ronald C. Cohen, Chair

Oxidative forms of reactive nitrogen (NO_y) impact air quality, nutrient dynamics, and climate. Our understanding of the sources and sinks of atmospheric NO_y that result from exchange between the atmosphere and biosphere is poorly constrained due to the lack of adequate instrumentation.

In this dissertation, I apply novel technologies to the question of NO_y exchange and describe observations of fluxes at the atmosphere-forest interface. I use thermal-dissociation laser-induced fluorescence, chemiluminescence, and the micrometeorological eddy-covariance method. Simultaneous observations of the rate and magnitude of exchanges and vertically resolved concentration measurements of the NO_y species (NO, NO_2, RO_2NO_2, $RONO_2$ and HNO_3) were measured in addition to a wide suite of relevant parameters including canopy structures, meteorological parameters, and associated chemical species as part of the Biosphere Effects on AeRosols and Photochemistry EXperiment (BEARPEX), which took place June 15 – July 31, 2009 at a Ponderosa pine plantation on the western slope of Sierra Nevada Mountains in California.

I present observational evidence for active within canopy chemistry resulting in simultaneous production and removal of NO_X within a forest canopy. My observations provide direct evidence for a NO_X canopy reduction factor and for an NO_2 compensation point. I also establish that an unusual peroxynitrate is formed within the canopy and then emitted to the atmosphere above underscoring the importance of coupling between biogenic volatile organic compounds and NO_X to the fluxes of NO_x, NO_y and BVOC.

Contents

List of Figures

List of Tables

Chapter 1

Nitrogen oxides exchanges in atmosphere-biosphere interactions

1.1 Summary of previous work

Nitrogen (N) is one of the basic elements of living creatures. Reactive nitrogen (Nr) is an activated form of N (as opposed to the unreactive dinitrogen molecule, N_2, that makes up 80% of Earth's atmosphere) and is produced via fixation processes including biological (microbial activities), electrical (lightning), and industrial (fertilization production via Haber–Bosch reaction) pathways. Even though Nr comprises a trivial amount, 3 Tg, of the total nitrogen on Earth—compare to the 4,000,000,000 Tg of N_2 (Jacob, 1999)—Nr is the main form of nitrogen directly involved in N cycling processes. Accordingly, much research has focused on global-scale N cycling of the reduced (e.g. ammonia) and oxidized (e.g. HNO_3) forms of N_r in order to understand ecosystem nutrient cycling.

In this dissertation, I focus on the role of nitrogen oxides in N_r cycling between the atmosphere and biosphere. Nitrogen oxides ($NO_y \equiv NO + NO_2 + RO_2NO_2 + RONO_2 + HNO_3 + HONO + NO_3 + N_2O_5$ …) are important to the chemistry of Earth's atmosphere because of their role in controlling the oxidative capacity of atmosphere and their effects on the composition of aerosol. They also influence carbon uptake by vegetation. In addition to the fertilizing effects of NO_y on vegetation (Hungate et al., 2003; Galloway et al., 2004; Morikawa et al., 2004a; Morikawa et al., 2004b; Takahashi et al., 2004; Teklemariam and Sparks, 2004; Takahashi et al., 2005a; Takahashi et al., 2005b; Lockwood et al., 2008; Sparks, 2009; Norby et al., 2010, Hietz et al., 2011) deleterious effects of nitrogen oxides are also well known; i.e. dehydration, chlorosis, and membrane damage (Hessen et al., 1997; Herman et al., 2001; Oka et al., 2004) and the acidification of soils and eutrophication of water (Makarov and Kiseleva, 1995; Pawlowski, 1997; Gbondo-Tugbawa and Driscoll, 2002; Zapletal et al., 2003; Chen et al., 2004). Recent studies also point out the climate impact via the fertilization effect of NOy deposition. (Townsend et al., 1996; Vitousek and Farrington, 1997; Vitousek et al., 1997; Holland and Lamarque, 1997; Holland et al., 1997; Ollinger et al., 2002a; Ollinger et al., 2002b; Hietz et al., 2011). (Hungate et al., 2003; Galloway et al., 2004; Hietz et al., 2011).

NO_y exchange across the biosphere-atmosphere interface remains poorly understood. Figure 1.1 describes the understanding of NO_y exchange that has emerged as a result of prior studies. The goal of this thesis is to test the understanding represented by this figure with direct observations of exchange rates for nitrogen oxides.

Analyses of previous experiments indicate that the dominant processes in the exchange of NO_y between the atmosphere and biosphere is NO emission resulting from soil microbial activities (biosphere to atmosphere) and HNO_3 deposition (atmosphere to biosphere). Freshly emitted NO is converted to NO_2 by reaction with ozone (O_3) within and above the canopy and NO_2 recycles back to NO via its photolysis reaction or oxidized further to form HNO_3 above the canopy (Figure 1.1). Subsequent chemistry eventually converts NO_2 to HNO_3. The deposition of HNO_3 is taken to be a permanent loss of NO_X from the atmosphere. The NO to NO_2 conversion and NO_2 photolysis, typically on a time scale of ~100 seconds in daytime, is comparable to the turbulent mixing time between the within and above canopy air masses. As a result, the magnitude and rate of vertical transport (the flux) of NO or NO_2 competes with the chemistry and thus the measureable flux for both species is expected to deviate from the flux that would be observed for a non reactive trace gas (e.g. water, or carbon dioxide). This flux divergence has been evaluated theoretically (Vila-Guerau de Arellano et al., 1993). Because the chemistry of NO and NO_2 is largely the inter conversion from one species to the other, the flux of their sum, NO_X, ($NO_X \equiv NO + NO_2$), is expected to behave as quasi-conserved tracer would. There are a few observational studies of NO_X exchange that qualitatively support this idea. For example, higher NO concentrations have been seen near the forest floor (Rummel et al., 2002) and enhanced ratios of NO_2 to NO_X (Horii 2002) have been reported within canopy owing to slower photolysis rates in a shaded canopy. However a detailed comparison of experiment and theory has yet to be reported.

In addition to the chemistry described above, large-scale chemical transport models invoke an ad hoc parameter, the so-called canopy reduction factor, to reconcile the observed O_3 with high soil NO emission rates in remote regions (Jacob and Wofsy, 1990; Yienger and Levy, 1995; Wang and Leuning, 1998). Canopy reduction factors are estimated to be 25-80% of soil NO emission. Several observational studies also support the idea of a "shielding effect of canopy"; with some observers reporting smaller amounts of NO_X well above the soil surface(Lovett and Lindberg, 1993; Hereid and Monson, 2001; Fang and Mu, 2006; Pang et al., 2009).

However, there is also considerable evidence that canopies should add to the atmospheric NO_x burden, not subtract from it. Leaf scale observations indicate that exchange of NO_x is bi-directional, that is plants can act either a source or sink of NO and/or NO_2 depending on conditions of the surroundings. The ambient concentration of NO_2 (or NO) where a plant changes from a source to a sink of NO_2 (or NO) is defined as the compensation point, C_{PT} (Conrad, 1996). If the ambient concentration is higher than the C_{PT}, vegetation consumes NO_2 (or NO). If the ambient concentration is lower than the C_{PT}, emissions occur. Reported C_{PT}s from branch enclosure studies of NO_2 range from 0.1-3ppb (Sparks et al., 2001; Raivonen et al., 2009; Breuninger et al., 2011; Chaparro-Suarez et al., 2011) implying most of remote regions of the globe act as NO_X sources. Previous reports about plant NO emission below 1ppb are also consist with that (Wildt et al., 1997). This is in direct conflict with the idea of a canopy reduction factor (Lerdau et al., 2000).

Although HNO_3, is represented in Figure 1.1, atmosphere-biosphere interactions of other higher oxides of nitrogen are completely absent. Recently, leaf level measurements (Okano et al., 1990; Sparks et al., 2003) and canopy-scale estimates (Doskey et al., 2004) of exchange for peroxy acyl nitrate (PAN: $CH_3C(O)OONO_2$), have led to suggestions that the PAN uptake rate is

significant – comparable to HNO_3 deposition in some locations. The laboratory measurements suggest PAN uptake is controlled by stomata. There is also one leaf-level study of alkylnitrates (ANs: $RONO_2$) showing that direct uptake of ANs and incorporation into amino acids within the leaves occurs (Lockwood et al., 2008).

One of the main obstacles to advancing our understanding of atmosphere-biosphere exchange of NO_y is the lack of technologies for sensitive high frequency measurements needed for eddy-covariance flux measurements. In the last few years, new technologies have made possible canopy scale measurements of the exchange of NO, NO_2 and the higher oxides. These studies provide evidence for new processes that are not represented in Figure 1.1. For example, upward exchange of ΣPNs and HNO_3 was reported by Farmer et al., (2006) and fluxes of speciated PNs were observed by Turnipseed et al., (2006); and by Wolfe et al., (2009). Both Farmer et al. and Wolfe et al. interpret the observations as evidence for rapid within canopy chemistry affecting the fluxes. The concept of rapid within canopy oxidation processes is also supported by several observational studies of biogenic volatile organic compounds (BVOCs) and their oxidation products (Holzinger et al., 2005; Karl et al., 2005; Bouvier-Brown et al., 2009a; Bouvier-Brown et al., 2009b; Park et al., 2012) and ozone deposition (Kurpius and Goldstein, 2003). In addition to the field observations, multi-layered canopy modeling studies also emphasize the importance of within canopy chemistry on NO_y, O_3, and BVOC exchange (Wolfe et al., 2011a; Wolfe et al., 2011b).

1.2 Overview of this work

In this thesis, I make use of these new techniques to obtain observations of nitrogen oxide fluxes using eddy covariance (EC). By coupling the highly specific and fast-time resolution thermal-dissociation laser-induced fluorescence (TD-LIF) for NO_2, PNs, ANs, and HNO_3 and a 2-channel chemiluminescence (2ch-CL) measurement for NO with well established micrometeorological knowledge, I was able to directly observe the fluxes and height resolved concentration, vertical gradients, simultaneously. A major advantage of this experiment was that it included a complete suite of simultaneous measurements of nitrogen oxides.

Using these new observations in this dissertation, I present evidence of active within canopy chemistry affecting the fluxes of nitrogen oxides. The new picture I propose is summarized in Figure 1.2. Instead of the simple canopy reduction process affecting NO and NO_2, shown as uptake by plants in Figure 1.1, I propose multiple mechanisms of higher nitrogen oxide formation within the canopy as shown in red arrows in Figure 1.2.

The detailed chemical cycling between NO_X and higher oxides and the connection to the biosphere plant involved processes is described in Figure 1.3. The red arrows are emission, representing a source of NO_X, and the blue and black arrows indicate the loss of NO_X via plant involved or chemical pathways, respectively. The processes outlined in this figure are the subject of Chapters 2-4 of this thesis.

In Chapter 2, I focus on the flux and gradient measurements of NO and NO_2 and infer the existence of NO_X loss processes within the canopy by analyzing the discrepancies between the flux and gradient relationships of both molecules as well as their sum. My finding from this chapter is consistent with the concept of a canopy reduction factor as suggested from large-scale chemical transport modeling studies. The observed fluxes of NO and NO_2 are generally upward. I compare the magnitude of fluxes with their vertical gradients and find the fluxes to be smaller than predicted from the gradients of NO_2 and NO_X alone. I argue this is evidence for NO_X loss processes within the canopy and investigate multiple chemical loss mechanisms associated with the formation of higher oxides. I suggest that the loss of NO_X is primarily due to the conversion of NO_X to peroxy and alkyl nitrates.

In Chapter 3, I present evidence for bidirectional fluxes of NO_2 at the canopy scale. The fluxes are shown to depend on ambient NO_2 in a manner consistent with the idea of a compensation point affecting NO_2 fluxes. The calculated exchange velocity of NO_2 is shown to be inversely correlated with the NO_2 concentration. Analysis of the NO_X cospectrum provides evidence for flux carrying eddies that have systematically different behavior at high and low NO_2.

In Chapter 4, I describe fluxes of total and speciated peroxynitrates. I find that the sum of specific peroxynitrate fluxes does not add to the total and use the difference to infer the production of an unidentified PN, denoted XPN, within the canopy. An upward flux of this molecule acts to counter the downward flux of the identified PNs with the net result that the deposition rate of total PNs is lower than the sum of the fluxes of individual molecules. Interestingly, this process is likely one of the loss processes contributing to within canopy NO_X removal and thus acting as a canopy reduction factor.

In Chapter 5, I briefly conclude with some ideas for future research on the atmosphere biosphere exchange of N and with a discussion of the broader implications of the results presented in CH's 2-4.

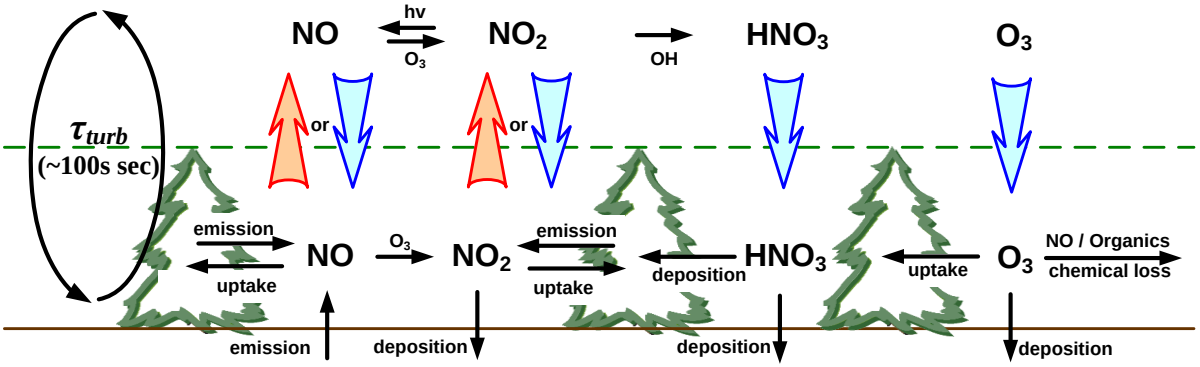

Figure 1.1. Schematic of the various interactions involved in the exchange of nitrogen oxides between the atmosphere and a forest canopy. Bold arrows in blue (downward) and red (upward) represent the direction of the flux of each species across the canopy surface.

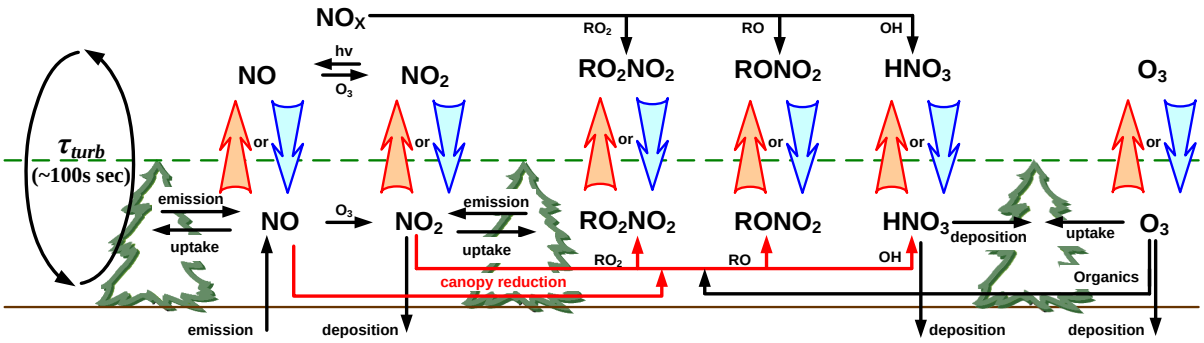

Figure 1.2. Updated schematic of the various interactions involved in the exchange of nitrogen oxides between the atmosphere and forest canopy. Bold arrows in blue (downward) and red (upward) represent the direction of the flux of each species across the canopy surface.

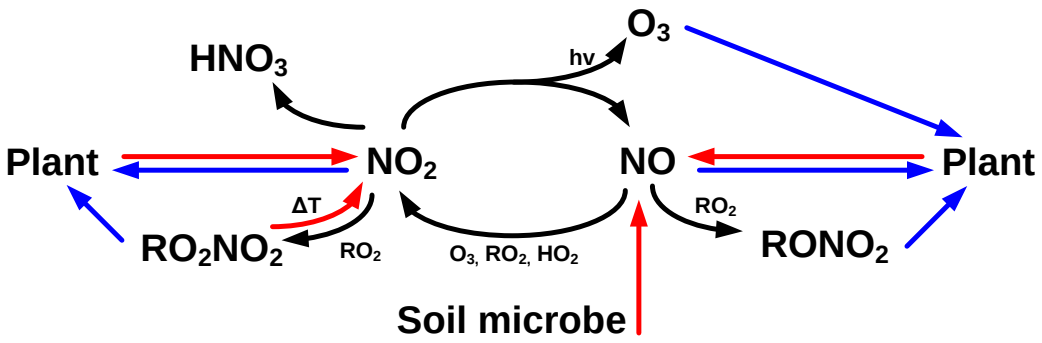

Figure 1.3. Nitrogen oxide cycling. Red arrows are NO_X sources and blue arrows are NO_y losses through direct plant uptake. The black arrows indicate the chemical processes.

Chapter 2

Eddy covariance measurements of NO and NO_2 fluxes over a ponderosa pine ecosystem: an observational evidence of canopy reduction processes

Abstract

Exchange of NO_X ($NO+NO_2$) between the atmosphere and biosphere is important for air quality, climate change, and ecosystem nutrient dynamics. There are few direct ecosystem scale measurements of the direction and rate of atmosphere-biosphere exchange of NO_X. As a result a complete description of the path of NO_X following emission from soils and/or plants to the free atmosphere remains poorly constrained and therefore debated. Here, we describe measurements of NO and NO_2 fluxes and vertical concentration gradients made during the Biosphere Effects on AeRosols and Photochemistry EXperiment 2009. In general, during daytime we observe upward fluxes of NO and NO_2 with counter-gradient fluxes of NO. We find that NO_X fluxes from the forest canopy are smaller than calculated using observed flux-gradient relationships for conserved tracers and also smaller than measured soil NO emissions. We interpret these differences as evidence for the existence of a "canopy reduction factor". We discuss the mechanisms that might explain the reduction factor and suggest it is primarily due to chemistry converting NO_X to its higher nitrogen oxides.

2.1. Introduction

The chemistry of reactive nitrogen oxides is one major factor determining the oxidation capacity and global ozone burden of troposphere. Reactive nitrogen oxides are also a nutrient (Sparks, 2009;Takahashi et al., 2005a; Takahashi et al., 2004; Teklemariam and Sparks, 2004; Lockwood et al., 2008) and interactions between available nitrogen in ecosystems and atmospheric N are many and complex, with exchange processes altering the patterns of N availability in the biosphere (Townsend et al., 1996; Vitousek and Farrington, 1997; Vitousek et al., 1997; Holland and Lamarque, 1997; Holland et al., 1997; Ollinger et al., 2002a; Ollinger et al., 2002b; Hietz et al., 2011). Nitrogen is the limiting nutrient for plant growth in most regions outside the tropics (Hungate et al., 2003; Galloway et al., 2004; Hietz et al., 2011), thus nitrogen deposited to the surface after atmospheric transport can act as fertilizer contributing to enhanced

carbon uptake (Morikawa et al., 2004a; Morikawa et al., 2004b; Takahashi et al., 2004; Takahashi et al., 2005a; Takahashi et al., 2005b; Sparks, 2009; Norby et al., 2010). For example, Norby et al. (2010) found that the availability of nitrogen was a major limiting factor for the CO_2 fertilization effect in the FACE (Free-Air CO_2 Enrichment) experiment. However, too much nitrogen deposition may impair ecosystem health (Hessen et al., 1997; Herman et al., 2001) by causing dehydration, chlorosis, membrane damage from peroxy acetal nitrate (PAN) (Oka et al., 2004) and/or ozone (O_3) (Moldau et al., 1991; Kasana, 1992; Ewert and Porter, 2000), or by inducing soil acidification and eutrophication (Makarov and Kiseleva, 1995; Pawlowski, 1997; Gbondo-Tugbawa and Driscoll, 2002; Zapletal et al., 2003; Chen et al., 2004).

A comprehensive understanding of NO_X exchange between the atmosphere and biosphere does not yet exist. Experimental studies have primarily focused on NO emissions from soils to the atmosphere (e.g. Butterbach-Bahl et al., 2002; Gasche and Papen, 2002; Gut et al., 2002a; Gut et al., 2002b; Rummel et al., 2002; van Dijk et al., 2002) or on the leaf-level transfer of NO and NO_2 using branch enclosures (Hereid and Monson, 2001; Chaparro-Suarez et al., 2011; and references therein). Studies at the canopy-scale often assume simple flux-gradient similarity relationships—meaning molecular movement is always along the gradient from high to low concentration—to infer the rate of exchange from vertically resolved observations (Mayer et al., 2011 and reference therein). Direct measurements of the direction and rate of exchange, the flux, at the canopy scale are few (Wesely et al., 1982; Wildt et al., 1997; Horii, 2002; Horii et al., 2004; Farmer et al., 2006).

Prior studies have constructed a picture of biosphere-atmosphere NO_X exchange as shown in Figure 2.1. In this model, NO is mainly emitted by soil microbial activity, is converted to NO_2 by reaction with O_3, and is then ultimately oxidized to nitric acid (HNO_3), which returns back to the biosphere via wet and dry deposition. The timescale of NO to NO_2 conversion by O_3 and the photolysis of NO_2 back to NO is typically ~100s in the daytime—comparable to that of the turbulent mixing time (τ_{turb}) within and out of a forest canopy. As a result, although the flux of either NO or NO_2 is expected to deviate from the flux of a conserved tracer, such as water, heat, or carbon dioxide (Vila-Guerau de Arellano et al., 1993), the flux of NO_X, their sum, is expected to behave as a quasi-conserved tracer.

This model of NO_X exchange is qualitatively supported by observational studies. For example, NO is observed to decrease as air is transported up through a canopy from the forest floor (e.g. Rummel et al., 2002) and the low light levels within a shaded canopy reduce NO_2 photolysis and enhance the NO_2 to NO_X ratio. For these reasons, downward NO fluxes and upward NO_2 fluxes have been observed as expected (e.g. Horii, 2002).

In contrast, calculations of ozone by large-scale chemical transport models parameterized with NO soil fluxes measured by chambers over-predict O_3 concentrations in comparison to aircraft and tower observations (e.g. Lerdau et al., 2000). To match observations, these models invoke a canopy reduction factor of 25-80% (Jacob and Wofsy, 1990; Yienger and Levy, 1995; Wang and Leuning, 1998). This parameter functions non-mechanistically to remove soil NO_X before it escapes the canopy, thus preventing its contribution to atmospheric ozone formation.

At the same time, laboratory observations at the leaf scale indicate bi-directional exchanges of NO_X by plant biota, where the direction and rate of exchange is controlled by a so-called "compensation point"—a concentration above which vegetation takes up NO_2 and/or NO but below which emissions occur. Direct observations of the NO_2 compensation point present real measurement challenges (Raivonen et al., 2003) and evidence suggests that compensation behavior is not fixed but rather varies by plant species, plant lifecycle, and environmental conditions (Raivonen et al., 2009). That said, compensation points are measured in the range of ambient NO_2 abundances and have been reported from 0.1 to 3 ppb (Sparks et al., 2001; Raivonen et al., 2009; Breuninger et al., 2011; Chaparro-Suarez et al., 2011) implying that most of the forests on Earth are a source of NO_X. This is in direct contradiction to the idea of a canopy reduction factor (Lerdau et al., 2000).

Recent field studies demonstrate very active within-canopy chemistry that is not included in Figure 1. With respect to nitrogen oxides, Farmer et al. (2006) observed upward exchanges of total peroxynitates, ΣRO_2NO_2, and HNO_3 and interpreted this as the formation of these molecules within a forest canopy. In addition, Wolfe et al. (2009) described the importance of chemical processes in speciated peroxynitrate exchange also finding observational evidence for within-canopy chemistry affecting observed fluxes. Several other experimenters have reported the occurrence of within-canopy chemistry affecting fluxes of biogenic volatile organic compounds (BVOCs) (Holzinger et al., 2005; Karl et al., 2005; Bouvier-Brown et al., 2009a; Bouvier-Brown et al., 2009b; Park et al., 2012) and ozone (Kurpius and Goldstein, 2003). A recent study from our group (Min et al., 2012a) further supports this idea, providing experimental evidence for upward fluxes of unidentified peroxynitrates formed within the forest canopy. Taken together these studies emphasize the importance of active chemistry not only for determining the magnitude but also for the direction of N exchange at the biosphere-atmosphere interface.

The Biosphere Effects on AeRosols and Photochemistry EXperiment (BEARPEX) included a component designed to provide comprehensive measurements of concentrations, vertical gradients, and fluxes of a wide suite of nitrogen oxides—NO, NO_2, total and speciated peroxynitrates, total and speciated alkylnitrates, HNO_3, and nitrous acid (HONO)—and therefore presents a direct opportunity to test our ideas about canopy-scale NO_X exchange. Analyses of peroxynitrate (Wolfe et al., 2009; Min et al., 2012a) and HONO (Ren et al., 2011) fluxes have been reported elsewhere. Here we present observations of vertical concentration gradients and fluxes of NO_2 and NO measured with laser induced fluorescence (LIF) and chemiluminescence, respectively, coupled to the eddy covariance flux method. We describe relationships between gradients and fluxes, present and interpret evidence for a canopy reduction factor, and explore the significance of chemistry within the canopy to the import/export of NO_X from the canopy.

2.2. Research site and instrumentation

The data used in this work were obtained as a part of BEARPEX 2009 **(**June 15 – July 31, 2009). The experiment was conducted over a managed Ponderosa pine plantation on the western slope of the Sierra Nevada Mountain range 75 km downwind of Sacramento, California and near to the University of California Berkeley Blodgett Forest Research Station (UC-BFRS, 38°53'42.9"N, 120°3757.9"W, 1315m). An overview of and results from BEARPEX can be found elsewhere (Cohen et al., 2012) and in the other articles in this special issue of ACP. A brief description of the field site and of instrumentation relevant to this paper follows.

Descriptions of the local meteorology by Choi et al. (2011) and Dillon et al. (2002) indicate that in the summer (May-September), winds at the BEARPEX site are characterized by daytime southwesterlies (210-240°) and nighttime northeasterlies (30°) with remarkably little variability in winds and transport patterns. As a result, this site samples air that has low concentrations of trace gases with anthropogenic sources early in the morning and higher concentrations in air transported from the west later in day. The westerlies bring air that has been exposed to a band of oak trees that are intense isoprene emitters (after 12:00). After 17:00 the westerlies bring isoprene and its oxidation products mixed with the urban plume from Sacramento.

There were two sampling towers at the site; a 15m walk-up tower on the south side of the site (hereafter south tower), and 18m scaffolding tower located 10m north of the south tower (hereafter north tower). On south tower, temperature, relative humidity, wind speed, net radiation, photosynthetically active radiation (PAR), water vapor, carbon dioxide (CO_2), and O_3 were monitored at 5 heights (1.2, 3.0, 4.9, 8.75, and 12.5m above the forest floor). At 12.5m, fluxes of water vapor, CO_2, and O_3 were measured. Vertical gradients of temperature, relative humidity, and wind speed were also measured on the north tower at 5 heights (1.2, 5.4, 9.2, 13.3, and 17.5m above the forest floor). Measurements from the north tower or an adjacent adjustable lift included NO, NO_2, HONO, total peroxy nitrates (ΣPNs, RO_2NO_2), total alkyl nitrates (ΣAN, $RONO_2$), HNO_3, hydroxyl radical (OH), hydroxy peroxy radical (HO_2), the OH reactivity, O_3, several individual PNs, several individual ANs, numerous volatile organic compounds (VOCs) including many biogenic VOCs (BVOCs), formaldehyde (HCHO), glyoxal, methylglyoxal, organic peroxides, and aerosol chemical and physical properties. Needle temperature, soil moisture, soil temperature, and soil heat flux were also monitored. In addition, soil NO emissions were measured using dynamic chamber set-up on July 2, 12 and 30th. All measurements were made at the 17.5m level and many were additionally recorded at one or more of the following heights: 1.2, 5.4, 9.2, and 13.3m. The upper canopy at this site is mainly Pinus ponderosa L., with a few scattered Douglas fir, white fir, and incense cedar. The understory is primarily mountain whitethorn (Ceanothus cordulatus) and manzanita (Arcostaphylos species) shrubs (see Misson et al., 2005, for a more detailed site description and history). The mean tree height was 8.8m and the leaf area index (LAI) was $3.7 m^2/m^2$ based on a tree survey conducted on July 17, 2009.

NO was measured using a custom built two-channel chemiluminescence NO detection system (2ch-CL) and NO_2 with two thermal-dissociation LIF systems (TD-LIF). The sampling

inlets for NO and NO_2 were collocated at 0.5, 5 (4.5), 9 (8.8) and 18 m (17.5) on the north tower and represent the forest floor, mid canopy, top canopy, and above canopy, respectively. At 18m, fluxes of NO and NO_2 were monitored along with 3-d wind and temperature from a sonic anemometer (Campbell Scientific CSAT3 3-D Sonic Anemometer). The measurements were combined to infer fluxes using eddy covariance (EC) (see Section 3). The sonic anemometer was pointing into the mean daytime wind stream with 0.02m vertical displacement and 0.2m horizontal displacement from the NO and NO_2 inlets.

The 2ch-CL system for the NO flux and vertical gradient measurements was based on the standard O_3 chemiluminescence method. A detailed description of the operating principle can be found elsewhere (Drummond et al., 1985 and references therein). Briefly, ambient NO is combined with an excess of O_3 (generated by electric discharge of O_2). The reaction of NO and O_3 produces exited state NO_2 molecules, which then fluoresce. One of the gold-plated detection cells was used for the flux measurement and the other one cell for the vertical concentration gradient measurement. The signals from photocathodes (flux channel: EMI 9658B, gradient channel: Hamamatsu H7421-50) were acquired at 5Hz. The cell pressures were maintained at 8-8.5 torr with pressure restricted at the inlet and with a fluorinated oil-sealed rotary vane pump. We operated the 2ch-CL system in free background checking mode, whereby during the sampling mode, 100% of the ozone flow was added directly into the detection cell to monitor the ambient NO concentration (for 24 seconds). The background signal was monitored by adding 50% of the O_3 to the sampling air prior to the detection cell to titrate ~90% NO (for 6 seconds). Incomplete titration of NO was employed to limit possible interferences from vibrationally excited OH molecules produced in the reaction of ozone with alkenes (Drummond et al., 1985). The other 50% of the ozone was added directly to the cell to minimize flow changes within the reaction cell between the sampling and the background mode.

Two TD-LIF systems were used for simultaneous flux and vertical gradient measurements of NO_2 and the higher nitrogen oxide species ΣPNs, ΣANs, and HNO_3. Details of LIF detection of NO_2 (Thornton et al., 2000) and application to EC flux measurement (Farmer et al., 2006) are described elsewhere. Briefly, thermal dissociation of each class of higher oxide generated NO_2 and a companion radical at the characteristic temperatures 180^{o}C for ΣPNs, 350^{o}C for ΣANs, and 600^{o}C for HNO_3, (Day et al., 2002) followed by detection of NO_2 by LIF. In both TD-LIF systems, excitation at 585nm was provided by Nd:YAG (Spectra Physics, average power of 2W at 532 nm, 30 ns pulse length) pumping a custom-built tunable dye laser operating at 8kHz. The wavelength of the dye laser beam was tuned to a specific, narrow rovibronic feature of NO_2 by rotating an etalon within the dye cavity. We alternated the laser frequency between a strong NO_2 resonance (8 sec) and the weak continuum adsorption (4 sec) to maintain a frequency lock on the spectral feature of interest. By adapting a supersonic expansion technique, we acquired ~10-fold higher sensitivity to NO_2 (Cleary et al., 2002). The fluorescence signal long of 700nm was collected and imaged onto a red sensitive photocathode (Hamamatsu H7421-50) and gated photon counting techniques (Stanford Research Systems, SRS 400) were employed to discriminate against prompt background signals. Laboratory measurements and comparison in the field showed the two TD-LIF instruments to have calibrations that were identical to within 4% (slope: 1.039 +/- 0.10 , R^2: 0.92). Allowing the intercept to vary from zero did not improve the R^2.

The cell pressures in the flux system were reduced to 0.17-0.19 Torr to achieve the high expansion ratios for the superconic jet cooling by using Lysholm twin screw blowers (Whipple model 2300 superchargers) backed by an oil-sealed rotary vane pump. The jet nozzles and this pump system combined to maintain a 580-700 sccm flow through each of the four cells (total flow of 2300 sccm). To reduce high frequency damping of turbulent eddies and interference from secondary chemistry in the heated inlet and sampling lines (100ft), we added a diaphragm bypass pump and maintained the total flow of a 13000 sccm. For the gradient system, critical orifices as pressures restrictors (AirLogic, F-2815-251-B85, 0.025" orifice diameter) were placed at the end of the inlet manifold to reduce the pressure along the sampling line.

Calibrations in the field were repeated once/twice per hour for both the NO and NO_2 instruments. NO_2 standard gas (4.9 ± 0.2 ppm NOx in N_2, PRAXAIR) was diluted to 3-20 ppb in zero air and added to system at the inlet tip. For NO, 2.25-6.7 ppb of NO (5.4 ppm ± 5% NO in N_2, PRAXAIR) was diluted with zero air and added at the inlet. Both cylinders were referenced to a library of calibration standards maintained in our laboratory. The mixing ratios were corrected (<2%) for quenching by water using the north tower RH measurement. To evaluate the background counts due to cell scatter and photocathode dark noise, we flowed excess zero air into the inlet once/twice per hour. The diagnostics for the NO and NO_2 flux instruments (calibration and zeroing) were completed within the first 3 minutes of every 30 minute duty cycle (Figure 2.2a). Flux data for both species were collected at 18m during the first 30 minutes, from the 3rd minute to the 30th minute, and for the last 30 minutes, from the 33rd minute to the 60th minute each hour (Figure 2.2a). NO and NO_2 at the lower levels were measured by switching between the 9, 5, and 0.5m heights and sampling at each height for 2 minutes (Figure 2.2b). Calibrations and zeros were completed in last 4 minutes from 56th to 60th minutes of every hour for both gradient systems (Figure 2.2b).

Data affected by exhaust plumes from a nearby propane electrical generator (mostly at night) and the infrequent wafts of car exhaust were removed prior to analysis. These spikes were defined as variations in the NO or NO_2 concentration in excess of 3 times the standard deviation of the 10-minute running mean. A few remaining spikes were identified through correlations with CO and removed by hand. Over the campaign, the NO_2 detection limit (defined as S/N = 2) was ~45 ppt (1 second) for the flux system and was ~10 ppt (1 minute) for gradient system. The NO detection limit for flux cell was ~58ppt (1 second) and for gradient cell was ~11 ppt (1minute) in midday (12:00-14:00).

2.3. Eddy-Covariance calculation

The flux of an atmospheric constituent (F_c), i.e. the turbulent mass transport of constituent (c) through a vertical reference layer, can be evaluated from the covariance between the concentration of c and the vertical wind (w) in a method known as eddy-covariance (EC) Eq. (2.1) (e.g. Foken, 2006; Lee et al., 2004; McMillen, 1988):

$$F_c = \int_{t0}^{t} w'c'\,dt = \frac{1}{n}\sum_{i=1}^{n}(w_i - \bar{w})(c_i - \bar{c}) = \overline{w'c'} \qquad (2.1)$$

In Eq. (2.1), the primes are the deviation from the mean, the subscripts i refer to individual high-time resolution measurements (NO or NO_2), and the bar indicates the mean over the averaging interval. In this work, the flux of NO_X, F_{NOX}, is defined as the sum of the separately calculated F_{NO} and F_{NO2}.

We used 5Hz data for the flux calculations and averaged for ~30 minutes—a time scale that spanned the range of the major flux-carrying eddies at this site (e.g. Wolfe et al., 2009; Farmer et al., 2006). Prior to calculating fluxes, we rotated the wind measurements to ensure that the vertical winds were normal to the shear plane (Baldocchi et al., 1988; McMillen, 1988). We also de-spiked and de-trended the concentration data, where spikes were defined as data greater than 3 times the standard deviation of the 10-minute running mean, and where the 10-minute running mean was also used for de-trending.

To synchronize the timing of wind and concentration measurements, the lag was determined from the maximum in covariance of the deviation from the mean of vertical wind speed and concentration. Figures 3a-c show the lag correlation between wind and temperature (as a check), NO, and NO_2, respectively. The data plotted in Figure 2.3 are the averaged midday (12:00-14:00) lag over the whole field campaign. As expected, 0 lag was observed between vertical wind speed and temperature since both quantities are synchronously measured by same instrument. Lag times for NO and NO_2 were measured to be 1.4 seconds and 2.6 seconds, times that were consistent with transport times in the tubing (<0.8 sec) plus the time difference between sonic anemometer computer and computers for 2ch-CL and TD-LIF.

To assure that each 30-minute flux was representative of the average surface exchange over the sampling period, we tested the calculated fluxes for stationarity (Farmer et al., 2006; Foken 2006; Wolfe et al., 2009). To do this, five equally divided subsets of each 30-minute flux period, F_{sub}, were averaged and compared with that of the full period, F_{30min}. If F_{sub} differed from F_{30min} by more than 30% then that measurement period was defined as non-stationary and that half hour excluded from further analysis (Foken and Wichura, 1996). Also, the calculated flux data with a tilt angle greater than 5^o from the wind rotation (Lee et al., 2004) and with a friction velocity smaller than 0.1m/s or larger than 1.5m/s (Foken 2006) were excluded for further analysis. Approximately 2/3 of the daytime and half the nighttime data remained after application of these filters.

We estimate the total systematic uncertainty in the NO and NO_2 flux estimation following Moore et al. (1986) and Massman (1991) (details are in Farmer et al., 2006 and Wolfe et al., 2009). Systematic uncertainties in EC fluxes arise from data acquisition sequencing, laser line-locking cycling or frequent background checking, sensor separation, inlet dampening, instrument time response, and concentration estimation. Random uncertainty arises from the statistics of photon counting. Flux underestimation caused by data acquisition sequencing and frequent background checking in the NO measurement (<2%) and laser line-locking cycling for the NO_2 measurements (<3%) were estimated for flux calculation by forcing the sonic temperature data to mimic the both the frequent background checking (NO) and laser line-locking cycling (NO_2) and

comparing this to the non-treated data. Sensor separation error and inlet dampening error were estimated using transfer functions as in Massman (1991) and Moore (1986). We found these effects were small, <2% for both the NO and NO_2 measurements. Flux estimation errors due to instrumental time response (Moore et al., 1986) are typically <0.2% (NO) and <0.7% (NO_2) for daytime. Errors from the absolute concentration estimation are 5 % for both of NO and NO_2 (see Day et al., 2002) and are accounted for in the systematic error. Random uncertainties in EC fluxes from the statistics of photon counting are <20% and <10% for NO and NO_2.

These errors are uncorrelated and combining them in quadrature, we calculate <6% systematic uncertainty in the NO and NO_2 fluxes and 56% and 10% random uncertainty in half hour average flux estimation. Variances due to precision terms decrease as the square root of the total number of half hour measurements and are therefore much smaller than the observed natural variability.

Spectral analysis supports the validity of the flux estimation from the instrumental setup and sensitivity. Spectral analyses of the fluxes are shown in Figure 2.4 and include the cospectral density (Figure 2.4a), the normalized cospectrum (Figure 2.4b), and the normalized cumulative cospectrum, or ogive, (Figure 2.4c) for both temperature and NO_X. We show each measurement for the time interval 9:00-12:00 when the chemistry affecting NO_X is slowest. By analyzing the NO_X cospectrum, rather than the spectra of NO and NO_2 separately, we are insensitive to the effects of the rapid chemical conversion of NO to NO_2 and vice versa.

The spectral analysis of NO_X provides additional evidence that our instruments for NO and NO_2, 2-ch CL and TD-LIF, observe the full range of flux carrying eddies at this site. We see in Figure 2.4a, that the observed cospectral density of sensible heat, *w'T'*, decreases in inertial sub-range (above 0.003 Hz) with a linear slope between that predicted by surface layer theory (-5/3) (Kaimal and Finnigan, 1994) and that slope observed previously at this site (-7/3) (Farmer et al., 2006; Wolfe et al., 2009). Because the cospectral density of vertical wind speed and NO_X as parallel to that of sensible heat, we have confidence that our sampling interval was long enough and the data acquisition time resolution fast enough to capture all the flux carrying eddies. Additionally, the comparable behavior observed in the *w'T'* and *w'*NO_X*'* cospectrum confirmed that those frequencies characteristic of our instruments' sampling and operative cycles (eg. regular patterns in on-line/off-line sequencing in both NO and NO_2) do not interfere with the measurements. Agreement between *w'T'* and *w'*NO_X*'* in the inertial sub-range (above 0.003 Hz), demonstrates that measured fluxes were not dampened by the sampling lines. Finally, we note that we observe both upward and downward NO_X fluxes at different frequencies. In Figures 4a-c triangles refer to downward fluxes and solid lines to upward fluxes.

The normalized cospectrum, shown in Figure 2.4b, indicates the fraction of the total flux at each frequency. It is calculated as the cospectra multiplied by the frequency and divided by the covariance of temperature, or NO_X, with the vertical wind, which is the integrated value under the curve. Generally, the shape of the normalized cospectrum of *w'*NO_X*'* is similar to that of *w'T'* with a maximum in the range 0.005-0.1 Hz (200-10 second), with values consistent with previous observations at this site (Farmer et al., 2006; Wolfe et al., 2009). A steeper falloff at high-frequencies (>0.01 Hz) for *w'*NO_X*'* (especially in the afternoon, not shown) than for *w'T'* was reported in previous studies of PAN at this site (Wolfe et al, 2009) and in a Loblolly pine

forest (Turnipseed et al., 2006) as well as for a variety of BVOCs at this site (Park et al., 2012). The deep feature seen at frequencies of 0.001-0.005 Hz is associated with downward fluxes (▲).

Figure 2.4c shows the normalized cumulative distributions of the cospectra and ogives of $w'T'$ and $w'NO_X'$. The ogive for $w'T'$ approaches a horizontal asymptote at both ends of the spectrum, providing additional confirmation that the sampling interval and time resolution was both long enough and the sampling frequency fast enough to capture all the important flux-carrying eddies. The ogive pattern of $w'NO_X'$ is generally comparable to that of $w'T'$, except for frequencies in the ranges 0.001-0.005 Hz and 0.1-1 Hz, where fluxes are downward. Here, we use the absolute value of the frequency weighted normalized cospectrum of $w'NO_X'$ for the ogive calculation noting that the frequencies of $w'NO_X'$ that are downward vary with time of day, suggesting they are not internally generated, but are rather the result of time-of-day dependent atmospheric processes.

2.4. Gradients and Fluxes

The diurnal variations in the concentrations of O_3, NO_X, NO, and NO_2 are shown in Figure 2.5 and are similar to previous observations at this site (Day et al., 2003; Farmer et al, 2006). The patterns are affected by transport from Sacramento, emissions from soils, deposition, and chemistry. O_3, NO_X, and NO_2 increase as air is transported in from the west carrying the remnants of emissions from the Sacramento metropolitan area and reach a maximum after sunset between 18:00 to 21:00. Generally, NO can be thought of as controlled by the amount of NO_X and local photochemistry. In the morning, we observe enhancements in NO and NO_2 and a decrease in O_3. Vertical gradients are also present. We observe the highest NO concentrations above the canopy, decreasing NO within the forest canopy and increasing NO concentrations again near the forest floor—except in the late afternoon when turbulent mixing is strongest and dry soils result in NO emissions that are at their daily minimum.

Typical NO mixing ratios above the canopy during BEARPEX 2009 ranged from 10 to 100 ppt with a daytime (9:00-18:00, local time) mean (± 1σ) of 45 ± 19 ppt. This concentration is ~20% lower than observed at this site during same time of year in 2001 (Day et al., 2003). The highest NO concentration near the forest floor was 270 ppt following rainfall on the evening of day 192 (July 11). The mixing ratio of NO_2 above the canopy varied from 80 to 550 ppt with a daytime mean concentration of 188 ± 86 ppt. This is a 65% decrease from the 533 ppt mean observed in 2001 (Day et al., 2003) and is in agreement with previously reported NO_X decreases in upwind Sacramento of approximately 13%/yr, which accumulate to an approximately 67% decrease between 2001 and 2009 (Cox et al., 2009; Russell et al., 2010; LaFranchi et al., 2011).

Figure 2.6 shows the vertical gradients of NO, NO_2, and NO_X throughout the course of the day: early morning (6:00-9:00, blue), late morning (9:00-12:00, cyan), midday (12:00-14:00, red), afternoon (14:00-18:00, magenta), evening (18:00-24:00, green) and night (24:00-6:00, black). For the purpose of discussion we define an enhancement factor (ΔX) to be the concentration

difference between each height and that measured above the canopy ($\Delta X = X_i - X_{18m}$). Positive values of ΔX indicate concentration enhancements and negative values indicate depleted concentrations relative to above the canopy. In Figure 2.6a, NO was depleted within the canopy and, in Figure 2.6b, NO_2 was enhanced at all times of day. In general, we observed the highest NO enhancement near the soil (except for night time) and larger NO_2 enhancements at mid- and top-canopy heights. This pattern is qualitatively explained by emissions of NO at the soil followed by the conversion of NO to NO_2 until the steady-state ratio is established by the reaction of NO with O_3 and photolysis of NO_2.

If soil NO emissions and the chemical cycling of NO/NO_2 are the only two process controlling NO_X, then we expect the gradient in the sum of NO and NO_2 to be a straight line connecting the enhanced concentration at forest floor with the above canopy (boundary layer value) so long as sufficient turbulent mixing exists (Vila-Guerau de Arellano et al., 1993; Gao et al., 1991; Jacob and Wofsy, 1990). This, however, is not what we observe (Figure 2.6c). Rather we observe a NO_X enhancement during daytime and depletion during nighttime within the canopy. In addition, the amount of the enhancement at the forest-floor, mid-canopy, and top-canopy heights changes within different time windows, indicating the existence of multiple processes other than soil NO emission and simple inter conversion of NO and NO_2. For example, the within-canopy gradients at 6:00-9:00 and 14:00-18:00 are opposite each other and the 6:00-9:00 NO_X gradient indicates the existence of a NO_X sink process as the height increases from mid to top- canopy, while the 14:00-18:00 gradient indicates a NO_X source process. This is a direct evidence for processes in addition to NO_X partitioning affecting the concentration gradient on the timescale of canopy exchange. While there have been a number of indirect lines of evidence for this idea (Jacob and Wofsy 1990; Yienger and Levy 1995; Wang et al., 1998; Lerdau 2000; Wolfe et al., 2011; Min et al., 2012a), to our knowledge these observations provide the first direct measurements.

In Figures 7a-c, we show the eddy-covariance fluxes of NO, NO_2 and NO_X. We observed upward fluxes from 9:00 to 15:00. Fluxes of NO and NO_x were slightly downward from 6:00-9:00. The midday (12:00-14:00) median fluxes of NO, NO_2 and NO_X are 0.32 ± 0.27, 0.67 ± 0.21 and 1.0 ± 0.43 ppt m/s. A comparison the direction of the observed flux of NO_2 and NO_X to the gradients in Figures 6b and c gives a picture of molecular movement consistent with standard ideas of turbulent transport moving material from a region of high to low concentration. For NO, however, the direction of the flux is counter to that of the concentration gradient ("counter-gradient").

The observed midday fluxes of NO_X of 1.0 ± 0.43 ppt m/s are smaller than the lower end of soil NO emission measured at this site (2.9-22.9 ppt m/s in the morning) and smaller than other studies in the region. For example, at the Schubert Watershed at the Sierra Nevada Foothill Research and Extension Center in an oak forest, soil NO_X emissions of 5.8-15 ppt m/s were observed during the summer (Herman et al., 2003) and typical soil NO fluxes reported in California are 1.9 ppt m/s - 19 ppt m/s (Anderson and Poth, 1989; Davidson et al., 1993). Comparison of these soil NO_X emissions to our ecosystem scale flux measurements suggests the existence of NO_X removal process within the canopy—a NO_X canopy reduction factor.

To evaluate the contribution of soil NO emission to the NO_2 flux by the reaction with O_3, we divide our system into a soil NO emission layer and a chemical conversion layer, where the latter layer includes the within and above canopy measurement heights. The noontime (12:00-14:00) ratio of NO and NO_2 in the conversion layer (estimated as the averaged value over all measured heights) is 1:4.7 indicating 0.83 NO_2 molecules are produced for every NO molecule emitted from soil emission layer. Using the lowest measured soil NO emission rate, we infer 0.3-4.3% of noontime downward flux of O_3 (14 nmol/m^2/s) is due to the conversion of NO to NO_2. A similar magnitude of O_3 loss (1-8%) via NO and NO_2 interconversion was calculated by Kurpius and Goldstein (2003). This conversion of NO to NO_2 induces a 1.0-1.7 ppt m/s NO_2 flux, which is 2-3 times bigger than the observed NO_2 flux (0.67 ± 0.21 ppt m/s), another piece of evidence supporting the existence of a canopy reduction process for NO_2.

2.5. Analysis

For a conserved tracer, the direction and magnitude of the flux is controlled by the local concentration gradient and the vigorousness of vertical mixing—the tracer moving from high to low abundance and the rate of movement determined by the strength of both the gradient and the turbulent mixing. This concept is known as flux-gradient similarity or Bowen ratio theory, and is often used for estimating the exchange rate of non-reactive (conserved) species from their concentration gradient information (e.g. Mayer et al., 2011 and references therein). Similarity theory holds for conserved tracers when observations of fluxes are made above the roughness sublayer (Raupach and Legg, 1984) and this criterion was met at BEARPEX 2009 (18m flux measurement height with 8.8m mean tree height), as evidenced by a comparison of the flux data of the sensible heat and 3 biogenic VOC species with longer chemical lifetimes than the turbulent transport time (Park et al., 2012).

The fluxes of reactive species cannot be completely described through simple application of similarity theory. This is because reactive species will, to some extent, undergo chemical transformations faster then they will be transported by turbulent diffusion (Vila-Guerau de Arellano et al., 1993; Gao et al., 1991; Jacob and Wofsy, 1990). However, similarity theory is still a powerful tool, as quantifying the flux due to turbulence transport, allows estimation of the effects of other within-canopy processes.

A visual representation of this idea is shown in Figure 2.8. The red line shows the gradient where the flux-gradient similarity holds and the blue line shows the gradient if the concentration is chemically, or otherwise, perturbed. This is known as Localized Near-Field (LNF) theory (Vandenhurk and Mcnaughton, 1995; Raupach, 1989). In the analysis below, we will assess the within-canopy behavior of NO, NO_2, and NO_X through pictorial relationships analogous to Figure 2.8.

In Figure 2.8, the green dashed line divides two layers: a within canopy layer and an above-canopy layer. C_1 is the measured concentration in the above canopy layer and C_2 is the measured

concentration within the canopy. Using similarity theory and the measured fluxes we calculate C_F, the concentration that would be observed for a conserved tracer. The difference between C_2 and C_F, defines C_N, represents the contribution to the concentration by other processes that act to perturb the flux gradient relationship. For conserved tracer with a chemical lifetime (τ_{chem}) longer than the turbulent mixing time (τ_{turb}), such as CO_2, H_2O and some less reactive BVOCs, C_N is zero. For reactive molecules as NO and NO_2, C_N will not be zero and, we can use C_N as a constraint on the extent to which chemistry occurring on fast timescales (i.e. faster than τ_{turb}) within the canopy.

To quantify C_F we use flux-gradient similarity, Eq. (2.2), (Meyer, 1986) and the mixing rate, *K*, the so called the eddy diffusivity constant, which is inferred from the observed sensible heat flux and temperature gradient. The difference between C_2, and C_F is then C_N.

$$\frac{\partial(C_F - C_1)}{\partial z} = \frac{F_X}{K} \tag{2.2}$$

In an illustrative test of our approach we present our results for the conserved tracer, water. In Figure 2.9, the blue circles represent the measured gradient of H_2O and the red circles show the gradient inferred from the H_2O flux (C_F) in the within-canopy layer at midday (12:00 to 14:00 hrs). As expected, the difference between C_2 and C_F in the within-canopy layer, C_N, shown as a black arrow, is negligibly small (<1% of C_1) with respect to the variability of H_2O and the measurement uncertainty (3%). This implies there are no important additional source/sink process(es) aside from turbulent transport.

Applying same analysis to NO and NO_2 (Figure 2.10), we find C_N, the difference between the measured concentration and C_F, is large compared to the measurement error. C_N for NO and NO_2 are -12.4±3.3 ppt (23% relative to C_1) and 64.7±4.7 ppt (44% relative to C_1). Repeating this analysis assuming the canopy top height and the concentration at that height as representative of the within canopy layer, instead of averaging through the entire canopy, results in C_N values of similar magnitude, 27% and 39% for NO and NO_2 respectively.

To understand contributions to C_N, we begin with analysis of how fast photochemistry interconverts NO and NO_2. Figure 2.10a indicates that to explain the observed NO flux, we need to account for 12ppt (C_N) more NO molecules than were observed in the canopy layer. Based on the observed gradient of NO, standard flux-gradient similarity predicts the downward flux of NO; however, we observed upward flux of NO (Figure 2.7). This counter-gradient flux can only be explained by the formation of NO during the transport process from within the canopy layer to the above canopy layer. This is reasonable as photolysis rates above the canopy should be faster than in the shade of the canopy. If the required NO is completely from NO_2 photolysis then a corresponding amount of NO_2 will be lost. Thus, roughly 20% of the C_N for NO_2 contributes 100% of C_N for NO, 12.4 (±3.3) ppt and the remainder (80% of C_N in NO_2, 52.3 ppt) must be accounted for via other mechanisms.

To validate the assumption that the counter-gradient flux of NO can be 100% explained by NO_2 photolysis, we use two different methods. First we use the photostationary state analysis of NO, NO_2, and O_3 over 100 seconds (τ_{turb}) and compare the remaining C_N of NO_2 after converting NO via photolysis (80% of C_N NO_2, 52.3ppt). We use Eq. (2.3) to estimate the magnitude of NO and NO_2 inter conversion on turbulent timescales and estimate the loss rate of NO_2 on a 100 second timescale.

$$L_{NO_2,net} = j_{NO_2} NO_2 - (k_{NO+O_3}[O_3] + k_{NO+HO_2}[HO_2] + k_{NO+RO_2}[RO_2])[NO] \quad (2.3)$$

The photolysis rate, j_{NO2}, is generated with the Tropospheric Ultraviolet and Visible (TUV) radiation model and then scaled with measured PAR. We treat RO_2 as equal to HO_2. Using the measured concentrations of NO, NO_2, O_3, HO_2, and temperature, we estimate a net loss of 22.8 ppt of NO_2, which is in excess of which is needed to explain the NO counter-gradient flux of 12.4 (±3.3) ppt.

The large value of C_N for NO_X (54.3±5.9 ppt, 29% relative to C_1) indicates the necessity of one or more within-canopy loss processes. To explore the mechanism(s) controlling the C_N for NO_X, we examine several chemical processes related to PNs, ANs, HNO_3, and HONO using our two-layer model. The magnitudes of each of the near-field processes for NO_X were inferred using Eq. (2.4) to estimate the contribution of certain processes on the ~100s timescale of turbulent mixing (τ_{turb}).

$$L_X = P_X = \frac{\partial}{\partial t}\int_{z1}^{z2} C_X(z)dz \quad (2.4)$$

Here, L_X (P_X) is the loss (production) rate of species x happening within the time window of turbulent air movement from within the canopy (height *z1*) to above the canopy (height *z2*). We choose 4.4m, averaged throughout the canopy, as a representative of *z1* and 18m above canopy layer as representative of *z2*.

PNs can act as either a net source or a sink of NO_X through thermal dissociation (+1 NO_2 molecule) or PN formation (-1 NO_2). Calculating the steady-state chemical production and thermal and chemical loss of PAN (LaFranchi et al., 2009; Wolfe et al., 2009), yields 5.3 ppt of NO_2 formed in 100s. This mechanism thus implies an enhancement of NO_X within the canopy, discussed in more detail in Min et al. (2012c). However, we have also suggested that a local biogenic precursor drives PN formation within canopy (Min et al., 2012a). This BVOC PN species, denoted XPN, exhibited an upward flux and is a candidate for NO_2 loss not included in our steady-state calculation. We estimate that the flux of this XPN to be 2.274±0.357 ppt m/s corresponding to 16.7 ppt of NO_2 loss within canopy and explaining 31% of the NO_X C_N.

BVOC driven AN formation from OH initiation can be calculated as:

$$P_{\sum AN} = \sum_i \alpha_i k_{OH+VOC_i}[OH][VOC_i] \quad (2.5)$$

Here, we estimate the effects of 2-methyl-3-butene-2-ol (MBO) and monoterpenes (two important BVOCs at the BEARPEX site (Bouvier-Brown et al., 2009a; Schade et al., 2000) on AN production (for 100s) and calculate 1.2-3.3 ppt (2.2-6%) and 0.11-0.6ppt (0.2-1.1%) NO_X is removed by AN formaion, respectively. A 3% branching ratio (α_i) (Rosen et al., 2004), we used for each molecule. If we instead use a branching ratio of 20%, we estimate 8.3-21.9 ppt (15-40%) and 0.77-2.0ppt (1.4-3.7%) NO_X is lost to MBO and monoterpene nitrates formation. If we consider AN formation from ozonolysis reactions of very reactive BVOCs, such as sesquiterpenes, in analogy to XPN formation through the channel described as BCSOZNO3 in MCM v3.2, we estimate additional 27 ppt (50%) of NO_X consumed. These calculations indicate chemical formation of nitrates is rapid enough to affect the fluxes.

Formation of HNO_3 is an important pathway to remove NO_X from the system by wet and dry deposition after formation. Gas phase reaction of NO_2 with OH has been known as a major source of HNO_3 formation in rural areas (heterogeneous formation HNO_3 from NO_2 hydrolysis is slower by an order of magnitude order than the gas phase formation rate). The production rate can be calculated as:

$$P_{HNO_3} = k_{OH+NO_2}[OH][NO_2] \quad (2.6)$$

Using the measured OH concentration, we estimate 0.6-2% of NO_X is lost through gas phase reaction at this site. Compared to ANs and PNs, HNO_3 formation is unimportant.

HONO formation is another candidate for altering the flux of NO_X. HONO flux measurements at this site were observed to be small (-0.11 ± 0.69ppt m/s) and downward indicating possibly contribute the enhancement of NO_X within canopy rather than loss.

Direct uptake through plant stomata might be responsible for the remaining NO_2 removal within the canopy. However, the daytime NO_2 concentration at this site of less than few hundred ppt suggests this site is a regime where NO_2 emissions from plant biota likely dominate. Further evidence of an NO_2 compensation point from canopy scale observations are presented in Min et al. (2012c).

Taken together as much as 100% of the C_N for NO_X (Table 2.1) can be explained by local chemical NO_X loss mechanisms and the formation of higher nitrogen oxides. A subsequent paper will examine fluxes of ANs to assess overall closure in the N budget.

2.6. Conclusions

We observed upward fluxes of NO and NO_2 from eddy-covariance flux measurements, large NO_2 and NO_X concentration enhancements within canopy, and counter-gradient fluxes of NO. Applying standard flux-gradient relationships indicates the existence of one or more NO_X loss processes within the canopy, in addition to conversion of NO to NO_2 by reaction with O_3 and

peroxy radicals. We investigate multiple chemical processes to explain the NO_X removal during vertical transport and conclude that the chemical formation of PNs and ANs can be responsible for the NO_X canopy reduction factor. This study provides observational evidence of an ecosystem scale canopy reduction factor, a factor that has been relied on to reconcile discordance between leaf-level, soil-level, and atmospheric modeling studies. We find it likely that much of this reduction is chemical—implying that the reactive nitrogen does escape the canopy and may be returned by further chemistry as NOx downwind.

Table 2.1. Possible within canopy NO_X consumption mechanisms.

Mechanisms	**NO_X consumption**
Un-identified PN formation	>31%
MBO and monoterpene nitrates formation	2.4-43.7%
Sesquiterpene nitrate formation	0-50%
HNO_3 formation	0.6-2%
HONO formation	~0%
Total NO_X loss	**34-100%**

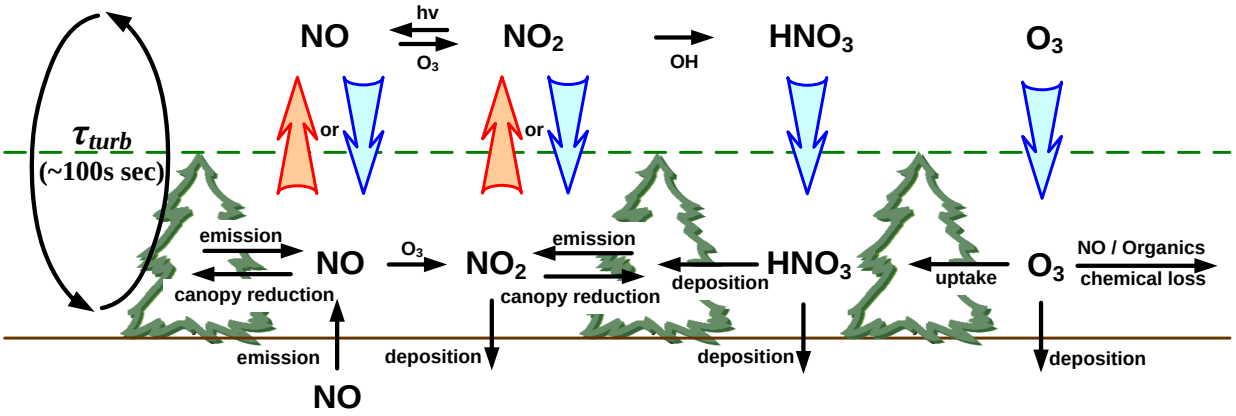

Figure 2.1. Schematic of the various interactions involved in the exchange of nitrogen oxides between the atmosphere and the forest canopy. Bold arrows in blue (downward) and red (upward) represent the direction of the flux of each species across the canopy surface.

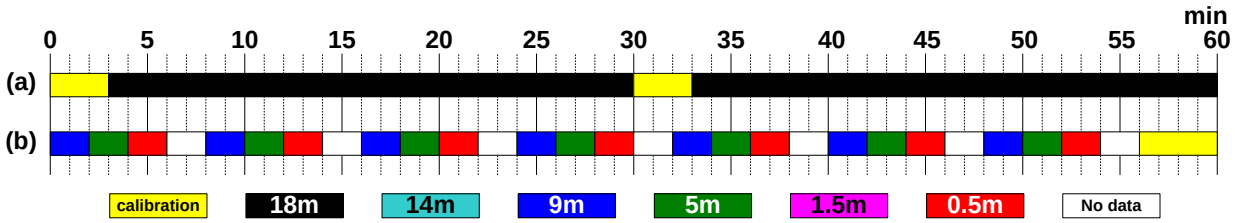

Figure 2.2. Data collection scheme for NO (2ch-CL) and NO_2 (TD-LIF) for flux (a) and vertical gradient (b) measurements. Colors represent the different measurement heights: 18m (black), 14m (light blue), 9m (blue), 5m (green), 1.5m (magenta), and 0.5m (red). Yellow periods are calibration cycles and white periods represent no data collected at that time.

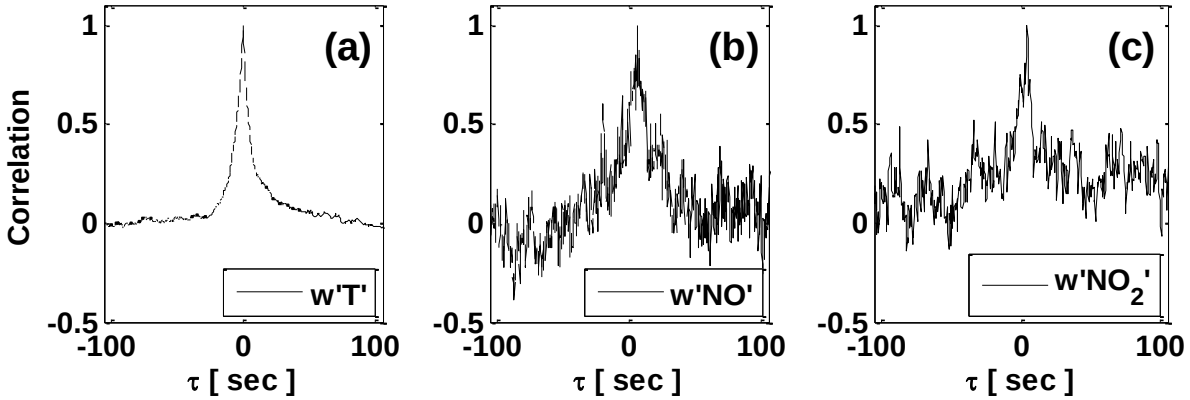

Figure 2.3. Lag calculation of w'T', w'NO' and w'NO_2'. Highest normalized correlation between wind and temperature/NO or NO_2 were observed as expected; 0 second for wind and temperature, 1.4 and 2.6 second for NO and NO_2.

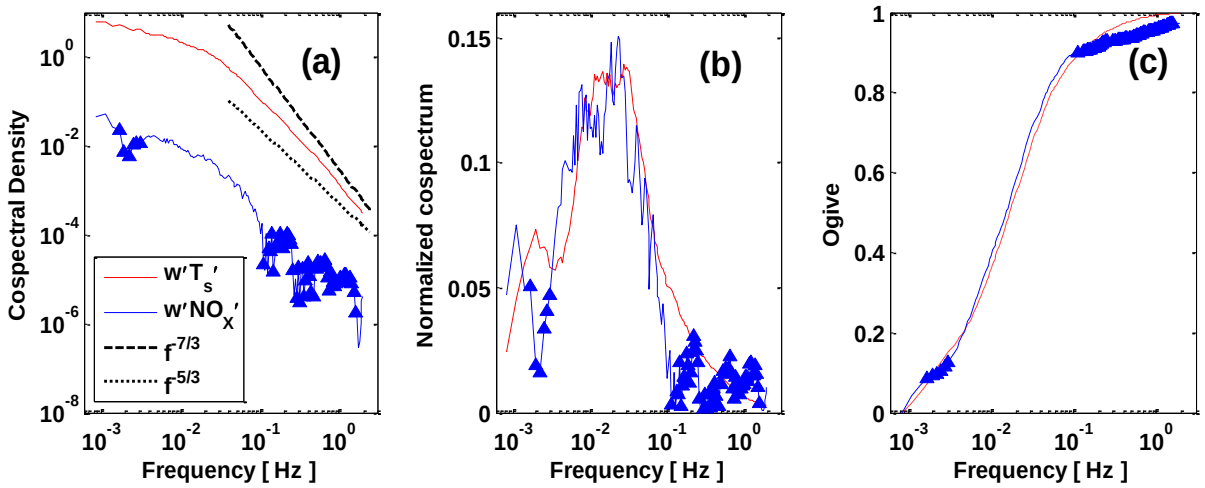

Figure 2.4. Equally spaced logarithmic averaged (200 bins) absolute cospectral density (a), frequency weighted cospectrum (b), and normalized cumulative distributions of the cospectra of temperature (red) and NO_X (blue) (c) with vertical wind from 9:00-12:00 when the chemical perturbation is small. Closed triangles represent the absolute value of the negative cospectral density, which has the opposite sign to the general flux direction. The black dotted lines in (a) are lines with slopes of −7/3 and −5/3 (see related text).

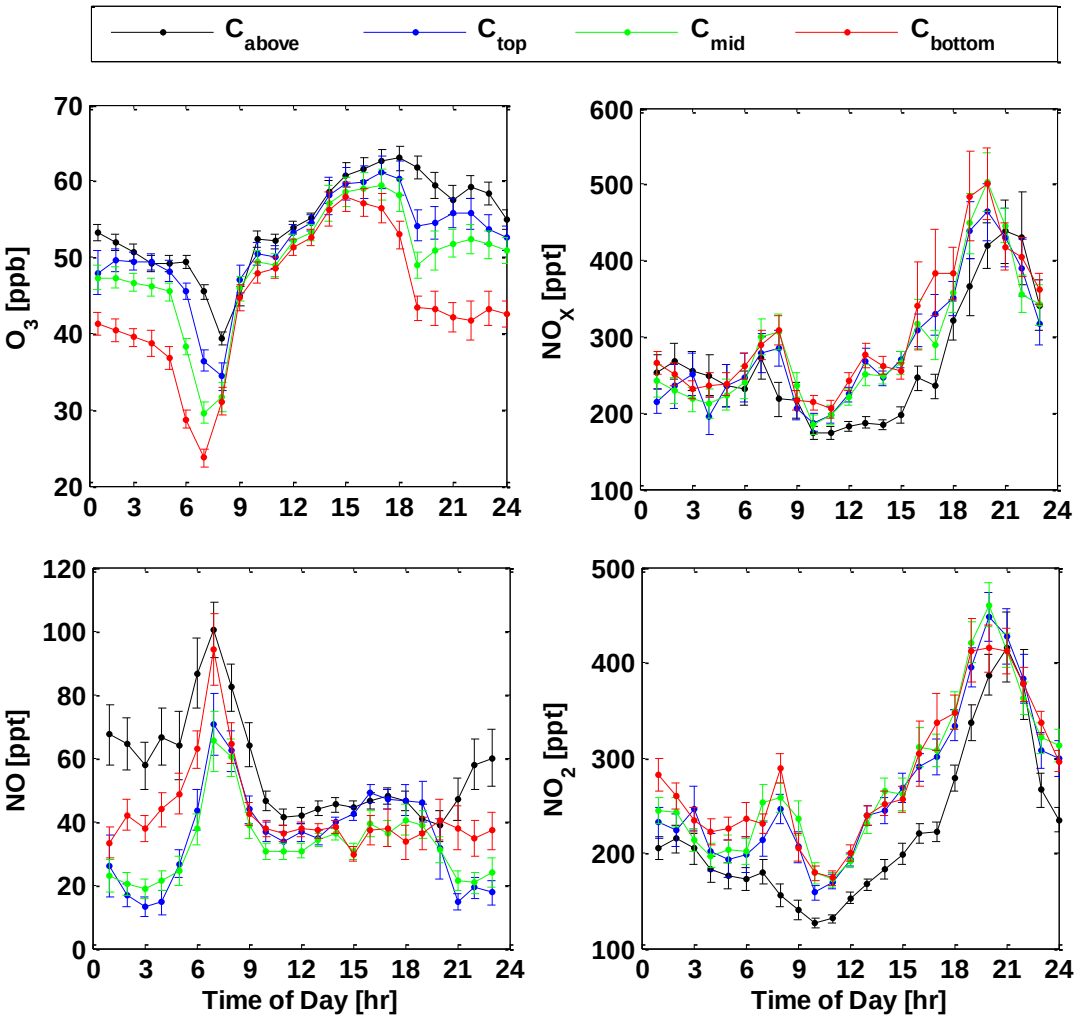

Figure 2.5. Diurnal patterns of O_3 (south tower), NO_X, NO, and NO_2. The data are one-hour mean values and the error bars represent the variation defined as the observed variability (± 1σ) divided by square root of the number of measurements in that time bin. Colors represent the measurement heights: above canopy (18m) in black, top canopy (9m) in blue, middle canopy (5m) in green, and forest floor (1.5m for O_3 and 0.5m for NO and NO_2) in red.

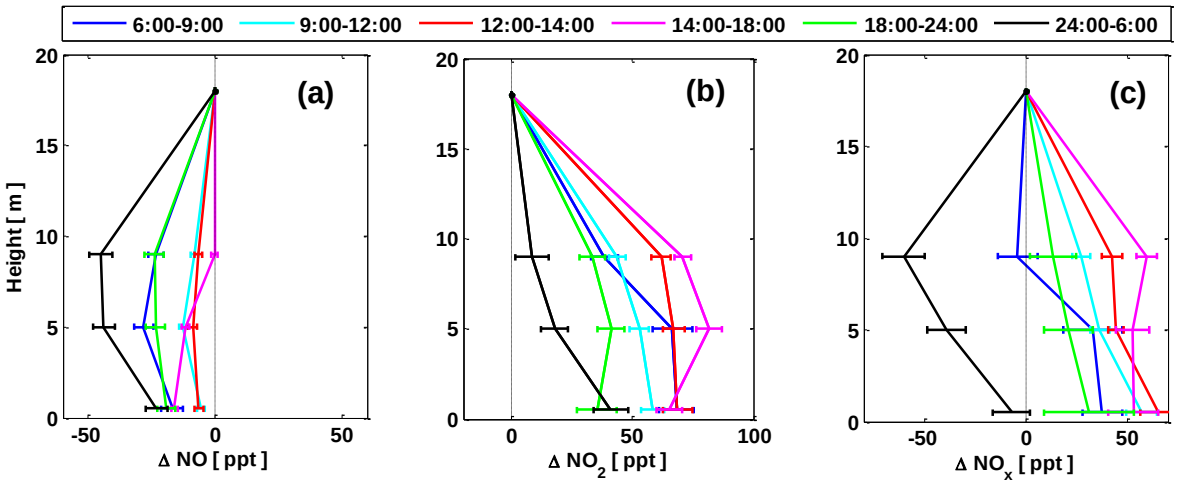

Figure 2.6. Vertical gradients of NO, NO_2, and NO_X. Dot and whiskers represent means and standard errors of the mixing ratio enhancement at each height. The colors represent the enhancement at 6 different times of day through the complete diurnal cycle: early morning (6:00-9:00, blue), late morning (9:00-12:00, cyan), midday (12:00-14:00, red), afternoon (14:00-18:00, magenta), evening (18:00-24:00, green) and night (24:00-6:00, black).

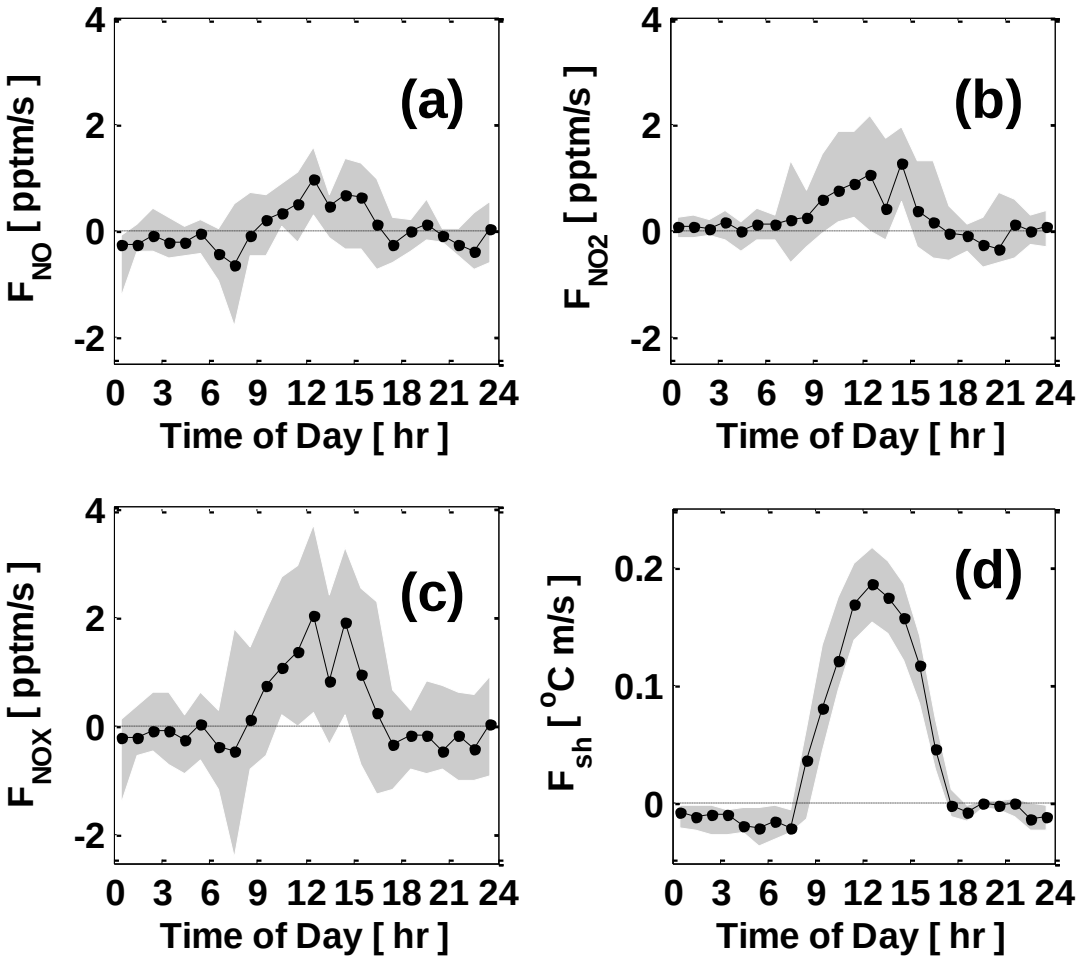

Figure 2.7. Diurnal patterns of the NO, NO_2, NO_X, and sensible heat fluxes in panels a, b, c, and d, respectively. All fluxes are upward indicating molecular motion from forest to atmosphere. Median midday (12:00-14:00) fluxes are 0.32 ± 0.27, 0.67 ± 0.21, and 1.0 ± 0.43 ppt m/s for NO, NO_2, and NO_X and that of sensible heat flux is 0.21 ± 0.08^{o}C m/s. Black line represent means and the gray areas give 25-75% of flux data for hourly bins.

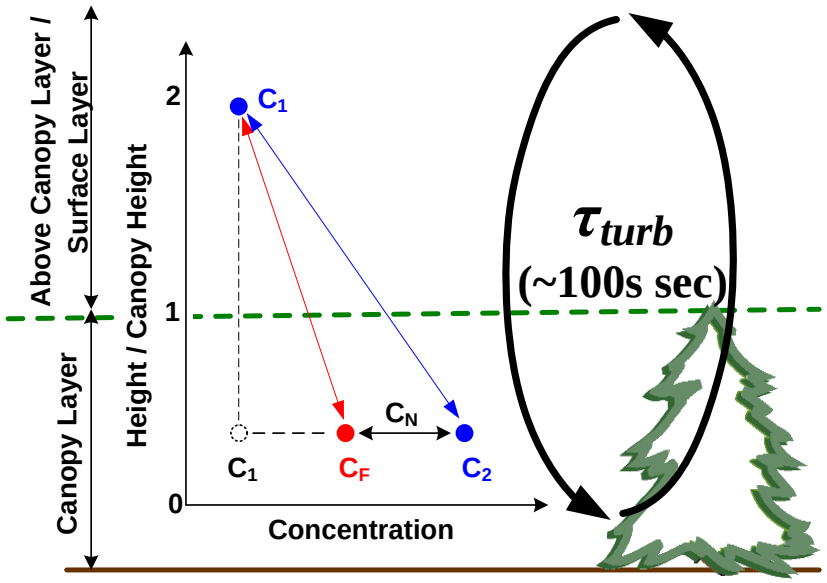

Figure 2.8. Schematic of our two-layered model based on the localized-near field, LNF, concept. C_1 represents the reference concentration, which for the above-canopy layer is defined as the measured concentration at height 18m. C_2 is the measured concentration within the canopy defined as the averaged concentration at 0.5, 5, and 9m. C_F is estimated concentration from the measured eddy-covariance flux and the eddy diffusivity calculated from sensible heat flux. C_N is the non-diffusive concentration estimated from the difference of C_2 and C_F while, C_F is the concentration from diffusion, where the standard flux-gradient relationship holds.

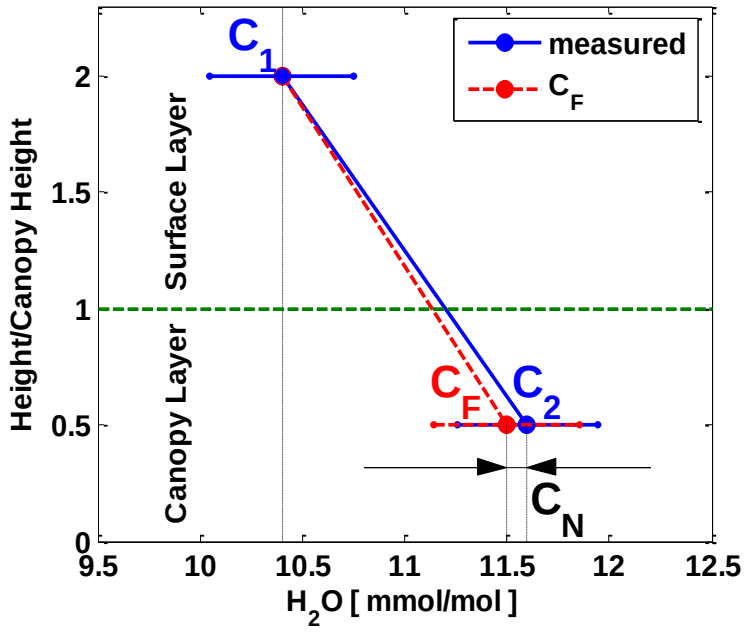

Figure 2.9. The estimated concentration, C_F (red) using standard flux-gradient similarities of H_2O during midday (12:00-14:00) is shown. Blue represents the measured vertical gradient. Closed circles and whiskers represent the mean and the variability of H_2O. The difference between blue and red in the within-canopy level is shown in black arrow indicates C_N and is negligibly small as expected for a conserved species.

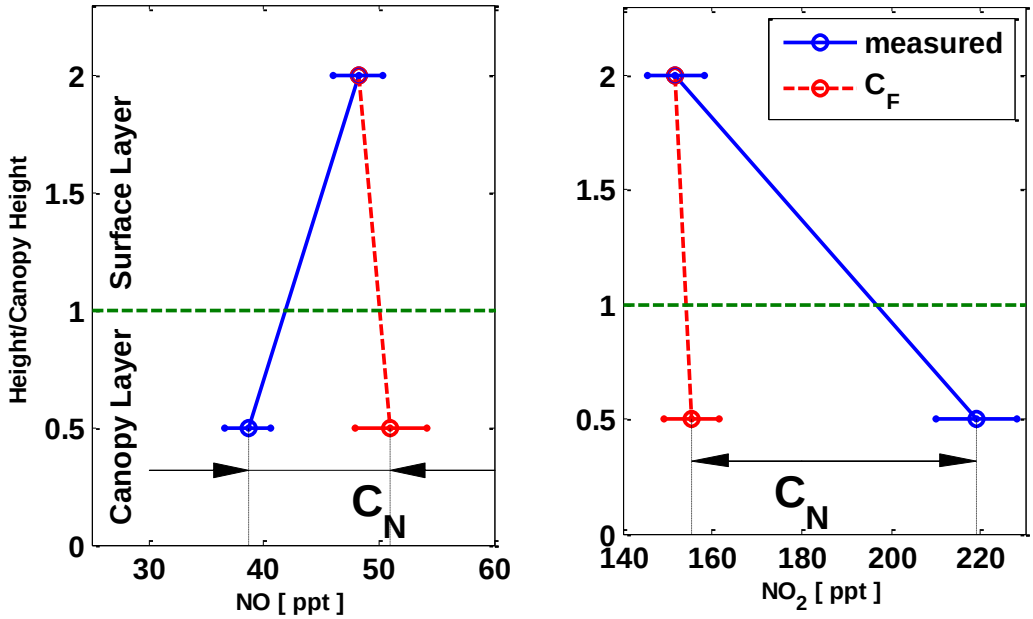

Figure 2.10. The estimated concentration, C_F, (red) using standard flux-gradient similarities of NO and NO_2 at midday (12:00-14:00). Blue represents the measured vertical gradient. Closed circles and whiskers are the mean and standard errors. The differences between blue and red points in the within-canopy layer are C_N.

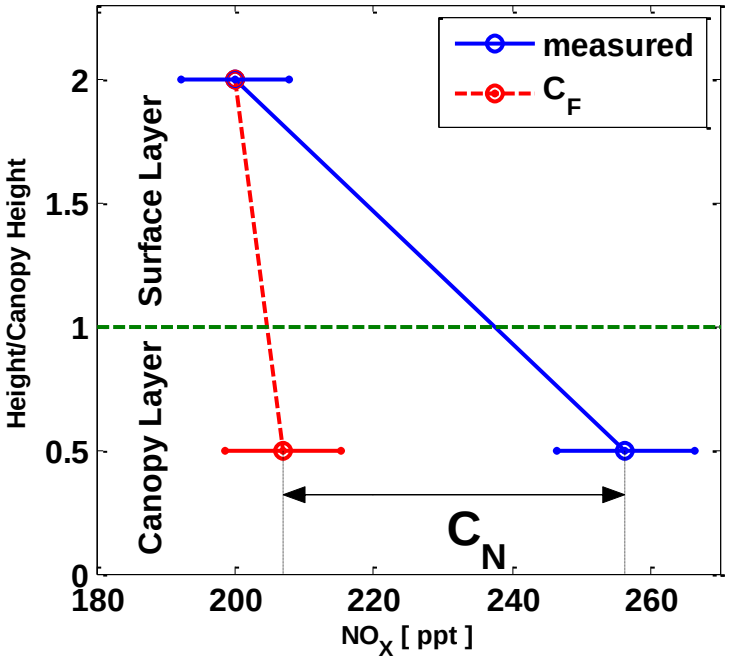

Figure 2.11. The estimated concentration, C_F, (red) using standard flux-gradient similarities of NO_X at midday (12:00-14:00). Blue represents the measured vertical gradient. Closed circles and whiskers are the mean and standard errors. The differences between blue and red points in the within-canopy layer are C_N.

Chapter 3

Observational evidence for an ecosystem scale NO_2 compensation point

Abstract

The effects of vegetation and chemistry on exchange of nitrogen oxides (NO_X = NO + NO_2) between the biosphere and atmosphere are poorly understood. We present an observational study of NO_2 exchange at the canopy scale, using eddy-covariance flux measurements along with simultaneous vertically resolved concentration measurements at multiple heights within the canopy. We derive exchange velocities for NO_2 and find they have an inverse relationship to NO_2 concentration and observe that the sign of the major flux carrying eddies varies with ambient NO_2 concentration. Relationships between exchanges rates of NO and NO_2 with those of carbon dioxide (CO_2), ozone (O_3) and photosynthetically active radiation provide constraints that help to elucidate the mechanisms controlling NO_2 exchange.

3.1 Introduction

The exchange of nitrogen oxides (NO_X = NO + NO_2) across the atmosphere-biosphere interface (Figure 3.1) affects (a) ecosystem nutrient cycling by influencing the amount of bioavailable N, (b) air quality as NO_X is a key atmospheric reactant, and (c) climate change as the dry and wet deposition of oxidized reactive N may act to fertilize plant growth and thus increases sequestration of CO_2 with the biosphere. Our current understanding of the atmosphere-biosphere exchange of NO_X is summarized in Figure 3.1. Soil NO emissions are the largest source of NO_X from the biosphere and the rapid inter conversion between NO and NO_2 resulting from the reaction of NO with O_3 and the photolysis of NO_2 determines the form of NO_X. To quantify the strength of the each arrow in Figure 3.1, multi-scale studies have been conducted at the inter-cellular (e.g. Rogers et al., 1979; Lee and Schwartz, 1981; Park and Lee, 1988; Okano et al., 1986; Nussbaum et al., 1993; Weber et al., 1995), leaf (e.g. Eller and Sparks, 2006; Teklemariam and Sparks, 2006; Chaparro-Suarez et al., 2011 and references therein), canopy (e.g. Hereid and Monson, 2001; Horii et al., 2004;Fang and Mu, 2006; Farmer et al., 2006; Min et al., 2012b), regional and global scale (e.g. Jacob and Wofsy, 1990; Yienger and Levy, 1995; Wang and Leuning, 1998; Ganzeveld et al., 2002; Delon et al., 2007) over the last few decades. Leaf-level studies, including inter-cellular studies, have largely focused on metabolic processes

of vegetation (plant centric), while canopy studies, including regional- and global-scale studies, have concentrated on the impacts of NO_x exchange across canopies on air quality and climate change (atmosphere centric). Broadly speaking, results from leaf and canopy perspectives are contradictory (Lerdau et al., 2000), as at the leaf scale plants are able to act as NO_X sources but at the canopy-scale vegetative canopies appear to act as NO_X sinks. We discuss both perspectives in detail below.

At the leaf scale the role of vegetation as source and/or sink of NO_2 is determined by the ambient NO_2 concentration. Bi-directional exchange of NO and NO_2 has been observed (e.g. Wildt et al., 1997; Chaparro-Suarez et al., 2011 and references therein) and a compensation point, C_{PT}, where the direction of net exchange changes sign has been identified for NO_2. The C_{PT} is defined as the ambient NO_2 concentration at which the net exchange of NO_2 becomes zero, below which the plant emits NO_2 and above which plants take up NO_2. This pivotal point is thought to be determined by a balance between the production and consumption of NO_2 by plants rather than the Henry's Law equilibrium of NO_2 between the atmosphere and the stomatal liquid (Conrad, 1996). Leaf-level branch enclosure studies have measured C_{PT}s for NO_2 ranging from 0.1 to 3.2 ppb (Chaparro-Suarez et al., 2011 and references therein). Most of the ecosystems on Earth experience lower ambient NO_2 concentrations than any reported C_{PT} implying that nearly all continental vegetation acts as a source of NO_2. Yet some branch enclosure studies have suggested mechanisms other than plant metabolic processes are responsible for the observed NO_2 emissions. For example UV induced NO_2 emissions from deposited nitric acid (HNO_3) or organic nitrates (Hari et al., 2003; Raivonen et al., 2006; Raivonen et al., 2009) have been proposed. Similar surface processes have been reported on snow and glass surfaces with emissions of NO_2, NO, and HONO observed (Beine et al., 2002; Zhou et al., 2003; Zhou et al., 2011). UV induced emissions will also mean canopies may act as sources of NO_X.

At the canopy scale, in order for chemical transport modeling studies to calculate reasonable concentrations of O_3 in remote regions, models invoke a "canopy reduction factor" to remove NO emitted from soils before it is injected into the atmosphere. This factor removes 25–85% of NO_X within the canopy prior to its escape depending on the strength of the local soil NO emission and location (Jacob and Wofsy, 1990; Yienger and Levy, 1995; Wang and Leuning, 1998; Ganzeveld et al., 2002; Delon et al., 2007). There is observational evidence to support this canopy shielding effect (Lovett and Lindberg, 1993; Hereid and Monson, 2001; Fang and Mu, 2006; Min et al., 2012b) including a description of its meteorological controlling factors (Pang et al., 2009). Previous work from our group directly observed a within canopy NO_X removal processes finding a canopy reduction factor was indeed needed to reconcile vertical NO_X concentration gradient and flux measurements (Min et al., 2012b) and we proposed that the chemical production of the higher nitrogen oxides such as peroxy nitrates and alkyl nitrates was the mechanism behind the reduction factor (Min et al., 2012a). Canopy reduction factors imply that in remote regions vegetative canopies function as NO_X sinks at ambient NO_X less than most values of C_{PT}.

In this paper, we (1) investigate whether —at the canopy scale— a forest acts as a source of NO_2 and (2) discuss how the existence of a CPT is consistent with the concept of a canopy reduction factor.

3.2 Methods

We use data collected during the BEARPEX 2009 campaign (June 15 – July 31, 2009) at a ponderosa pine plantation and located adjacent to the University of California at Berkeley Blodgett Forest Research Station (38°53'42.9"N, 120°3757.9"W and 1315m) on the western slope of the Sierra Nevada Mountains in California. A detailed description of the local meteorology, along with a campaign overview and other BEARPEX analyses can be found elsewhere (Cohen et al., 2012; articles in this special issue of ACP).

Briefly, the summer wind patterns are highly regular and characterized by flow from the southwest (210-240°) during daytime and from the northeast (30°) during nighttime. The dominant upper canopy trees are Pinus ponderosa L. with a few Douglas fir, white fir, and incense cedar. The lower canopy is mainly composed of mountain whitethorn (Ceanothus cordulatus) and manzanita (Arcostaphylos species) shrubs. The canopy height, defined by the mean tree height, was 8.8 m with a 3.7 m^2/m^2 leaf area index (LAI). The leaf area density was estimated following Wolfe et al. (2011) and Misson et al. (2005).

All data in this study were measured from an 18 m tall scaffolding tower (hereafter the "north tower") with the exception of O_3, which was measured from a 15 m walk-up tower (hereafter the "south tower") and the two towers were 10 m apart. Vertically resolved concentration measurements of NO and NO_2 were made at multiple heights (0.5, 4.5, 8.8 and 17.5 m) using a two-channel chemiluminescence system (2ch-CL) and two thermal-dissociation laser-induced fluorescence systems (TD-LIF). In addition, higher oxides of nitrogen i.e. PNs, ANs and HNO_3 were also measured from same TD-LIFs and by two independent chemical-ionization mass spectrometry (CIMS) methods (Wolfe et al., 2009; Beaver et al., 2012). Details on the NO and NO_2 measurement configurations and data acquisition sequences are described in Min et al. (2012b).

At a height of 17.5 m on the north tower, a sonic anemometer (Campbell Scientific CSAT3 3-D Sonic Anemometer) was placed adjacent to the NO and NO_2 inlets with minimal displacement (0.02 m vertical and 0.2 m horizontal displacement) to monitor 3-D wind information to calculate fluxes. Fast response O_3 sensor using a chemiluminescence technique (Coumarin 47) and high-resolution infrared gas analyzer for CO_2 and H_2O (Licor 6262) were placed at a height of 12.5 m on the south tower with a sonic anemometer (Applied Technologies, Inc., Boulder, CO). Photosynthetically active radiation (PAR) was also measured. Detailed information on the setup and operating principles for the O_3 measurements can be found in Fares et al. (2010).

The flux, F_C, is a measure of the direction and vertical transport rate of atmospheric constituent, C. In this study F_C is calculated using the eddy-covariance method (EC) utilizing high-time resolution measurements (<1 Hz) of 3D-wind information and, in this paper, concentration observations of NO, NO_2, O_3, and CO_2. The eddy covariance flux is directly inferred from the deviation of covariances between C and vertical wind speed, w, ($F_C=\overline{w'C'}$, Foken, 2006; Lee et al., 2004; McMillen, 1988). The exchange velocity of C, V_C, is defined as

the concentration normalized flux ($V_C = F_C/[C]$). Details of the EC flux observations and procedures used in this paper can be found in Min et al. (2012b).

To explore the mechanism controlling the NO_2 exchange, we use the normalized exchange velocity (nV_c). nV_c is defined as the exchange velocity of species C (V_C) divided by the maximum exchange velocity ($nV_C = V_C/Vmax_C$). The nV_C is useful because it normalizes out the variations in the exchange rate caused by strong turbulent mixing since the V_{maxC} describes the aerodynamic limit of exchange rate. The calculation of nV_C is described in Appendix A.

3.3 Vertical gradients of NO and NO_2

If the strength and direction of NO_2 emissions from the canopy is dictated by a C_{PT} then it is expected to be ambient NO_2 concentration dependent. Accordingly, Figure 3.2 shows the vertical gradients of NO, NO_2, and NO_X under high (red) and low (blue) NO_2 conditions. We define high and low NO_2 using the NO_2 concentration at 17.5 m (this is the above canopy NO_2 concentration) and a dividing line of 180 ppt. In early afternoon (12:00-15:00) we have a nearly equal number of 30 minute NO_2 flux observations, n_{high} = 67 and n_{low} = 73 binning the data in this way. We found that different time windows and/or concentration criteria do not affect our conclusions. We also sorted by day of week defining Saturday and Sunday as weekends and Tuesday, Wednesday, and Thursday as weekdays, where weekends have low NO_2 and weekdays have high NO_2 (this site is downwind of the city of Sacramento). Again, results were similar as when sorted above and below 180 ppt.

In the bottom panels of Figures 2, the gradients are shown as difference (ΔC) of each measured concentration with respect to the above canopy concentrations at 17.5 m ($\Delta C = C_{height} - C_{17.5m}$). Within canopy concentrations greater than that above the canopy have positive values of ΔC and within canopy concentrations that are smaller negative ones. In the first plot in Figure 3.2 the normalized leaf area density is shown along the measurement profile. The time derivative of NO_2, Φ, is calculated as:

$$\Phi = k_{NO+O_3}[NO][O_3] - j_{NO_2}[NO_2] \quad (3.1)$$

When the system reaches photostationary state Φ equals 0. The photolysis rate of NO_2, j_{NO2} is inferred from the photolysis rate calculated with the Tropospheric Ultraviolet and Visible (TUV) radiation model and an extinct rate that is assumed to depend on the leaf area density and scaled by PAR. We estimate 90% of the radiation is attenuated at the bottom of the canopy following Wolfe et al (2011).

We observe that less NO and more NO_2 and NO_X exist within the canopy than above. NO_2 and NO_X both peak near the forest floor. The depletion of NO within canopy is due to the conversion of NO to NO_2 by reaction with O_3 and reduced photolysis of NO_2 within the canopy. The positive Φ at 0.5m confirms that conversion of NO emitted from the soil to NO_2 persists to

at least that height above the soil. By 5m NO and NO_2 are nearly in photostationary state ($\Phi \approx 0$). Above the canopy, we find NO and NO_2 are in photostationary state and that this is independent of the ambient NO_2. The higher photolysis rate above the canopy means that NO_2 is more quickly converted to NO compared to the shaded regions in the middle and at the top of the canopy. The observed gradients of NO and NO_2 are qualitatively consistent with the generally held model of biosphere-atmosphere NO_X exchange, described in Figure 3.1, where soil NO emissions are the major source of NO_X. In this model, NO_2 exchange is controlled by the soil NO emission rate and chemical cycling between NO_2-O_3-NO, which happens sufficiently rapidly (~100 seconds) to affect the concentration within the canopy, the gradients, and the fluxes. The calculated Φ also supports this zero order model; the positive deviation from 0 near the forest floor indicates the soil NO emissions are a source of NO_2 and the Φ at 17.5m is close to 0 indicating that above canopy NO_X is in photosationary state. If NO and NO_2 inter conversion from soil NO emission was the only within canopy process taking place, we would expect NO_X to be conserved and to be described by a straight line pinned at the surface NO_X concentration. However, this is not what we observe. Rather, we see more NO_X within canopy than above. The drop in NO_X concentration from within the canopy to above the canopy (~50 ppt) is due to the presence of processes that we ascribe to a canopy reduction factor (via comparisons with flux data) in Min et al. (2012b).

One interesting phenomenon shown in Figure 3.2 is that the shapes of the NO_2 and NO_X gradients are dependent on NO_2 while the shape of the NO gradient is not. The bottom panel of Figure 3.2, we show that NO_2 is 55 (± 12) ppt greater within the canopy compared to above the canopy, specifically near the forest floor, when NO_2 concentrations are high, and 82 (± 10) ppt greater within the canopy when the above canopy NO_2 concentrations are low. At the same time, we do not observe any difference in NO in high versus low NO_2 concentration conditions. This is in part due to correlation with O_3 that result in higher photostatioinary state NO_2/NO ratios at high NO_2. This may also be an indication of a NO_X source other than soil NO. We observe greater NO_2 and NO_X concentrations with respect to the concentration at 17.5m at low NO_2 than we do at high NO_2, mostly apparent in lower canopy region, suggesting that this NO_X source is affected by ambient NO_2 concentration and that it may be related to plant function. This within canopy NO_X source is consistent consists with the mechanisms assumed to be responsible for a compensation pint for NO_2.

3.4 Exchange velocities of NO and NO_2

The NO_2 concentration dependence of the exchange velocity ($V_{NO2}=F_{NO2}/[NO_2]$) during the daytime (9:00-18:00) is shown in Figure 3.3. The mean and median V_{NO2} are shown as black diamonds and red lines; the blue boxes mark the central 50%. For the most part, the observed V_{NO2} is positive indicating that, in the aggregate, NO_2 exchange is upward from the biosphere to the atmosphere. V_{NO2} peak (1-2 cm/s) at 50-100 ppt of NO_2 and substantially decrease as NO_2 concentration increase. V_{NO2} is nrear zero in the range 300-500 ppt of NO_2.

In Figure 3.4, the daytime V_{NO2} is separated into three ambient NO_2 concentration regimes: low (NO_2 < 125 ppt, n = 85), mid (155 ppt < NO_2 < 192 ppt, n = 85) and high (240 ppt < NO_2, n = 84). The distribution of V_{NO2} under low NO_2 conditions spreads toward higher exchange velocities (Figure 3.3, top panel) compared to the distribution under high NO_2 conditions (Figure 3.3, bottom panel). Possible explanations for this behavior include a compensation point for NO_2 exchange—if there is a C_{PT} then NO_2 emissions would be larger at low NO_2. An alternative speculation is that emissions of NO are anticorrelated with NO_2 concentration. However, we are unaware of any process that would result in anticorrelation of NO emission and NO_2 concentration.

In Figures 5 and 6, we present the normalized NO (nV_{NO}) and NO_2 (nV_{NO2}) exchange velocity plotted versus photosynthetically active radiation (PAR) and CO_2, respectively. We find that nV_{NO} and nV_{NO2} exhibit different dependences on these two parameters. The nV_{NO} shows no dependence on PAR while nV_{NO2} is negative at low PAR and increases more or less linearly with PAR. The difference in the PAR dependence is direct evidence that nV_{NO} and nV_{NO2} are controlled by different processes. In addition, it also suggests that soil NO emissions and NO/NO_2 conversion are not the only source of NO_2. If soil NO were the only source of NO_2, and the chemistry of NO to NO_2 conversion controlled the NO_X partitioning, we would expect to correlated PAR dependence for both species

The dependence of nV_{NO} and nV_{NO2} on nV_{CO2} (Figure 3.6) also provides information that the processes controlling NO are not the same as those that control NO_2. In Figure 3.6 we observe a linear increase of nV_{NO2} with increases in nV_{CO2}, where faster upward movement of NO_2 molecules is correlated with a faster CO_2 deposition rate except for the smallest nV_{CO2}. No clear relationship exists between nV_{NO} and nV_{CO2}. The correlation with nV_{CO2} and nV_{NO2} may be an indication of the connection between the within canopy NO_2 source and plant processes. However, CO_2 flux is correlated with PAR and it is difficult to disentangle a purely radiative effect from one involving plant stomata.

3.5 Cospectral analysis

Cospectral analysis can be used to characterize the contributions of the different frequency eddies to the total flux. Min et al. (2012b) show that our NO and NO_2 instruments, 2-ch CL and TD-LIF, observe the full range of flux carrying eddies without any significant biases in frequency. Here, we interpret the cospectrum of reactive species by comparison to the cospectrum of conserved tracers. The frequency weighted and covariance normalized cospectrum of sensible heat ($nCo_{w'Ts'}$), NO_2 ($nCo_{w'NO2'}$), NO ($nCo_{w'NO'}$) and O_3 ($nCo_{w'O3'}$) are shown in Figure 3.7. These curves represent the fraction of the total flux at each frequency. Higher frequencies are smaller eddies and lower frequencies are larger ones. The frequency weighted and covariance normalized cospectrum, $nCo_{w'c'}(\upsilon)$, is calculated as:

$$nCo_{w'c'}(v) = \frac{vCo(v)}{\sigma_{w'c'}} \tag{3.2}$$

$$Co(v) = real\left(\frac{fft(w')^{*}\, fft(c')}{T}\right) \tag{3.3}$$

In Eq. 3.3 fft(w') and fft(c') stands for the Fourier transforms of the deviation of vertical wind and concentration from the mean over sampling period, T, (30 minutes for this study) and * stands for the complex conjugate. The cospectrum, $Co_{w'c'}(\upsilon)$, is the real part. $nCo_{w'c'}(\upsilon)$ is calculated as cospectrum multiplied by each frequency, υ, and divided by the covariance of C with w, $\sigma_{w'c'}$, at that frequency.

We show the frequency weighted normalized cospectra in both the high (>180 ppt, top panel) and low (<180 ppt, bottom panel) NO_2 regime at 17.5 m within the 12:00-15:00 time window. Black lines are $w'Ts'$, which are always positive, green lines are $nCo_{w'NO2'}$, light blue dashed lines are $nCo_{w'NO'}$, and yellow lines are $nCo_{w'O3'}$. Both positive and negative signs are observed in the cospectral density for NO_2, NO and O_3.

Generally, the shape of $nCo_{w'O3'}$ and $nCo_{w'Ts'}$ are similar to each other, although opposite in sign, with the maximum flux contribution from frequencies in the range 0.005 Hz to 0.1 Hz (200-10 second). We infer these are the dominant flux carrying eddies at this site. The sign of the cospectrum is an indication of the direction of the flux; positive indicating upward from the canopy to the atmosphere and negative from the atmosphere to the canopy.

We do not observe significant differences in the flux-carrying eddy frequencies of $nCo_{w'Ts'}$ and $nCo_{w'O3'}$ under high verses low NO_2 conditions. We do, however, see strong differences in the cospectrum of $nCo_{w'NO2'}$ and $nCo_{w'NO'}$. In the bottom panel, at low NO_2, we see upward fluxes of NO_2 for eddies slower than the frequency of 0.1 Hz (longer time scales than 10 seconds). These flux carrying eddies are not apparent at high NO_2. At first glance this is surprising as the measurement precision is better at high NO_2 and if fluxes were independent of concentration, we would expect better S/N in the higher NO_2 cospectrum. In contrast, we observe downward or weaker upward motions of NO and NO_2 under high NO_2 conditions at the same frequencies where the maximum upward flux-carrying eddies are observed at low NO_2 (0.013-0.02 Hz). The NO and NO_2 cospectra exhibit coupling at some frequencies -one is up while the other is down - especially for longer eddies that reach the forest floor or small eddies that circle above the canopy.

Providing further evidence that these differences are real and require an explanation, we observed a concentration dependence of the cospectrum at other times of day. We also found that other nitrogen oxides exhibit bidirectional features. The HNO_3 cospectrum is downward at all frequencies, while NO, NO_2, $\sum$PNs and $\sum$ANs cospectra all have bi-directional components.

3.6 Discussion

Faster V_{NO2}s are observed in lower NO_2 conditions (50-100 ppt) and V_{NO2} gradually decreases and becomes near zero in the range 300-500 ppt of NO_2 which has some parallels to leaf level studies reporting emission at low NO_2. The absence of deposition at any NO_2 makes us reluctant to label the effect a "compensation point". However, the mechanism is consistent with that idea. The daytime mean NO_2 concentration at this site is 188 ± 86 ppt (± 1σ) falling at the lower range of previously reported C_{PT}s from leaf-level studies. The C_{PT} of the ponderosa pine has not yet been measured, although the compensation points for other conifers have been studied and are in the range 0.1-3ppb (e.g. Rondon and Granat, 1994; Gessler et al., 2002; Hari et al., 2003; Raivonen et al., 2009; Chaparro-Suarez et al., 2011). The observed gradient in NO_2 is consistent with greater emission at low ambient NO_2. Moreover, there are more upward frequency features in flux carrying eddies at lower NO_2 than at high NO_2. The dependence of nV_{NO} and nV_{NO2} on nV_{CO2}, and PAR suggest there is a below canopy NO_X source that is independent of soil NO emission and the associated NO/NO_2 conversion. We hypothesize that this component of the local NO_X source is related to the shrubs and trees in the forest surrounding our observing site.

In Chapter 2, we showed from our interpretation of measured fluxes and their gradients that there are within canopy sinks of NO_X and equated these sinks to a mechanistic description of the canopy reduction factor. We show in this chapter that the presence of a canopy reduction factor does not necessarily conflict with presence of an ambient NO_2 dependent source from vegetation (Figure 3.8). Direct or indirect NO_2 emissions from plants are a potential source for within canopy NO_X in addition to soil NO. However, it is the total within canopy NO_X regardless of its source, that is removed prior to escape from the canopy by the reduction factor; shown as BVOC-NO_2 in Figure 3.8. Consequently it is difficult to directly observe NO_2 fluxes associated with NO_2 emissions by the forest. In this case, it is only the multiple lines of evidence from simultaneous flux and gradient measurements that point to emission from the biota within the forest.

3.7 Conclusions

We observed the NO_2 exchange rate dependence on NO_2 concentration using canopy scale measurements of EC fluxes and vertically resolved concentrations. Spectral analysis, the observed gradients and the fluxes suggest the existence of one or more mechanisms, which drive bi-directional NO_2 exchange as the net flux is unidirectional upward. From the comparison of the NO and NO_2 exchange rate dependence on PAR and CO_2 we speculate that processes that are directly or indirectly related to stomatal conductance affect NO_2. To our knowledge, this is the first observational study of NO_2 emission sources at the canopy scale and it is consistent with mechanisms that could cause a compensation point.

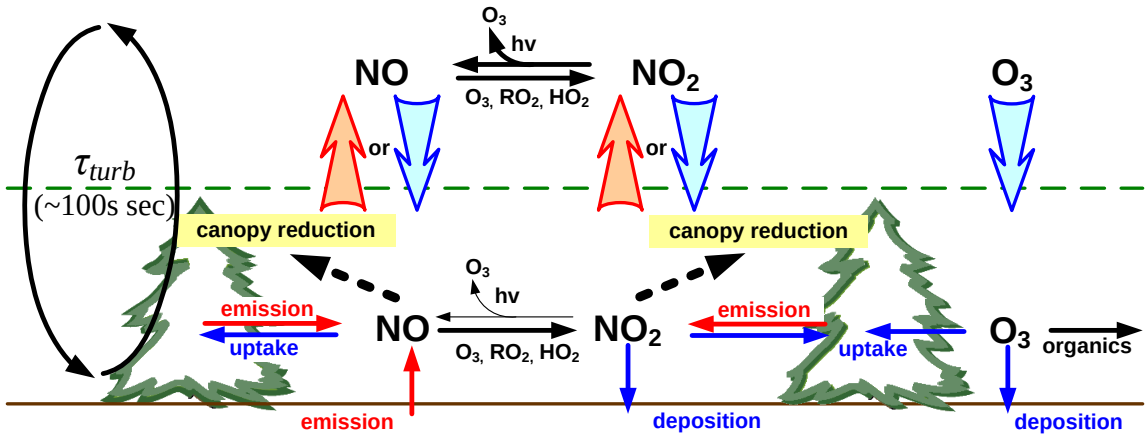

Figure 3. 1. Schematic of the atmosphere-biosphere exchanges of nitrogen oxides between. Bold arrows in blue (downward) and red (upward) represent the direction of the flux of each species across the canopy surface. Canopy reduction is in black dashed arrows within canopy.

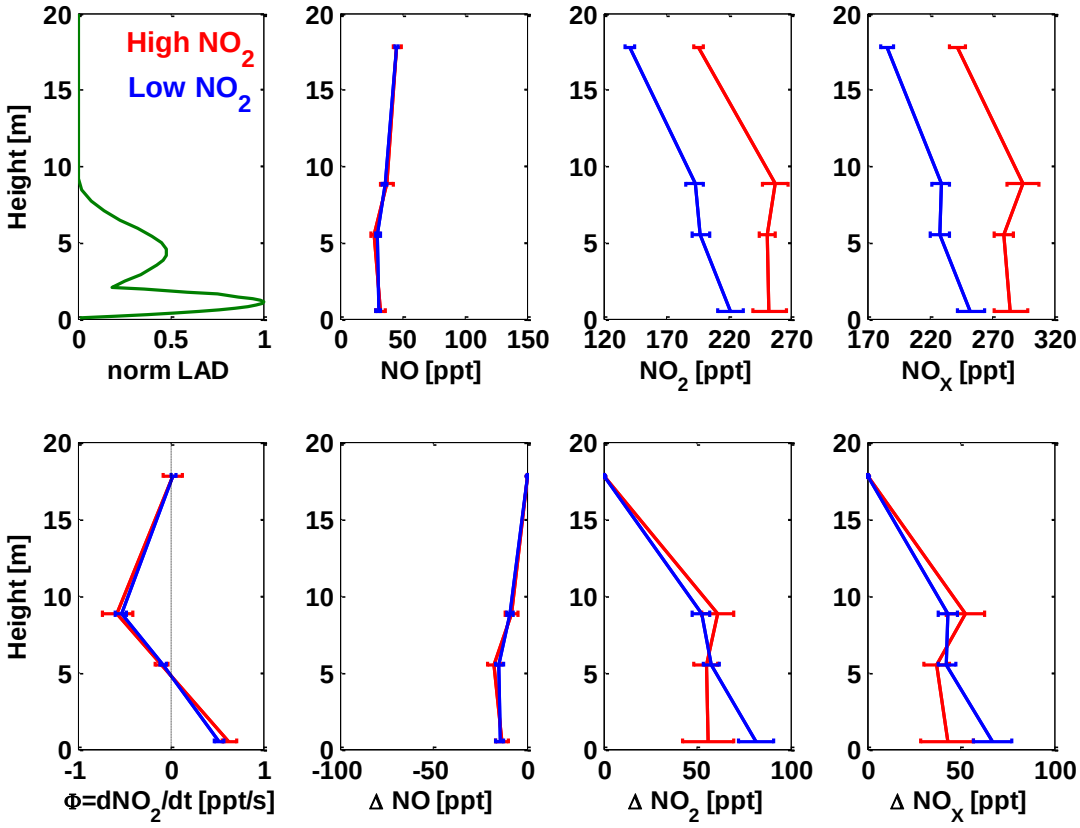

Figure 3.2. Normalized vertical gradients of NO, NO_2, and NO_X under high and low NO_2 conditions during the early afternoons (12:00-15:00) along with the normalized leaf area density (norm LAD). The horizontal bars are the 1σ variance divided by square root of number of data points and indicating the natural variability.

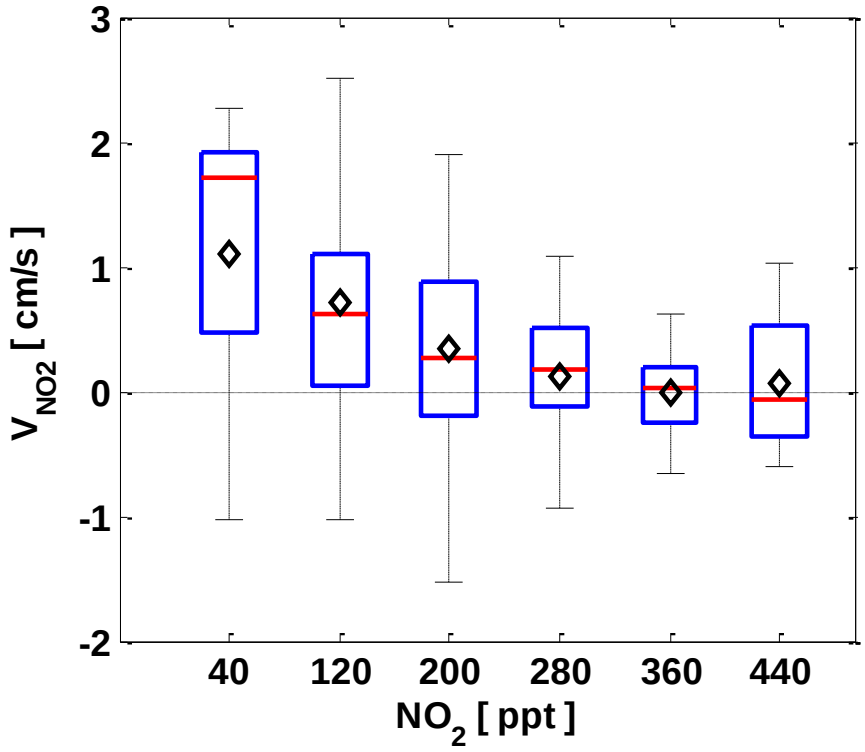

Figure 3.3. The NO_2 concentration dependence of the NO_2 exchange velocity during the daytime (9:00-18:00). The blue boxes represent the lower and upper quartile values and red lines and black diamonds indicate the median and mean V_{NO2}. Whiskers extend out to 99.3%. Bins with less than 5 points are ignored.

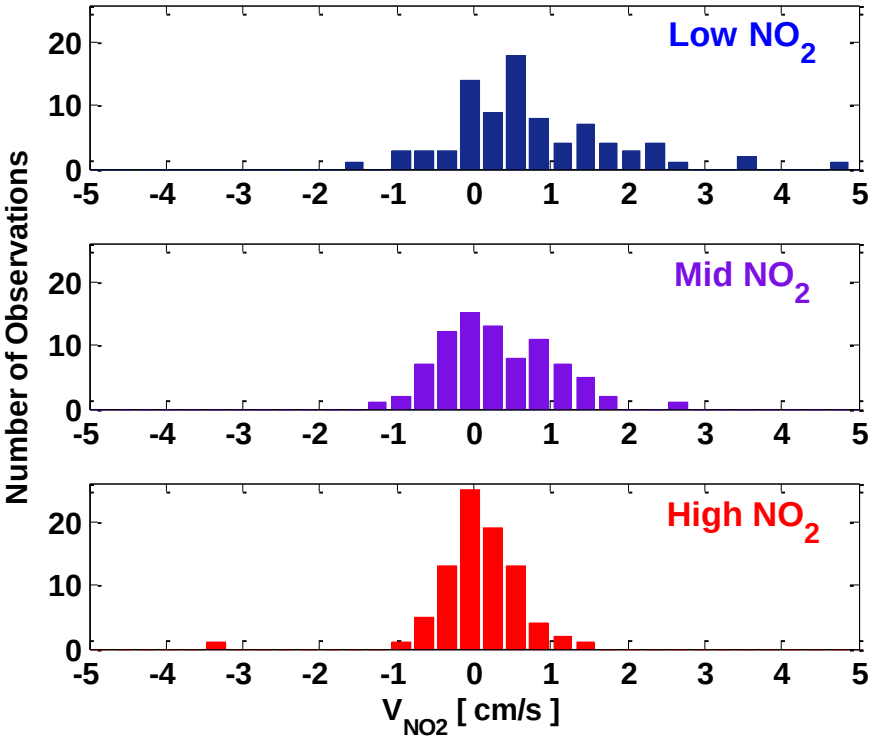

Figure 3.4. Histograms of V_{NO2} observations separated into three different NO_2 concentration regimes. Upper (blue), middle (green), and lower (red) panels represent low (<125 ppt), middle (155-190 ppt) and high (>240 ppt) above canopy NO_2 concentrations during the daytime (9:00-18:00). The low NO_2 category has 85 and the mid and high categories have 84 observations each.

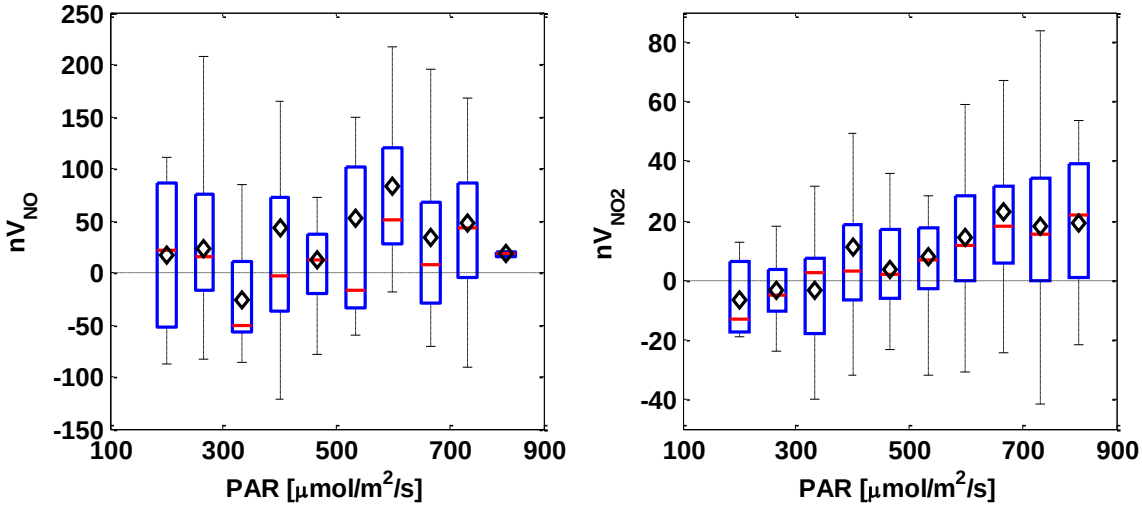

Figure 3.5. Normalized exchange velocity of NO and NO_2 vs. PAR during daytime (9:00-18:00). The blue boxes represents lower and upper quartile values and the red lines and and black diamonds indicate the median and mean nV_{NC}. Whiskers extend to 99.3%.

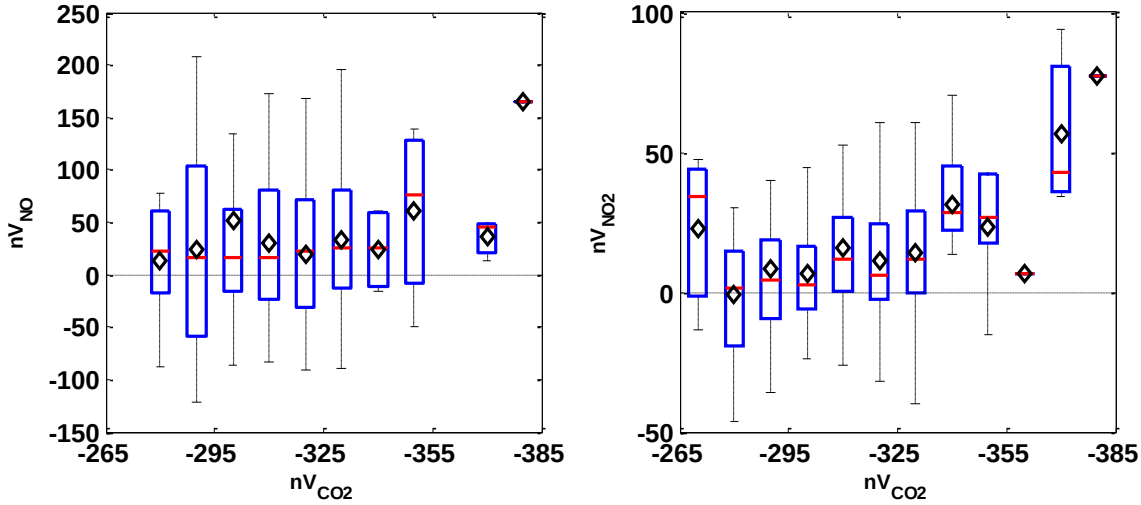

Figure 3.6. Normalized exchange velocities of NO and NO_2 vs. the normalized exchange velocities of CO_2 during the daytime (9:00-18:00). Blue boxes outline the lower and upper quartile values and the red lines and black diamonds indicate the median and mean. Whiskers extend to 99.3%. Negative sign indicate downward motion and bigger number of nV_{CO2} indicate faster uptake of CO_2.

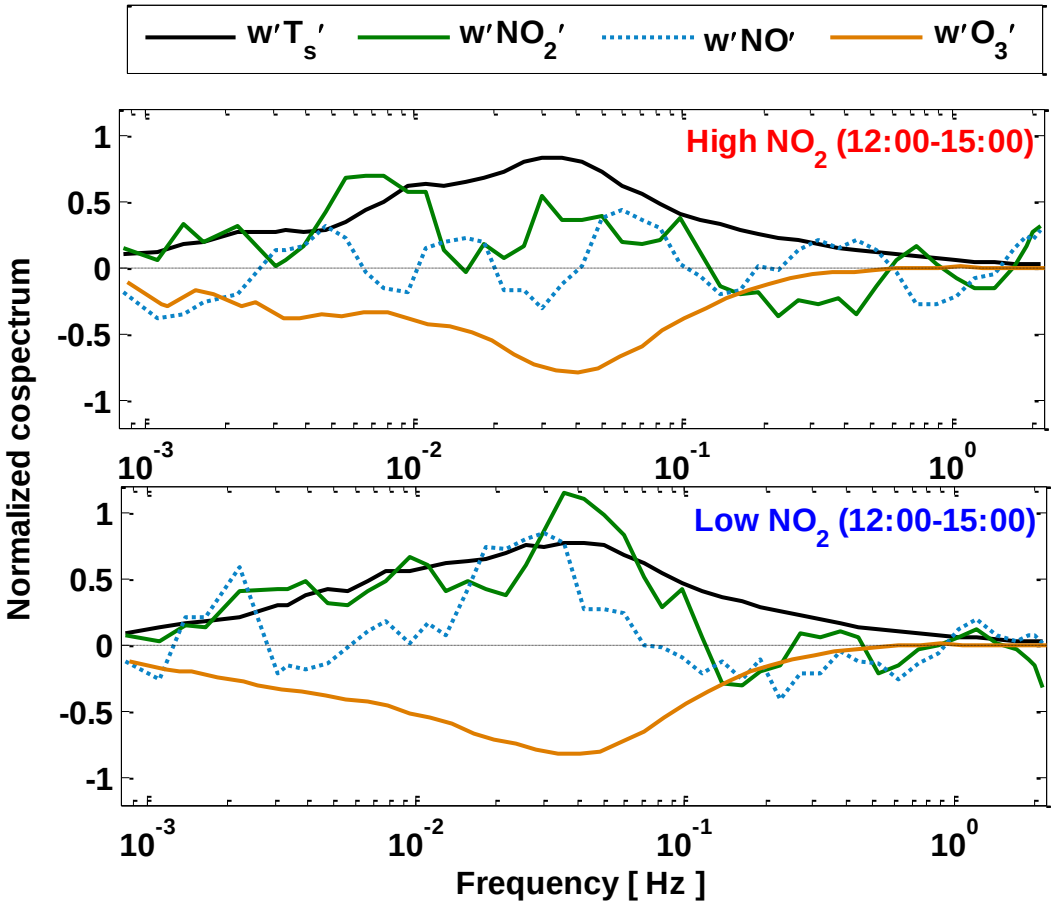

Figure 3.7. Equally spaced logarithmic averaged (100 bins) frequency weighted normalized spectra of sensible heat (w'Ts', black), NO_2, (w'NO_2', green), NO (w'NO', light blue), and O_3 (w'O_3', yellow) under high NO_2 conditions (upper panel) and low NO_2 conditions (lower panel).

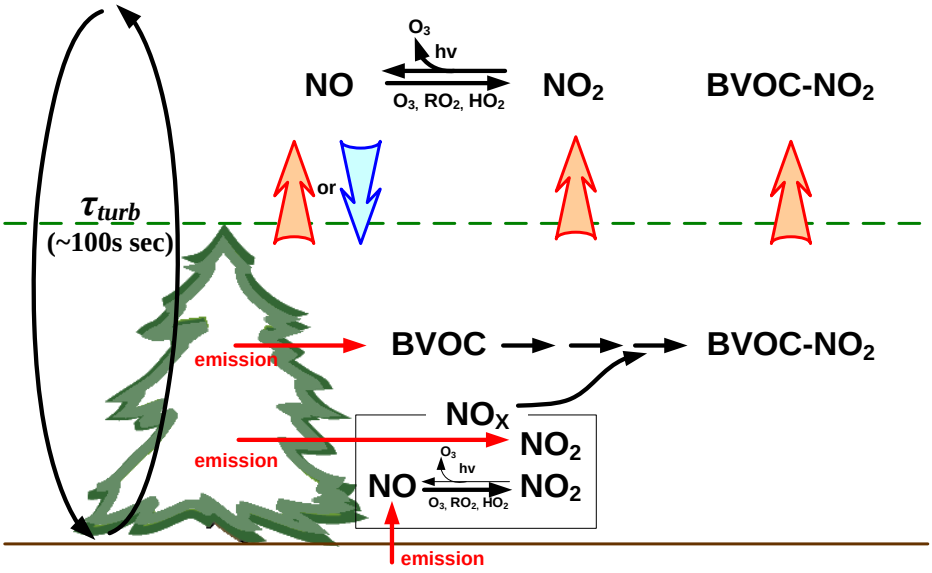

Figure 3.8. Conceptual model of NO_2 sources and sinks within the canopy and its exchange in atmosphere-biosphere interactions in low NO_2 condition. Bold arrows represent the exchanges in forest-atmosphere interphone; deposition is in blue and emissions in red. Solid red arrows indicate source processes and black arrows indicate chemical mechanisms take place.

Chapter 4

Observations of atmosphere-biosphere exchange of total and speciated peroxynitrates: nitrogen fluxes and biogenic sources of peroxynitrates

Abstract

Peroxynitrates are responsible for global scale transport of reactive nitrogen. Recent laboratory observations suggest that they may also play an important role in delivery of nutrients to plant canopies. We measured eddy covariance fluxes of total peroxynitrates (ΣPNs) and three individual peroxynitrates (APNs ≡ PAN + PPN + MPAN) over a ponderosa pine forest during the Biosphere Effects on AeRosols and Photochemistry EXperiment 2009 (BEARPEX 2009). Concentrations of these species were also measured at multiple heights above and within the canopy. While the above-canopy daytime concentrations are nearly identical for ΣPNs and APNs, we observed the downward flux of ΣPNs to be 30-60% slower than the flux of APNs. The vertical concentration gradients of ΣPNs and APNs vary with time of day and exhibit different temperature dependencies. These differences can be explained by the production of peroxynitrates other than PAN, PPN, and MPAN within the canopy (presumably as a product from oxidation of local biogenic VOC emissions) and upward fluxes of these PN species. The impact of this implied peroxynitrate flux on the interpretation of NO_X fluxes and ecosystem N exchange is discussed.

4.1. Introduction

Peroxynitrates, PNs (RO_2NO_2 ≡ acyl peroxynitrates + non-acyl peroxynitrates) represent 25% or more of the reactive nitrogen in the troposphere. PNs are thermally unstable at characteristic surface temperatures but have very long lifetimes (days to weeks) aloft. As a result, peroxynitrates are temporary reservoirs of NO_X (≡ NO + NO_2) affecting regional and global tropospheric ozone formation (Hudman et al., 2004; Zhang et al., 2008; Parrish et al., 2009; Fiore et al., 2011) by sequestering NO_X at the source and then releasing it in downwind rural and remote regions. PNs may also have a significant influence on climate via their effects on available nitrogen and thus ecosystem productivity (Bytnerowicz and Fenn, 1996; Goulding et al.,

1998; Sparks et al., 2003; Teklemariam and Sparks, 2004; Sparks, 2009) and via their phytotoxicity and thus ecosystem health (Okano et al., 1990; Goulding et al., 1998). Recent research has brought attention to new mechanisms by which peroxynitrates might participate in linking the atmospheric and biospheric N cycles (Townsend et al., 1996; Holland et al., 1997; Teklemariam and Sparks, 2004; Sparks, 2009).

Measurements at the leaf scale (Okano et al., 1990; Sparks et al., 2003) and studies assuming assume flux-gradient similarity (Doskey et al., 2004) have suggested that the direct uptake of PAN ($CH_3C(O)OONO_2$) by plants is fast and controlled by stomatal processes. Early work focused only on PAN's phototoxicity (Taylor, 1969; Ordin et al., 1971; Okano et al., 1990; Oka et al., 2004) assuming exclusively negative impacts due to foliar uptake on ecosystem health (Bytnerowicz and Fenn, 1996). In contrast, Sparks (2009) pointed out that direct foliar uptake of atmospheric reactive nitrogen to biota could be a major source of global N input to ecosystems. Teklemariam and Sparks (2004) estimated as much as 20% of regional dry deposition of N occurs via foliar uptake of PAN and that this addition could serve to enhance productivity (Teklemariam and Sparks, 2004). To the extent that stomatal processes dominate, PN deposition will occur according to spatial and temporal patterns that are different from HNO_3, as HNO_3 deposition is thought to be controlled only by turbulent transport to surfaces and, as a result, PN deposition could be an even larger percentage of the total in some locations.

New measurement techniques have enabled the use of eddy-covariance methods (Turnipseed et al., 2006; Farmer et al., 2006; Wolfe et al., 2009) providing more detailed observations of the rate of exchange of PNs between the atmosphere and biosphere. Analyses of these recent experiments indicate that a complex interplay of chemistry and turbulent exchange occurs, making it difficult to isolate direct foliar uptake, but providing information about a variety of other chemical and micrometeorological processes. All of these new experiments suggest that our current understanding of the mechanisms governing ecosystem exchange of PNs is poor. Turnipseed et al. (2006) found the deposition of PAN to be four times faster than estimated based on a resistance analogy to H_2O. Farmer et al. (2006) found that the net flux of total PNs (ΣPNs) were upward - contrary to all prior expectations. Wolfe et al. (2009) observed downward fluxes of speciated PNs, at the same site as Farmer et al. (2006) but three years later, and observed that three individual PNs each deposits at a different rate (Wolfe et al., 2009).

Building on the prior experiments by Farmer et al. (2006) and Wolfe et al. (2009), we measured fluxes and gradients of total and speciated peroxynitrates (ΣPNs and APNs, respectively) above a ponderosa pine forest during the Biosphere Effects on AeRosols and Photochemistry EXperiment 2009 (BEARPEX 2009). Our goal was to develop an observational database that could provide insights into the chemistry and ecosystem biology that affect forest-atmosphere PN exchange. These measurements provide evidence for processes that result in both the upward and downward exchange of PNs and indicate that the net is a subtle balance between these opposing processes. They also provide evidence for PN formation from one or more unidentified VOC, within the forest canopy. These molecules, hereafter denoted XPNs, are then transported to the atmosphere above.

4.2. Research Site and Instrumentation

The observations used in this work were collected at a research site located on the western slope of the Sierra Nevada Mountains from June 15 to July 31 in 2009 as a part of the BEARPEX field campaign. An overview of this experiment is found in Cohen et al. (in prep.) and in the articles included in this special issue of ACP. The BEARPEX research site was located 75km downwind of Sacramento, California at a managed ponderosa pine plantation owned by Sierra Pacific Industries and near the University of California at Berkeley Blodgett Forest Research Station (38°53'42.9"N, 120°3757.9"W, and 1315m). In the summer (May to September), wind patterns at the site are controlled by the topography and are characterized by southwesterlies (210-240°) during daytime and northeasterlies (30°) at night. More detailed descriptions of the local and regional meteorology are available elsewhere (Dillon et al., 2002; Cahill et al., 2006; Choi et al., 2011; Bianco et al., 2011). The forest at this site is dominantly Pinus ponderosa L., planted in 1990, with some Douglas fir, white fir, and incense cedar. The canopy understory is largely mountain whitethorn (Ceanothus cordulatus) and manzanita (Arcostaphylos spp.) shrubbery (up to 2m in height). The average canopy heights in 2004, 2006, and 2009 were 5.1m, 7.9m, and 8.8m, respectively and the leaf area indices (LAI) determined to be $2.1 m^2/m^2$, $3.2 m^2/m^2$ and $3.7 m^2/m^2$ by onsite surveys conducted on April 8, 2004, October 4, 2006, and July 17, 2009 (following Misson et al., 2005).

At the BEARPEX site, there were two walk up towers separated by a distance of 10m, a 15m tower (south tower) and an 18m tower (north tower). On the south tower, meteorological parameters, including temperature, relative humidity, wind speed, net radiation, photosynthetically active radiation (PAR), and chemical species (water vapor, CO_2, and O_3) were monitored at 5 heights (1.2, 3.0, 4.9, 8.75, and 12.5m). Fluxes of water vapor, CO_2 and O_3 were also measured at 12.5m. On the north tower, vertical gradients of meteorological parameters were also monitored, including temperature, relative humidity and wind speed. Chemical species observed on the north tower, or on an adjacent height adjustable lift, included NO, NO_2, HONO, ΣPNs and PAN, PPN ($CH_3CH_2C(O)OONO_2$), MPAN ($CH_3C(CH_2)C(O)OONO_2$), total alkyl nitrates (ΣANs) and several speciated ANs, HNO_3, OH, HO_2, total OH reactivity, O_3, numerous BVOCs, formaldehyde, glyoxal, methylglyoxal, and several organic peroxides. Aerosol chemical and physical properties were also measured. While some measurements were made only at the 17.5m height many others were also collected at one or more of the following heights 0.5, 2.4, 5.4, 9.2 and 13.3m. For simplicity, we refer to these measurement heights as 0.5, 2, 5, 9, 13 and 18 m in the remainder of this text. Needle temperature, soil moisture, soil temperature, and soil heat flux were also monitored. Observations are available at http://www.cchem.berkeley.edu/rccgrp.

In this study we focus on the measurements of ΣPNs, PAN, PPN, MPAN, and meteorological parameters summarized in Table 4.1. The inlets for the flux measurements used in this study shared a single sonic anemometer (Campbell Scientific CSAT3 3-D Sonic Anemometer) located 0.2m horizontal and <0.01m vertical displacement from TD-CIMs inlet and with the same 0.2 m horizontal and 0.03m vertical displacement from the TD-LIF inlet.

Thermal dissociation – laser induced fluorescence (TD-LIF) was used for the measurement of NOyi (NO_2, ΣPNs, ΣANs and HNO_3). Briefly, thermal dissociation of each of these classes of higher oxides converts them to NO_2 and a companion radical at 180°C for ΣPNs, 350°C for ΣANs, and 600°C for HNO_3 (Day et al., 2002). NO_2 is then detected by LIF (Thornton et al., 2000). Two autonomous homebuilt TD-LIF systems were deployed at BEARPEX 2009 for the simultaneous measurement of fluxes and gradients. In both systems, excitation of a 585nm rovibronic feature of NO_2 was provided by a frequency doubled Nd:YAG laser (Spectra Physics, average power of 2 W at 532 nm, 30 ns pulse length) pumping a custom-built tuneable dye laser operating at 8kHz. The fluorescence signal long of 700nm was imaged onto a red sensitive photocathode (Hamamatsu H7421-50) and gated photon counting techniques (Stanford Research Systems, SRS 400) were employed to discriminate against prompt background signals. Laboratory measurements and in-field comparisons showed the two TD-LIF instruments to have calibrations that were identical to within 3% (±2.5%, 1σ, R^2=0.92).

The APNs, PAN, PPN, and MPAN, were measured by thermal dissociation – chemical ionization mass spectrometry (TD-CIMS) with an iodide reagent ion source. A detailed instrument description, including a discussion of the specific configuration for the BEARPEX measurements, is presented in Wolfe et al. (2009). Briefly, thermally dissociated acyl peroxy (PA) radicals are reacted with iodide ion to form carboxylate anions, which are detected using a quadrupole mass spectrometer. Masses corresponding to PAN (m/z=58.7), PPN (m/z=72.7) and MPAN (m/z=84.7) were detected at 3.3Hz time resolution.

The sampling inlets for ΣPNs, as well as NO_2, ΣANs, and HNO_3, and APNs were co-located. The time sequence of the observations is shown in Figure 4.1. Fluxes from the TD-LIF system measurements were measured at 18m during the first 30 minutes from the 3rd minute to the 30th minute and the last 30 minutes from the 33rd minute to the 60th minute each hour (Figure 4.1. row a). NOyi measurements at the other heights were collected by switching between the 9, 5, and 0.5m heights sampling at each height for 2 minutes (Figure 4.1. row b).

TD-CIMS measurements had two different modes, a flux divergence mode (Figure 4.1. row c) and a normal mode (Figure 4.1. row d). During the flux divergence mode (day of year 165-183), concentrations at 18m and 13m were measured for 15 minutes each, alternating between either the first or last 30 minutes of the hour and measuring concentrations at 18, 13, 9, 5, 2 and 0.5m for 3 minutes each for the other 30 minutes of each hour. After day 183, fluxes were only monitored at 18m, from the 0th minute to the 25th minute (Figure 4.1. row d).

The data used in this study are from days after 176 when the TD-CIMS measurements were more reliable. Data affected by exhaust plumes from a nearby propane power generator (mostly at night) and the occasional wafts of car exhaust were removed prior to analysis. These spikes are defined as variations in the ΣPN or APN concentration in excess of 3 times the standard deviation of the 10-minute running mean. A few remaining spikes were identified through correlations with CO, NO, and NO_2 and removed by hand.

To ensure the time synchronous comparison of measurements by multiple instruments, 30-minute data resolution was calculated as the averaged value of the 0th to the 30th minute and from the 30th to the 60th minute at each height and is representative of the first and the last halves of

each hour. For the vertical gradients in Figure 4.6, 1-hour data resolution was achieved by averaging from the 0^{th} to 60^{th} minute.

The comparison of daytime (9:00-18:00) measurements of ΣPNs and APNs at 18m is shown in Figure 4.2. The measurements are identical to within 5%, and a least-square linear fit, forcing the intercept through zero, yields a slope of 1.02±0.026 with R^2=0.92. If we allow the intercept to vary we find a slope of 1.047±0.038 and an 8ppt intercept, however there is no improvement in the R^2. The quality of the comparison between ΣPN and APN measurements is consistent with previous studies (Wooldridge et al., 2010). It should be noted that attempts to cross-calibrate with a pure PAN source in the field were unsuccessful and that each instrument was calibrated independently with respect to a different reference gas.

4.3. EC flux calculation

Detailed procedures for flux calculations are described elsewhere for ΣPNs (Farmer et al., 2006) and APNs (Wolfe et al., 2009). Briefly, 3-D winds are rotated using the 2-step natural wind coordinate rotation, and concentrations data are de-spiked and de-trended using a 10-minute running mean. The time lag between wind and concentration signals is calculated by shifting the concentration time series relative to the winds and optimizing the covariance calculated by Eq. (4.1). Since this lag should depend only on the physical setup (particularly the inlet residence time), a single average lag was applied to all data. The eddy-covariance flux, F_c, of species c is calculated using the covariance between the vertical wind speed, w, and the mixing ratio of c by Eq. (4.1).

$$F_C = \frac{1}{n}\sum_{i=1}^{i=n}(w_i - \bar{w})(c_i - \bar{c}) = \overline{w'c'} \qquad (4.1)$$

In this study, c corresponds to ΣPNs, PAN, PPN, and MPAN, and w represents the vertical wind speed. The primes in Eq. (4.1) are the deviation from the mean, the subscripts i refer to individual fast time resolution measurements, and the bar indicates the mean of n data points over the course of a single measurement period (15 – 30 min).

Several filters were applied to the derived fluxes to assure they are accurate. To assess stationarity (e.g. whether a 30-minute flux was representative of the average surface exchange over the sampling period), each flux measurement period (~30min) was divided into 5 equal periods and the averaged flux of each subset, F_{sub}, was compared to the 30-minute total flux, F_{30min}. If the ratio F_{sub}/F_{30min} differed from unity by more than 30% then the measurement period was determined to be non-stationary and that entire half hour was removed from the dataset (Foken and Wichura, 1996). Flux data with large tilt angles (>5^o) were also rejected (Lee et al., 2004). We also applied a frictional velocity filter keeping only that data with a range of frictional velocities between 0.1m/s and 1.5m/s (Foken, 2006). After the application of all filters, 67% of daytime and 61% of nighttime data remained and were used to calculate the flux.

The flux of the sum of individual APNs, F_{APNs}, is defined as the sum of the separately calculated PAN, PPN, and MPAN fluxes. We calculated the ΣPN flux, $F_{\Sigma PNs}$, using the concentration difference between ambient (NO_2) and the 180°C (NO_2 + ΣPNs) channel. Nearly identical results are obtained if we calculated the flux of NO_2 and the flux of (NO_2 + ΣPNs) taking the difference to be the ΣPN flux.

TD-LIF systematic uncertainty (Farmer et al., 2006; Min et al., 2012b) terms in $F_{\Sigma PNs}$ estimation, include the line-locking cycle for the dye laser data acquisition scheme (<3%), sensor separation and inlet dampening (<2%), instrument response time (<8%), and the absolute concentration estimation (<15%). The random uncertainty term follows the statistics of photon-counting (<10%). Assuming all errors are uncorrelated, we calculate 17% systematic uncertainty (9% without errors from the concentration estimation) in $F_{\Sigma PNs}$ and 10% random uncertainty in half hour average $F_{\Sigma PNs}$.

Systematic and random uncertainties in F_{APNs} measured by TD-CIMS are described in Wolfe et al. (2009). Systematic terms are the sensor separation and inlet dampening (<2%), response time (<12%), and the absolute calibration of the sum of all three APNs, which is taken to be 22% using the root-mean-square of 21% for PAN and PPN and 31% for MPAN weighted by their relative abundances. The total systematic error in F_{APNs} is 25% (12% without errors from the concentration estimation). Random terms follow counting statistics and are <20% for half hour average flux measurements.

Many uncertainties are common to both techniques. The uncertainty in the measured concentration differences is constrained to be less than 5% based on the data shown in Figure 4.2 and the 4.7% slope derived from a fit allowing the intercept to vary. We believe this is a conservative estimate as the difference is 2% when the intercept is fixed at zero and allowing the intercept to vary in the fit did not reduce the R^2. Combining this 5% concentration with the 9% and 12% systematic uncertainties from other terms governing the behavior of each instrument as described above, we find the total systematic uncertainty in the difference in flux of ΣPNs and APNs (F_{XPNs}) to be 15% if we assume the three terms are uncorrelated. Variances due to precision terms decrease as the square root of number of half hour measurements and are much smaller than the observed natural variability. The natural variability dominates is shown by the vertical bars in the figures.

4.4. Results

As has been described previously, ΣPN and APN abundances at the BEARPEX site reflect advection of precursors from the city of Sacramento (~5h upwind) and from the nearer-field upwind oak belt (~3h upwind) (Dillon et al., 2002; Farmer et al., 2006; Day et al., 2009; LaFranchi et al., 2009; Wolfe et al., 2009). The concentrations of all PN species increased from noon to 18:00 (PST) and high concentrations of ΣPNs and APNs persisted past midnight (Figure 4.3). Both instruments observed similar diurnal patterns at all heights

Figure 4.4 shows the diurnal pattern of XPNs — the difference between ΣPNs and APNs (XPNs ≡ ΣPNs – APNs) at the different heights. At 18m, XPNs increase beginning at 18hrs to a concentration of approximately 100ppt and are indistinguishable from zero between 9 and 18 hrs. In contrast, near the forest floor XPNs approach 100ppt during the afternoon (15:00-18:00) when the above canopy values are at a minimum. In the middle of the canopy there is an apparent transition region. While it is theoretically possible that the ΣPNs signal could be due to N_2O_5, we expect the contribution of N_2O_5 to the XPN is negligible since the lifetime of NO_3 at this site characterized to reaction with BVOC is too short to sustain concentrations of N_2O_5 that are more than a fraction of a ppt.

The diurnal pattern in eddy covariance ΣPN and APN fluxes (Figure 4.5) are similar in shape and direction with peak downward fluxes around 15hrs. This general pattern is similar to the APN flux observations reported by Wolfe et al. (2009) using measurements 2 years earlier at this same study site. Both the APN and ΣPN measurements give fluxes that are opposite in sign to the observations of ΣPN fluxes also made at this site during summer 2004 (Farmer et al., 2006). While the sign of the two flux measurements is the same, the magnitude of ΣPN and APN fluxes are significantly different. We observe a 30-60% slower deposition rate of ΣPNs than of APNs with a maximum difference during the daytime (9:00-18:00). This is surprising given the concentrations at 18m, the height where we observed fluxes, are identical to within 2-5%.

Two pieces of information provide hints about the source of the flux difference. For convenience we define Δc to be the mixing ratio difference of species c from 18m to height i, as:

$$\Delta c = c_i - c_{18m}, \tag{4.2}$$

Positive values of Δc indicate enhancements in species c at height i relative to 18m while negative values of Δc indicate a depletion of c at height i relative to 18m. Figure 4.6 shows the vertical gradients (Δc) of ΣPNs and XPNs at five different times of day. During the daytime, ΣPNs and XPNs are larger within the canopy than above. At night, values of both observables are much lower near the forest floor than above the canopy indicating loss rates of ΣPNs or XPN are faster than the production rates. These profiles are suggestive of a daytime source of XPNs within the canopy.

A second piece of evidence indicating a within canopy source of XPNs is the temperature dependence of the XPN concentration at different heights. Figure 4.7 shows observations of the temperature dependence in the morning period (6:00-12:00), when large flux differences were observed alongside relatively shallow gradients. During this time period XPNs at 18m decrease with increasing temperature while at the forest floor (0.5m) XPNs increase with temperature. XPNs at 5m and 9m (not shown here) are intermediate between these two features. The temperature dependence of XPN at each height indicates that the production process is stronger within the canopy and that XPN loss processes dominate above the canopy. Although we chose this time interval to map directly to the time window shown in Figure 4.6, we arrive at the same conclusions if we use a narrower time window such as 6:00-9:00 or 9:00-12:00.

4.5. Discussion

We have investigated a variety of possible issues with our instrumentation finding no source of error able to explain the flux and gradient differences. This leads us to believe that there is an upward flux of one or more peroxynitrates that is or are not measured by the TD-CIMS. Other evidence supporting this suggestion is indicated by the temperature and PAR dependence of the XPN fluxes and exchange velocities, *Vex*, (Figure 4.8). We defining the flux and *Vex* of XPNs as in Eq. (4.3):

$$F_{XPNs} = F_{\Sigma PNs} - F_{APNs} \quad \text{or} \quad Vex_{XPNs} = \frac{F_{XPNs}}{[XPN]} \tag{4.3}$$

F_{XPNs} and Vex_{XPNs} are independent of canopy temperature below 20°C and then increase steeply with increasing temperature. F_{XPNs} and Vex_{XPNs} increase with PAR to 1200 μmol/m^2/s then decrease. These features are similar to previously reported behavior for BVOC emissions at this site (Lee et al., 2005; Holzinger et al., 2005; Schade and Goldstein, 2001).

We can estimate the source strength needed to produce the observed XPN flux by assuming steady-state XPN chemical production and XPN flux out of the canopy:

$$F_{XPNs} \approx F_{P-XPNs}. \tag{4.4}$$

Here, $F_{P\text{-}XPNs}$ is the net chemical production of XPNs. Other terms in the flux budget including thermochemical loss, plant uptake, and canopy storage are calculated to be more than a factor of 10 smaller and can be neglected. The flux of XPNs, during daytime (2.3±0.4 ppt m/s : mean ± 1σ divided by square root of number of data points) is then approximately the integral of chemical production within the canopy. To calculate the chemical production rate, we assume the canopy integrated chemical production of 2.3 ppt m/s occurs uniformly from the forest floor to the 18m measurement height (Eq. 4.5). The PA radical concentration needed to support the observed flux of XPNs is calculated by solving Eq. (4.5) and Eq. (4.6) for XO_2 using an average daytime concentration of NO_2 of 250ppt and a rate constant for $k_{XO2+NO2}$ of 1.1x10^{-11} cm^3/molec/sec, chosen in analogy to the rate for PAN formation at 298 K and 868 mbar (Tyndall et al., 2001):

$$F_{P-XPNs} = \int_{z0}^{z} (P_{XPNs}) dz = 2.3(\pm 0.4)\ pptm/s \tag{4.5}$$

$$P_{XPNs} = k_{xo2+NO2}[XO_2][NO_2] \tag{4.6}$$

Solving for XO_2, we find a concentration of 2.3±0.7 ppt. This is about 10% of the average daytime HO_2 observed at the site (22±11 ppt) (Mao et al., in prep). One plausible candidate for BVOC inducing XPN formation is sesquiterpene (SQT) oxidation. The observed sesquiterpene concentration within canopy at this site is approximately 85ppt during daytime. Using *β*-caryophyllene as an example, the OH and O_3 reaction rate constants are 1.97×10^{-11}

cm^3/molec/sec and 1.16×10^{-14} cm^3/molec/sec, respectively (Shu and Atkinson, 1994; Shu and Atkinson, 1995). The typical concentrations of OH and O_3 within the canopy during BEARPEX 2009 were 0.16ppt and 54ppb. For a 100-second canopy mixing timescale (Wolfe et al., 2009), we calculate 198ppt of oxygenated BVOC (oBVOC) produced during SQT oxidation within the canopy. The source of XO_2 can be estimated considering the reaction of this oBVOC with OH radical, Eq. (4.7).

$$\frac{d(XO_2)}{dt} = k_{oBVOC+OH}[oBVOC][OH] \tag{4.7}$$

Solving for the rate constant to form an XO_2 radical using this estimate of oBVOC and the observed OH we find a rate constant of 2.3×10^{-11} cm^3/molec/sec which is in the range of typical rate constants for the reaction of OH with aldehydes, confirming the plausibility of a sesquiterpene source of XPNs.

In addition to the reasonable value for the inferred rate constant there is laboratory and computational evidence supporting the idea that BVOC emitted by forest canopies can result in upward fluxes of PNs. For example, in a recent chamber study PNs built on a more complex organic framework than the three APNs observed in our study were observed during *β*-caryophyllene ozonolysis (Jenkin et al., 2012). Several other studies have discussed production of PNs built on a larger carbon backbone, including *α*-pinene (Noziere and Barnes, 1998), *d*-limonene (Leungsakul et al., 2005) and nonanal (Bowman et al., 2003) derived PNs. Using a canopy box model, Wolfe et al (2011) found upward fluxes of an PN derived from 2-methyl-3-buten-2-ol oxidation. This molecule is not likely the source or our upward flux as the chemical mechanism has been revised and that particular product is not formed (Carrasco et al., 2006), however the calculations show that products form and are transported out of the canopy on the relevant time scales.

4.6. Implications of XPNs formation

The formation of XPNs within the canopy suggests a complex array of effects on PN fluxes and, more broadly, on the biosphere-atmosphere exchange of reactive nitrogen. The first consequence is that the sign of the total PN flux depends on the relative magnitude of the upward flux of XPN and downward fluxes of PAN, PPN and MPAN. This offers one possible explanation for the upward ΣPN flux previously observed at this site (Farmer et al., 2006). If this is the case, in the Farmer et al., measurements, the upward flux of XPNs was a consequence of vegetation acting as a source of PN precursors rather than, as is often assumed, a sink through stomatal uptake. Explaining both data sets requires the biogenic source of PN precursors at the BEARPEX site to have decreased over the last decade.

A second implication is the possible role of XPNs in explaining poorly understood canopy reduction factors for soil NO_X emissions. XPN formation affects the total N flux, as upward

fluxes of XPNs function to transfer within canopy NO_2 to the ΣPN pool. XPN formation is a plausible within canopy NO_X loss process and is consistent with the long standing discussion about missing NO_X sinks within canopies, which are parameterized as a canopy reduction factors and widely invoked in global models. These models otherwise find the strength of soil NO_X emissions lead to dramatic overestimates of O_3 (e.g. Jacob and Wofsy, 1990). Deposition to vegetation is the most studied NO_X sink process. However, the role of vegetation with respect to the NO_X flux is still controversial (Lerdau et al., 2000). Here, we suggest that XPN formation is one possible mechanism of NO_X loss within the canopy.

4.7. Conclusions

We observed a significant (30-60%) difference between the deposition rate of ΣPNs, and that of the sum of three speciated PNs. The difference in these fluxes suggests formation within the canopy of PNs other than PAN, PPN and MPAN. The time of day and temperature dependence of the vertical gradient of XPNs also supports this idea. We show the flux of XPN must be upward, indicating the possibility that local vegetation acts as a source of PN rather than as a passive PN sink, a mechanism that can explain the upward ΣPN flux reported by Farmer et al. (2006). In this mechanism, oxidation of biogenic VOC may affect not only the magnitude of PN fluxes but also NO_X fluxes supporting the ideas of a the strong connection between turbulent transport and chemical processes in biosphere-atmosphere exchange, as proposed by Wolfe et al. (2009 and 2011) and Farmer et al. (2006) and offering at least a partial explanation for canopy reduction factors.

Table 4.1. Vertical placement of measurements used in this study on north tower.

Height[m]	Met Data	NOyi (TD-LIF)	APNs (CIMS)
18 (17.5)	T, RH	NO_2, ΣPNs, ΣANs, HNO_3	PAN, PPN, MPAN
13 (13.3)	T, RH	—	PAN, PPN, MPAN
9 (8.8)	T, RH	NO_2, ΣPNs, ΣANs	PAN, PPN, MPAN
5 (5.4)	T, RH	NO_2, ΣPNs, ΣANs	PAN, PPN, MPAN
2 (2.4)	T, RH	—	PAN, PPN, MPAN
0.5 (0.5)	NA/	NO_2, ΣPNs, ΣANs	PAN, PPN, MPAN

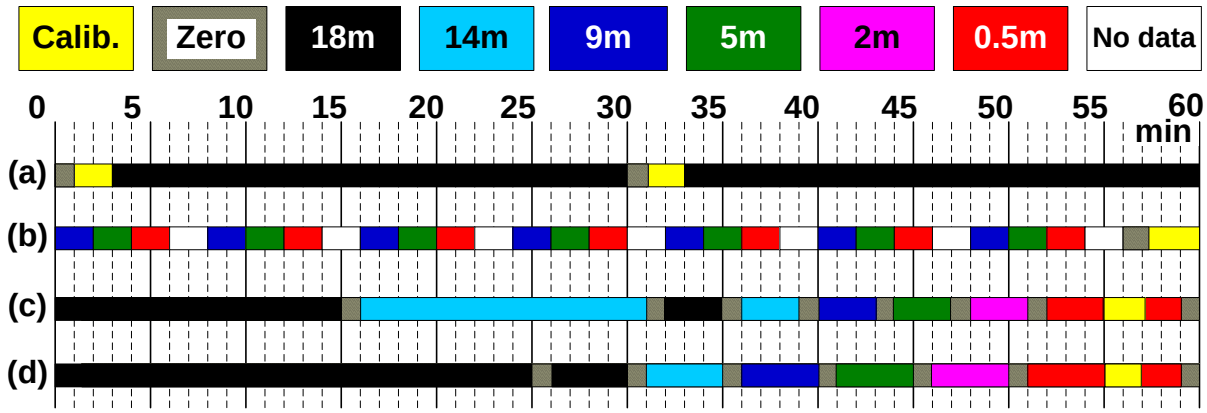

Figure 4.1. Colors represent difference measurement heights of 18m (black), 14m (light blue), 9m (blue), 5m (green), 2m (magenta) and 0.5m (red). Yellow and shaded periods are calibration and zero cycles and white periods represent no data collected at that time. (a) Flux measurement of ΣPNs, (b) vertical gradient measurements from ΣPNs, (c) APNs measurement over the flux-divergence mode, (d) same as (c) but over the normal mode.

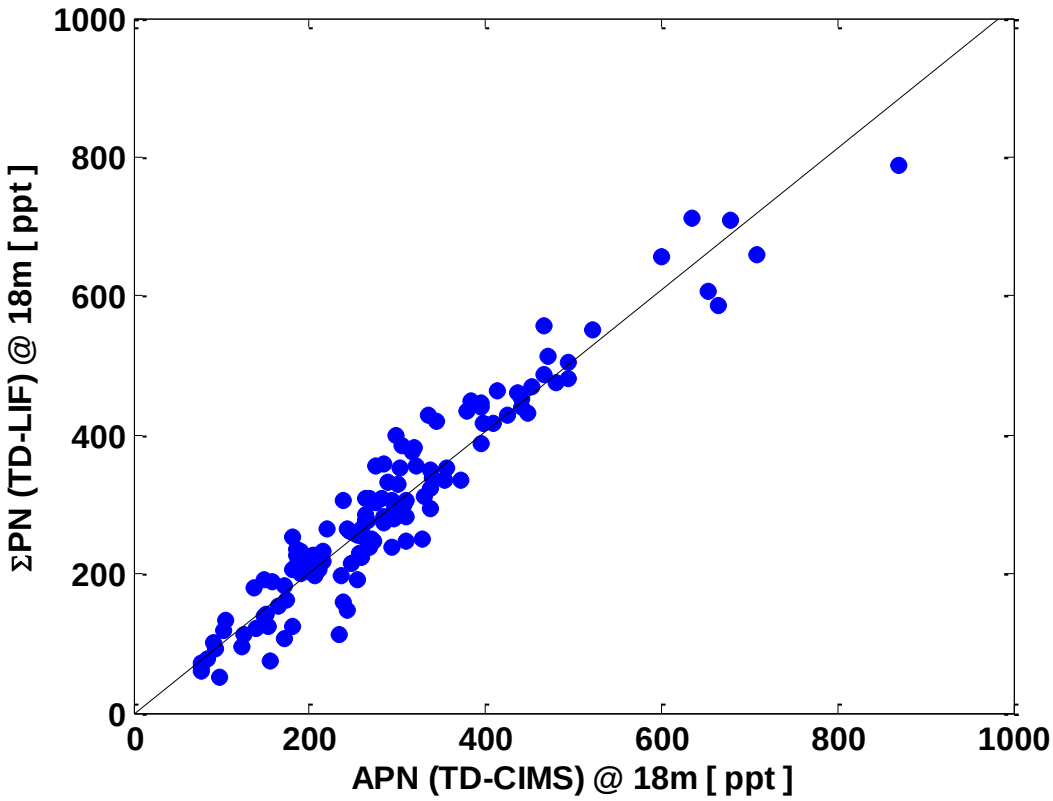

Figure 4.2. Comparison of TD-LIF ΣPNs and TD-CIMS APNs measurements from 9:00 to 18:00 hrs PST (blue circles). The slope of the line fitted line (black) is 1.02 with the intercept fixed at 0 (R^2=0.92).

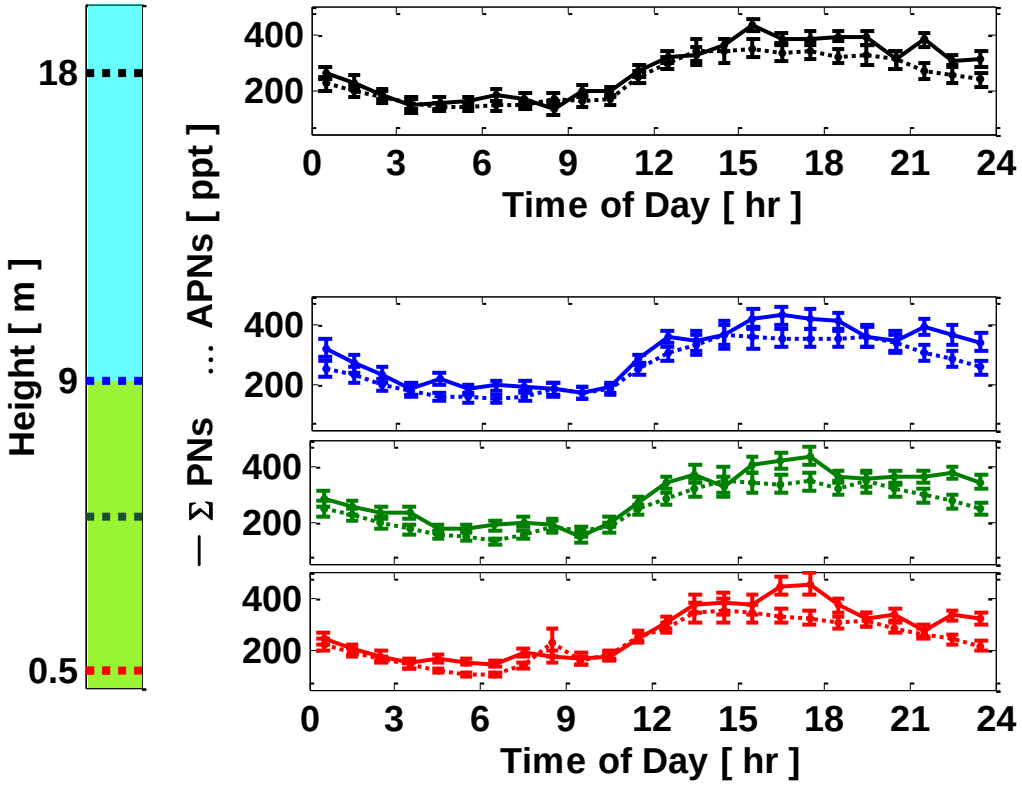

Figure 4.3. Diurnal patterns of ΣPNs (solid lines) and APNs (dashed lines) at each height. The vertical bars are the 1σ variance divided by square root of number of data points. The left box indicates the measurement height, with green at or below the 9 m average canopy height and blue above that point. Dashed lines are the specific measurement heights.

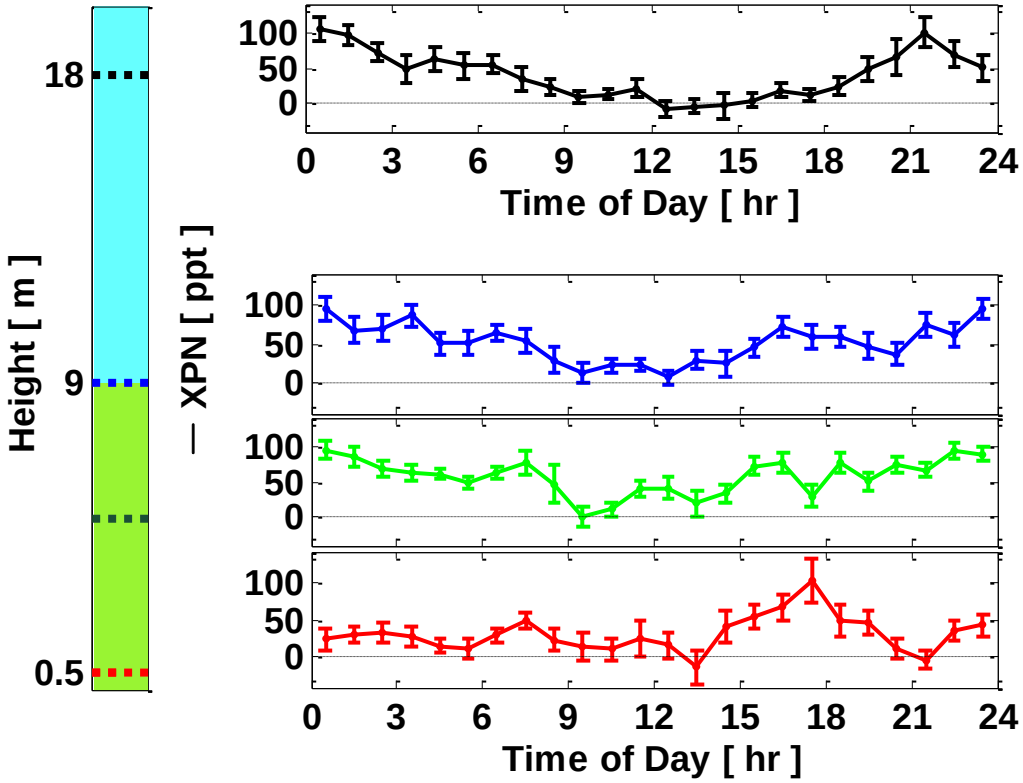

Figure 4.4. Diurnal pattern of XPNs at different heights. The vertical bars represent the 1σ variance divided by square root of number of data points in the observations. The left box indicates the measurement height, with green at or below the 9 m average canopy height and blue above that point. Dashed lines are the specific measurement heights.

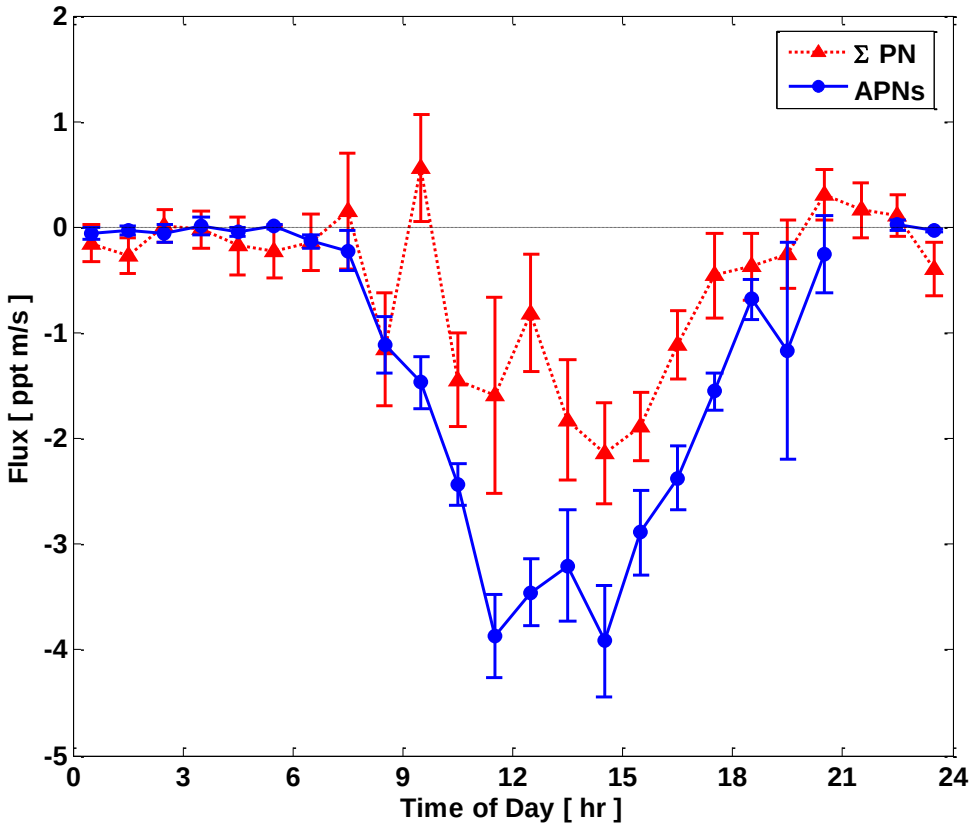

Figure 4.5. Diurnal pattern of $F_{\Sigma PNs}$ and F_{APNs}. The vertical bars are the 1σ variance divided by square root of number of data points. Both species exhibit a downward flux, indicating the dominance of in-canopy sinks, though PNs 30-60% less negative than F_{APNs} during daytime.

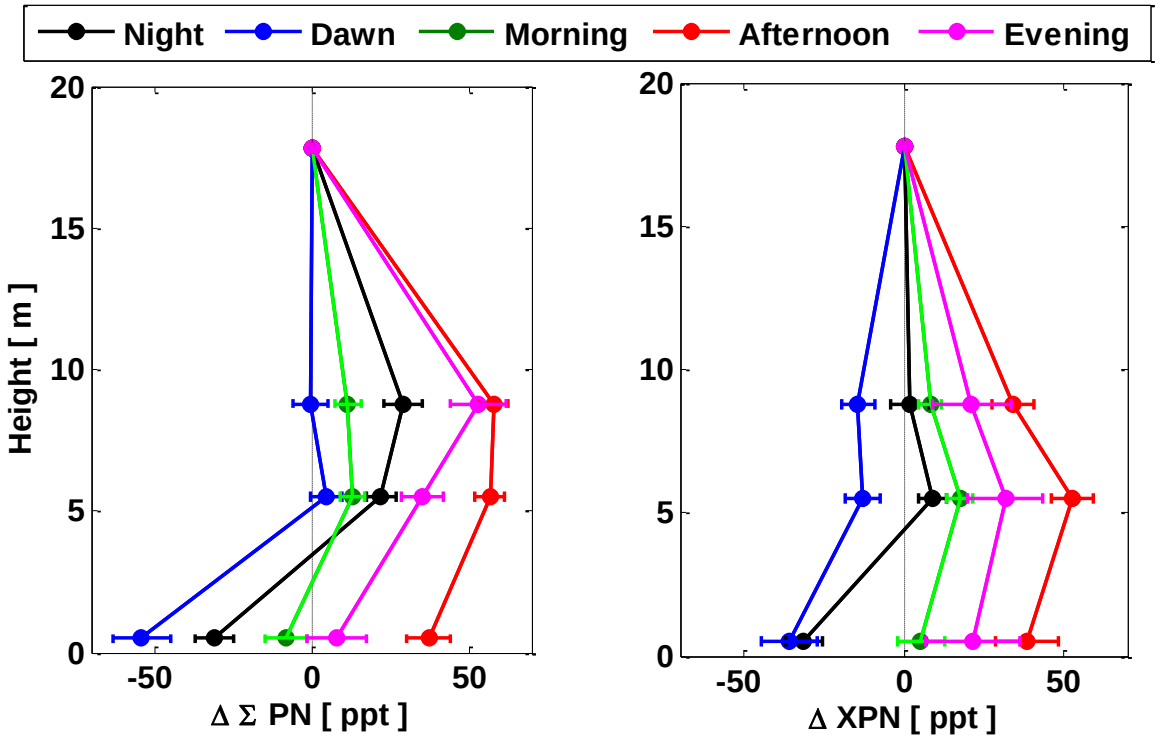

Figure 4.6. Diurnal pattern of vertical mixing ratio differences of ΣPNs (left) and XPNs (right) with respect to the 18m mixing ratios. The horizontal bars are the 1σ variance divided by square root of number of data points. Positive values of ΔΣPN and ΔXPN indicate enhanced concentrations and negative values represent depleted concentration compared to 18m. Colors represent the time of day black (21:00-3:00), blue (3:00-6:00), green (6:00-12:00), red (12:00-18:00) and magenta (18:00-21:00).

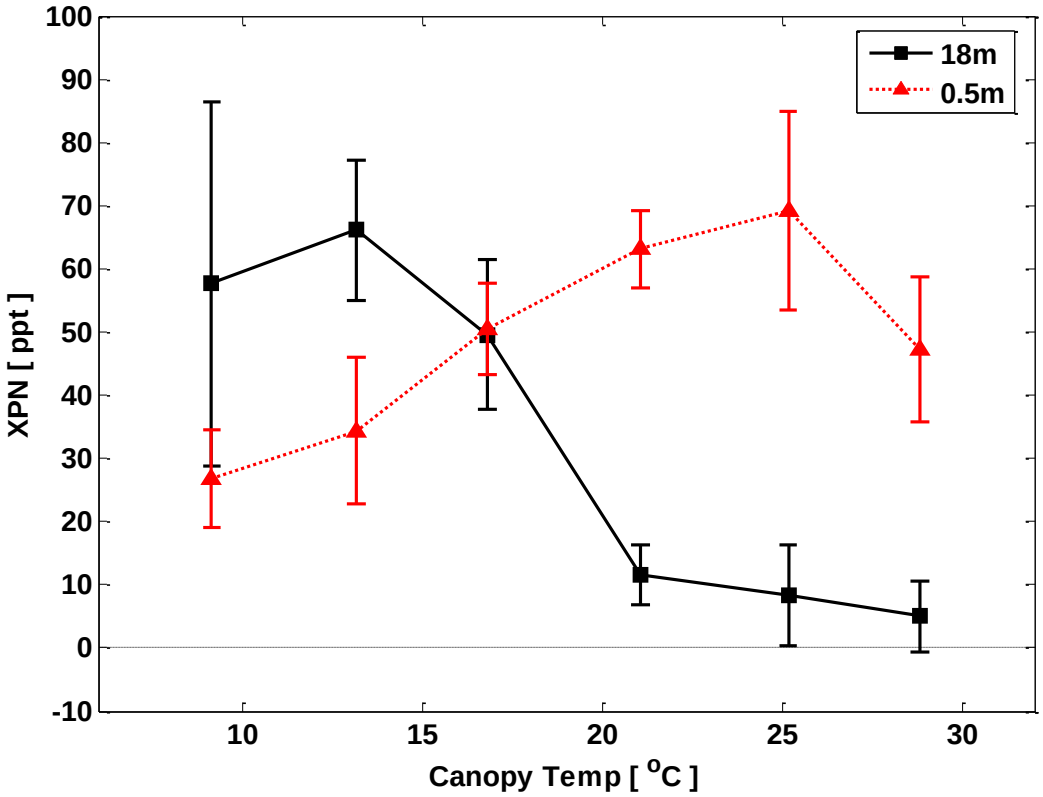

Figure 4.7. Temperature dependence of XPNs at 0.5 and 18m during mornings (6:00-12:00). The vertical bars represent the 1σ variance divided by square root of number of data points.

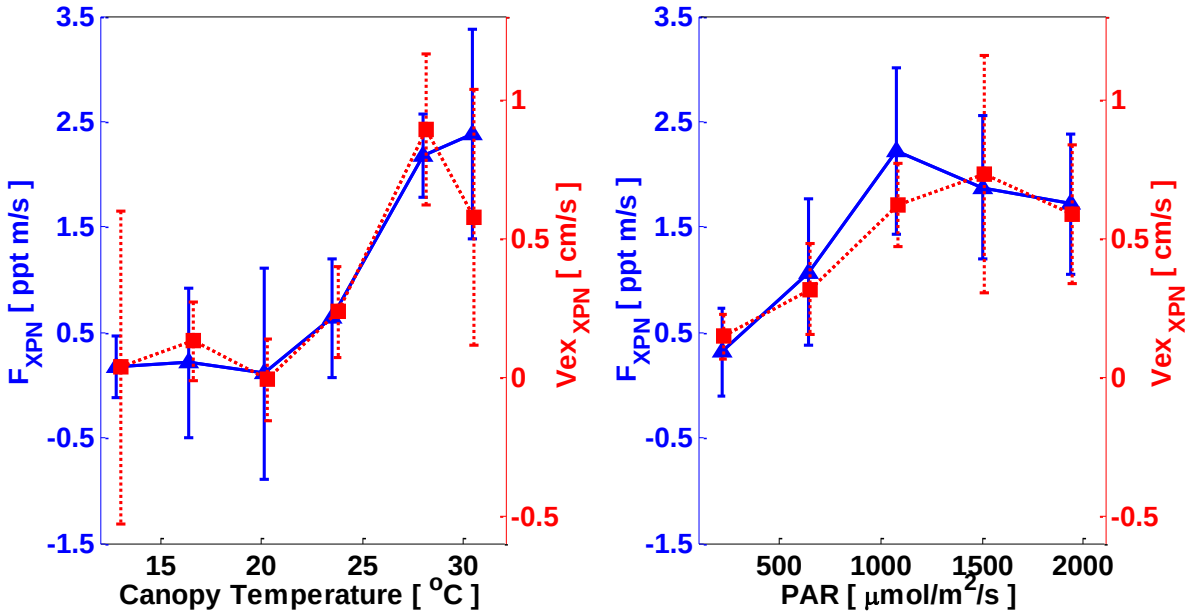

Figure 4.8. Canopy temperature (left) and PAR (right) dependence of F_{XPNs} and Vex_{XPNs}. The vertical bars are the 1σ variance divided by square root of number of data points.

Chapter 5

Conclusion

5.1 Summary of this work

The study of biosphere-atmosphere exchanges requires an interdisciplinary approach: air masses within the canopy are affected by plant biota and the escaping efficiencies of molecules from the canopy to the atmosphere are determined by both micrometeorological factors and chemical reactions of molecules taking place during vertical transport. For a comprehensive understanding, we must integrate knowledge from forestry, micrometeorology, and atmospheric chemistry, especially when we consider reactive species.

In this dissertation, I focused on the exchange of reactive nitrogen oxides, NO_y, specifically NO, NO_2, RO_2NO_2, $RONO_2$, and HNO_3. By merging the eddy covariance method and state of the art measurement techniques for NO_y species, I directly measured the exchange rates and magnitudes along with vertically resolved abundances as a part of the collaborative Biosphere Effects on AeRosols and Photochemistry EXperiment (BEARPEX). The findings described in the previous chapters are summarized below.

In Chapter 2, I described observational evidence for removal of NO_x within a canopy. Canopy reduction factors are currently used as non-mechanistic parameters invoked in models to reconcile the gap between observed soil NO emissions and modeled O_3 concentrations in remote regions. Typically 25-80% of the NO emissions are removed within a canopy before transport into the boundary layer where they would contribute to the formation of O_3 (Jacob and Wofsy, 1990; Yienger and Levy, 1995; Wang and Leuning, 1998). Smaller fluxes of NO_X than are expected based on the vertical gradients I measured during BEARPEX 2009 indicate that there is a removal process within the canopy. Multiple mechanisms were considered and formation of higher oxides of nitrogen was shown to be an important (perhaps sole) mechanism for canopy reduction of NO_x.

In Chapter 3, I showed that even as the canopy is removing NOx the exchange rate of NO_2 is inversely correlated with NO_2 concentration—in other words there are processes akin to an NO_2 compensation point.

In Chapter 4, I examined the fluxes of some of the higher oxides of nitrogen—total peroxynitrates. I found that the total flux was smaller than the sum of fluxes for the 3 most abundant peroxy nitrates. Analysis suggests that a small concentration of a peroxynitrate derived

from BVOC is produced within the canopy and that upward flux of this species is responsible for the differences observed.

5.2 Recommendations for future work

From the research summarized above, I am able to augment our understanding of how reactive chemistry impacts the vertical movement of molecules out of a forest canopy to the boundary layer above. These results and conclusions raise new questions for the further investigation and I list some of these questions below:

1) What chemical form of PNs and ANs are responsible for NO_X loss within the canopy? To explore this question, mechanistic studies of the conversion of larger carbon backbone compounds to higher nitrogen oxides are recommended. There are a few previous laboratories studies that suggest this possibility (Noziere and Barnes, 1998; Bowman et al., 2003; Leungsakul et al., 2005; Jenkin et al., 2012). Attempts to understand the detailed kinetic mechanisms in laboratories along with monitoring corresponding molecules in ambient air are recommended.

2) What mechanism(s) drive(s) the NO_2 compensation point? Is the compensational behavior observed at the canopy scale directly controlled by plant metabolic processes or by a process external to plant function? Branch enclosure tests with high performance instruments with simultaneous measurements of a complete set of NO_y species spanning the NO_2 concentration from 0 to 3ppb are highly recommended. Previous branch enclosure studies have not attempted to thoroughly investigate at concentrations below 1 ppb because of their instrumental limitations (Chaparro-Suarez et al., 2011 and references therein). Canopy modeling studies taking into account both compensational behavior of plants and complex chemistry are also recommended to investigate the vegetation impact on tropospheric chemistry.

3) Expand the interpretation of cospectra for reactive species to the formation of the higher nitrogen oxides and O_3. During BEARPEX 2009, I saw upward eddies at some frequencies for PNs, ANs, HNO_3, and O_3 even though their net fluxes were all downward. Can this analysis be used to better understand the existence of active within canopy chemistry? The cospectral analysis of reactive species will further link the fields of micrometeorology and atmospheric chemistry. Can we convert the observed frequencies to length information so as to spatially locate sources?

4) What are the regional and global impacts of within canopy NO_X to NO_Z conversion? Prior to this work, most PNs and HNO_3 were thought to be formed during transport from urban areas and then deposited to remote regions; however, along with previous observations of upward fluxes of PNs and HNO_3 (Farmer et al., 2006) and the XPN work described in chapter 4, there is evidence that NO_X's influence extends further downwind than conventionally thought by slowing the PN and HNO_3 deposition rate or even through upward fluxes from the forest to the atmosphere.

5) How are carbon and nitrogen coupled on regional and global scales? Traditionally, carbon and nitrogen coupling is thought to be limited to the CO_2 fertilization effect. How for example, might XPN change our understanding of the CO_2 fertilization effect though its influence on BVOC fluxes? The carbon balance needs to be taken into account for BVOCs and CO_2, where NO_X may perturb the BVOCs exchange. Further developing our understanding of carbon and nitrogen cycling through, particularly, observational approaches may help us better predict the impacts of climate change.

References

Anderson, I. C., and Poth, M. A.: Semiannual losses of nitrogen as NO and N_2O from unburned and burned chaparral, Global Biogeochem, 3, 121-135, 1989.

Baldocchi, D. D., Hicks, B. B., and Meyers, T. P.: Measuring Biosphere-Atmosphere Exchanges of Biologically Related Gases with Micrometeorological Methods, Ecology, 69, 1331-1340, 1988.

Beine, H. J., Honrath, R. E., Domine, F., Simpson, W. R., and Fuentes, J. D.: NO_X during background and ozone depletion periods at Alert: Fluxes above the snow surface, J Geophys Res-Atmos, 107, Artn 4584, doi:10.1029/2002jd002082, 2002.

Bianco, L., Djalalova, I. V., King, C. W., and Wilczak, J. M.: Diurnal Evolution and Annual Variability of Boundary-Layer Height and Its Correlation to Other Meteorological Variables in California's Central Valley, Bound.-Lay. Meteorol., 140, 491-511, doi:10.1007/s10546-011-9622-4, 2011.

Bouvier-Brown, N. C., Goldstein, A. H., Gilman, J. B., Kuster, W. C., and de Gouw, J. A.: In-situ ambient quantification of monoterpenes, sesquiterpenes, and related oxygenated compounds during BEARPEX 2007: implications for gas- and particle-phase chemistry, Atmos Chem Phys, 9, 5505-5518, 2009a.

Bouvier-Brown, N. C., Holzinger, R., Palitzsch, K., and Goldstein, A. H.: Large emissions of sesquiterpenes and methyl chavicol quantified from branch enclosure measurements, Atmos Environ, 43, 389-401, doi:10.1016/j.atmosenv.2008.08.039, 2009b.

Bowman, J. H., Barket, D. J., and Shepson, P. B.: Atmospheric chemistry of nonanal, Environ Sci Technol, 37, 2218-2225, doi:10.1021/Es026220p, 2003.

Breuninger, C., Oswald, R., Kesselmeier, J., and Meixner, F. X.: The dynamic chamber method: trace gas exchange fluxes (NO, NO_2, O_3) between plants and the atmosphere in the laboratory and in the field, Atmos. Chem. Phys. Discuss., 4, 5183-5274, 2011.

Butterbach-Bahl, K., Breuer, L., Gasche, R., Willibald, G., and Papen, H.: Exchange of trace gases between soils and the atmosphere in Scots pine forest ecosystems of the northeastern German lowlands 1. Fluxes of N_2O, NO/NO_2 and CH_4 at forest sites with different N-deposition, Forest Ecol Manag, 167, 123-134, 2002.

Bytnerowicz, A., and Fenn, M. E.: Nitrogen deposition in California forests: A review, Environ. Pollut., 92, 127-146, 1996.

Cahill, T. M., Seaman, V. Y., Charles, M. J., Holzinger, R., and Goldstein, A. H.: Secondary organic aerosols formed from oxidation of biogenic volatile organic compounds in the Sierra Nevada Mountains of California, J. Geophys. Res., 111, doi:10.1029/2006jd007178, 2006.

Carrasco, N., Doussin, J. F., Picquet-Varrault, B., and Carlier, P.: Tropospheric degradation of 2-hydroxy-2-methylpropanal, a photo-oxidation product of 2-methyl-3-buten-2-ol: Kinetic and mechanistic study of its photolysis and its reaction with OH radicals, Atmos. Environ., 40, 2011-2019,

Chaparro-Suarez, I. G., Meixner, F. X., and Kesselmeier, J.: Nitrogen dioxide (NO_2) uptake by vegetation controlled by atmospheric concentrations and plant stomatal aperture, Atmos Environ, 45, 5742-5750, doi:10.1016/j.atmosenv.2011.07.021, 2011.

Chen, X. Y., Mulder, J., Wang, Y. H., Zhao, D. W., and Xiang, R. J.: Atmospheric deposition, mineralization and leaching of nitrogen in subtropical forested catchments, South China, Environ Geochem Hlth, 26, 179-186, 2004.

Choi, W., Faloona, I. C., McKay, M., Goldstein, A. H., and Baker, B.: Estimating the atmospheric boundary layer height over sloped, forested terrain from surface spectral analysis during BEARPEX, Atmos Chem Phys, 11, 6837-6853, doi:10.5194/acp-11-6837-2011, 2011.

Cleary, P. A., Wooldridge, P. J., and Cohen, R. C.: Laser-induced fluorescence detection of atmospheric NO_2 with a commercial diode laser and a supersonic expansion, Appl Optics, 41, 6950-6956, 2002.

Cohen, R. C., Goldstein, A. H., and the BERPEX Science team: The Biosphere Effects on Aerosol and Photochemistry EXperiment (BEARPEX), Atmos. Chem. Phys. Discuss., in preparation, 2012.

Conrad, R.: Soil microorganisms as controllers of atmospheric trace gases (H_2, CO, CH_4, OCS, N_2O, and NO), Microbiol Rev, 60, 609-+, 1996.

Davidson, E. A., Matson, P. A., Vitousek, P. M., Riley, R., Dunkin, K., Garciamendez, G., and Maass, J. M.: Processes Regulating Soil Emissions of NO and N_2O in a Seasonally Dry Tropical Forest, Ecology, 74, 130-139, 1993.

Day, D. A., Wooldridge, P. J., Dillon, M. B., Thornton, J. A., and Cohen, R. C.: A thermal dissociation laser-induced fluorescence instrument for in situ detection of NO_2, peroxy nitrates, alkyl nitrates, and HNO_3, J. Geophys. Res., 107, doi:10.1029/2001jd000779, 2002.

Day, D. A., Dillon, M. B., Wooldridge, P. J., Thornton, J. A., Rosen, R. S., Wood, E. C., and Cohen, R. C.: On alkyl nitrates, O_3, and the "missing NOy", J Geophys Res-Atmos, 108, Artn 4501, doi:10.1029/2003jd003685, 2003.

Day, D. A., Farmer, D. K., Goldstein, A. H., Wooldridge, P. J., Minejima, C., and Cohen, R. C.: Observations of NO_X, ΣPNs, ΣANs, and HNO_3 at a Rural Site in the California Sierra Nevada Mountains: summertime diurnal cycles, Atmos. Chem. Phys., 9, 4879-4896, 2009.

Delon, C., Serca, D., Boissard, C., Dupont, R., Dutot, A., Laville, P., De Rosnay, P., and Delmas, R.: Soil NO emissions modelling using artificial neural network, Tellus B, 59, 502-513, doi:10.1111/j.1600-0889.2007.00254.x, 2007.

Dillon, M. B., Lamanna, M. S., Schade, G. W., Goldstein, A. H., and Cohen, R. C.: Chemical evolution of the Sacramento urban plume: Transport and oxidation, J Geophys Res-Atmos, 107, Artn 4045, doi:10.1029/2001jd000969, 2002.

Doskey, P. V., Kotamarthi, V. R., Fukui, Y., Cook, D. R., Breitbeil, F. W., and Wesely, M. L.: Air-surface exchange of peroxyacetyl nitrate at a grassland site, J. Geophys. Res., 109, doi:10.1029/2004jd004533, 2004.

Drummond, J. W., Volz, A., and Ehhalt, D. H.: An Optimized Chemi-Luminescence Detector for Tropospheric No Measurements, J Atmos Chem, 2, 287-306, 1985.

Eller, A. S. D., and Sparks, J. P.: Predicting leaf-level fluxes of O_3 and NO_2: the relative roles of diffusion and biochemical processes, Plant Cell Environ, 29, 1742-1750, doi:10.1111/j.1365-3040.2006.01546x, 2006.

Ewert, F., and Porter, J. R.: Ozone effects on wheat in relation to CO_2: modelling short-term and long-term responses of leaf photosynthesis and leaf duration, Global Change Biol, 6, 735-750, 2000.

Fang, S. X., and Mu, Y. J.: Air/surface exchange of nitric oxide between two typical vegetable lands and the atmosphere in the Yangtze Delta, China, Atmos Environ, 40, 6329-6337, doi:10.1016/j.atmosenv.2006.05.041, 2006.

Farmer, D. K., Wooldridge, P. J., and Cohen, R. C.: Application of thermal-dissociation laser induced fluorescence (TD-LIF) to measurement of HNO_3, ΣANs, ΣPNs, and NO_2 fluxes using eddy covariance, Atmos Chem Phys, 6, 3471-3486, 2006.

Fiore, A. M., Levy, H., and Jaffe, D. A.: North American isoprene influence on intercontinental ozone pollution, Atmos. Chem. Phys., 11, 1697-1710, doi:10.5194/acp-11-1697-2011, 2011.

Foken, T., and Wichura, B.: Tools for quality assessment of surface-based flux measurements, Agr Forest Meteorol, 78, 83-105, 1996.

Foken, T.: Micrometeorology, Springer-Verlag, Berlin Heidelberg, Germany, 2006.

Galloway, J. N., Dentener, F. J., Capone, D. G., Boyer, E. W., Howarth, R. W., Seitzinger, S. P., Asner, G. P., Cleveland, C. C., Green, P. A., Holland, E. A., Karl, D. M., Michaels, A. F., Porter, J. H., Townsend, A. R., and Vorosmarty, C. J.: Nitrogen cycles: past, present, and future, Biogeochemistry, 70, 153-226, 2004.

Ganzeveld, L. N., Lelieveld, J., Dentener, F. J., Krol, M. C., Bouwman, A. J., and Roelofs, G. J.: Global soil-biogenic NO_X emissions and the role of canopy processes, J Geophys Res-Atmos, 107, Artn 4298, doi:10.1029/2001jd001289, 2002.

Gao, W., Wesely, M. L., and Lee, I. Y.: A Numerical Study of the Effects of Air Chemistry on Fluxes of NO, NO_2, and O_3 near the Surface, J Geophys Res-Atmos, 96, 18761-18769, 1991.

Gasche, R., and Papen, H.: Spatial variability of NO and NO_2 flux rates from soil of spruce and beech forest ecosystems, Plant Soil, 240, 67-76, 2002.

Gessler, A., Rienks, M., and Rennenberg, H.: Stomatal uptake and cuticular adsorption contribute to dry deposition of NH_3 and NO_2 to needles of adult spruce (Picea abies) trees, New Phytol, 156, 179-194, 2002.

Goulding, K. W. T., Bailey, N. J., Bradbury, N. J., Hargreaves, P., Howe, M., Murphy, D. V., Poulton, P. R., and Willison, T. W.: Nitrogen deposition and its contribution to nitrogen cycling and associated soil processes, New. Phytol., 139, 49-58, 1998.

Gut, A., Scheibe, M., Rottenberger, S., Rummel, U., Welling, M., Ammann, C., Kirkman, G. A., Kuhn, U., Meixner, F. X., Kesselmeier, J., Lehmann, B. E., Schmidt, W., Muller, E., and Piedade, M. T. F.: Exchange fluxes of NO_2 and O_3 at soil and leaf surfaces in an Amazonian rain forest, J Geophys Res-Atmos, 107, Artn 8060, doi:10.1029/2001jd000654, 2002a.

Gut, A., van Dijk, S. M., Scheibe, M., Rummel, U., Welling, M., Ammann, C., Meixner, F. X., Kirkman, G. A., Andreae, M. O., and Lehmann, B. E.: NO emission from an Amazonian rain forest soil: Continuous measurements of NO flux and soil concentration, J Geophys Res-Atmos, 107, Artn 8057, doi:10.1029/2001jd000521, 2002b.

Hari, P., Raivonen, M., Vesala, T., Munger, J. W., Pilegaard, K., and Kulmala, M.: Atmospheric science - Ultraviolet light and leaf emission of NO_X, Nature, 422, 134-134, doi:10.1038/422134a, 2003.

Hereid, D. P., and Monson, R. K.: Nitrogen oxide fluxes between corn (Zea mays L.) leaves and the atmosphere, Atmos Environ, 35, 975-983, 2001.

Herman, D. J., Halverson, L. J., and Firestone, M. K.: Nitrogen dynamics in an annual grassland: oak canopy, climate, and microbial population effects, Ecol Appl, 13, 593-604, 2003.

Herman, F., Smidt, S., Huber, S., Englisch, M., and Knoflacher, M.: Evaluation of pollution-related stress factors for forest ecosystems in central Europe, Environ Sci Pollut R, 8, 231-242, 2001.

Hessen, D. O., Henriksen, A., Hindar, A., Mulder, J., Torseth, K., and Vagstad, N.: Human impacts on the nitrogen cycle: A global problem judged from a local perspective, Ambio, 26, 321-325, 1997.

Hietz, P., Turner, B. L., Wanek, W., Richter, A., Nock, C. A., and Wright, S. J.: Long-Term Change in the Nitrogen Cycle of Tropical Forests, Science, 334, 664-666, doi:10.1126/science.1211979, 2011.

Holland, E. A., Braswell, B. H., Lamarque, J. F., Townsend, A., Sulzman, J., Muller, J. F., Dentener, F., Brasseur, G., Levy, H., Penner, J. E., and Roelofs, G. J.: Variations in the predicted spatial distribution of atmospheric nitrogen deposition and their impact on carbon uptake by terrestrial ecosystems, J Geophys Res-Atmos, 102, 15849-15866, 1997.

Holland, E. A., and Lamarque, J. F.: Modeling bio-atmospheric coupling of the nitrogen cycle through NO_X emissions and NOy deposition, Nutr Cycl Agroecosys, 48, 7-24, 1997.

Holzinger, R., Lee, A., Paw, K. T., and Goldstein, A. H.: Observations of oxidation products above a forest imply biogenic emissions of very reactive compounds, Atmos. Chem. Phys., 5, 67-75, 2005.

Horii, C. V.: Tropospheric reactive nitrogen speciation, deposition and chemistry at Harvard Forest, Ph.D., Harvard University, Cambridge, MA, U.S.A., 2002.

Horii, C. V., Munger, J. W., Wofsy, S. C., Zahniser, M., Nelson, D., and McManus, J. B.: Fluxes of nitrogen oxides over a temperate deciduous forest, J Geophys Res-Atmos, 109, Artn D08305, doi:10.1029/2003jd004326, 2004.

Hudman, R. C., Jacob, D. J., Cooper, O. R., Evans, M. J., Heald, C. L., Park, R. J., Fehsenfeld, F., Flocke, F., Holloway, J., Hubler, G., Kita, K., Koike, M., Kondo, Y., Neuman, A., Nowak, J., Oltmans, S., Parrish, D., Roberts, J. M., and Ryerson, T.: Ozone production in transpacific Asian pollution plumes and implications for ozone air quality in California, J. Geophys. Res., 109, doi:10.1029/2004jd004974, 2004.

Hungate, B. A., Dukes, J. S., Shaw, M. R., Luo, Y. Q., and Field, C. B.: Nitrogen and climate change, Science, 302, 1512-1513, 2003.

Jacob, D. J., and Wofsy, S. C.: Budgets of Reactive Nitrogen, Hydrocarbons, and Ozone over the Amazon-Forest during the Wet Season, J Geophys Res-Atmos, 95, 16737-16754, 1990.

Jenkin, M. E., Wyche, K. P., Evans, C. J., Carr, T., Monks, P. S., Alfarra, M. R., Barley, M. H., McFiggans, G. B., Young, J. C., and Rickard, A. R.: Development and chamber evaluation of the MCM v3.2 degradation scheme for Î-caryophyllene, Atmospheric Chemistry and Physics Discussion, 12, 2891–2974, doi:10.5194/acpd-12-2891-2012, 2012.

Kaimal, J. C., and Finnigan, J. J.: Atmospheric boundary layer flows: their structure and measurement, Oxford University Press, New York, NY, USA, , 1994.

Kasana, M. S.: Effects of Ozone Fumigation on a Tropical Fiber Plant, Kenaf (Hibiscus-Cannabinus L), Agr Ecosyst Environ, 38, 61-70, 1992.

Kurpius, M. R., and Goldstein, A. H.: Gas-phase chemistry dominates O_3 loss to a forest, implying a source of aerosols and hydroxyl radicals to the atmosphere, Geophys Res Lett, 30, Artn 1371, doi:10.1029/2002gl016785, 2003.

LaFranchi, B. W., Wolfe, G. M., Thornton, J. A., Harrold, S. A., Browne, E. C., Min, K. E., Wooldridge, P. J., Gilman, J. B., Kuster, W. C., Goldan, P. D., de Gouw, J. A., Mckay, M., Goldstein, A. H., Ren, X., Mao, J., and Cohen, R. C.: Closing the peroxy acetyl nitrate budget: observations of acyl peroxy nitrates (PAN, PPN, and MPAN) during BEARPEX 2007, Atmos. Chem. Phys., 9, 7623-7641, 2009.

LaFranchi, B. W., Goldstein, A. H., and Cohen, R. C.: Observations of the temperature dependent response of ozone to NO_X reductions in the Sacramento, CA urban plume, Atmos Chem Phys, 11, 6945-6960, doi:10.5194/acp-11-6945-2011, 2011.

Lee, A., Schade, G. W., Holzinger, R., and Goldstein, A. H.: A comparison of new measurements of total monoterpene flux with improved measurements of speciated monoterpene flux, Atmos. Chem. Phys., 5, 505-513, 2005.

Lee, X., Massman, W., and Law, B.: Handbook of micrometeorology: a guide for surface flux measurement and analysis, Kluwer Academic Publishers, Dordrecht, The Netherlands, 2004.

Lee, Y. N., and Schwartz, S. E.: Evaluation of the Rate of Uptake of Nitrogen-Dioxide by Atmospheric and Surface Liquid Water, J Geophys Res-Oc Atm, 86, 1971-1983, 1981.

Lerdau, M. T., Munger, L. J., and Jacob, D. J.: Atmospheric chemistry - The NO2 flux conundrum, Science, 289, 2291-+, 2000.

Leungsakul, S., Jeffries, H. E., and Kamens, R. M.: A kinetic mechanism for predicting secondary aerosol formation from the reactions of d-limonene in the presence of oxides of nitrogen and natural sunlight, Atmos Environ, 39, 7063-7082, doi:10.1016/j.atmosenv.2005.08.024, 2005.

Lockwood, A. L., Filley, T. R., Rhodes, D., and Shepson, P. B.: Foliar uptake of atmospheric organic nitrates, Geophys Res Lett, 35, Artn L15809, doi:10.1029/2008gl034714, 2008.

Lovett, G. M., and Lindberg, S. E.: Atmospheric Deposition and Canopy Interactions of Nitrogen in Forests, Can J Forest Res, 23, 1603-1616, 1993.

Makarov, M. I., and Kiseleva, V. V.: Acidification and nutrient imbalance in forest soils subjected to nitrogen deposition, Water Air Soil Poll, 85, 1137-1142, 1995.

Mao, J., Ren, X., Van Duin, D. M., Cohen, R. C., Park, J.-H., Goldstein, A. H., Paulot, F., Beaver, B. R., Crounse, J. D., Wennberg, P. O., DiGangi, J. P., Henry, S. B., Keutsch, F., N., Park, C., Schade, G. W., Wolfe, G. M., Thornton, J. A., Brune, W. H. : Insights into hydroxyl measurements and atmospheric oxidation in a California forest, Atmos. Chem. Phys. Discuss., in preparation, 2012.

Massman, W. J.: The Attenuation of Concentration Fluctuations in Turbulent-Flow through a Tube, J Geophys Res-Atmos, 96, 15269-15273, 1991.

Mayer, J. C., Bargsten, A., Rummel, U., Meixner, F. X., and Foken, T.: Distributed Modified Bowen Ratio method for surface layer fluxes of reactive and non-reactive trace gases, Agr Forest Meteorol, 151, 655-668, doi:10.1016/j.agrformet.2010.10.001, 2011.

McMillen, R. T.: An Eddy-Correlation Technique with Extended Applicability to Non-Simple Terrain, Bound-Lay Meteorol, 43, 231-245, 1988.

Meyer, K.: Effects of Fuel-Element Vibrations on Spectral Density of Neutron-Flux Fluctuations in Pressurized Water-Reactors, Kernenergie, 29, 49-50, 1986.

Min, K. E., Pusede, S. E., Browne, E. C., LaFranchi, B. W., Wooldridge, P. J., Wolfe, G. M., Harrold, S. A., Thornton, J. A., and Cohen, R. C.: Observations of atmosphere-biosphere exchange of total and speciated peroxynitrates: nitrogen fluxes and biogenic sources of peroxynitrates, Atmospheric Chemistry and Physics Discussion, 12, 6205-6233, 2012a.

Min, K.-E., Pusede, S. E., Browne, E. C., LaFranchi, B. W., Wooldridge, P. J., and Cohen, R. C.: Eddy covariance measurements of NO and NO_2 fluxes over a ponderosa pine ecosystem: an observational evidence of canopy reduction processes, Atmospheric Chemistry and Physics Discussion, in preparation, 2012b.

Min, K.-E., Pusede, S. E., Browne, E. C., LaFranchi, B. W., Wooldridge, P. J., and Cohen, R. C.: Observational evidence for an ecosystem scale NO_2 compensation point, Atmospheric Chemistry and Physics Discussion, in preparation, 2012c.

Mission, L., Tang, J., Xu, M, Mckay, M., and Goldstein, A. H.; Influences of recovery from clear-cut, climate variability and thinning on the carbon balance of a young ponderosa pine plantation, Agr. Forest Meteorol., 130, 207-222, 2005.

Moldau, H., Sober, J., Karolin, A., and Kallis, A.: CO_2 Uptake and Respiration Losses in Vegetative Bean-Plants Due to Ozone Absorption, Photosynthetica, 25, 341-349, 1991.

Moore, C. J.: Frequency-Response Corrections for Eddy-Correlation Systems, Bound-Lay Meteorol, 37, 17-35, 1986.

Morikawa, H., Takahashi, M., Sakamoto, A., Matsubara, T., Arimura, G. I., Kawamura, Y., Fukunaga, K., Fujita, K., Sakurai, N., Hirata, T., Ide, H., Nonoyama, N., and Suzuki, H.: Formation of unidentified nitrogen in plants: an implication for a novel nitrogen metabolism, Planta, 219, 14-22, doi:10.1007/s00425-003-1200-7, 2004a.

Morikawa, T., Oikawa, A., Wadano, A., Yano, K., Sakurai, N., Suzuki, H., Saito, K., Shibata, D., and Ohta, D.: Plant metabolomic analyses by FT-ICR/MS, GC/MS, and LC/MS, Plant Cell Physiol, 45, S206-S206, 2004b.

Norby, R. J., Warren, J. M., Iversen, C. M., Medlyn, B. E., and McMurtrie, R. E.: CO_2 enhancement of forest productivity constrained by limited nitrogen availability, P Natl Acad Sci USA, 107, 19368-19373, doi:10.1073/pnas.1006463107, 2010.

Noziere, B., and Barnes, I.: Evidence for formation of a PAN analogue of pinonic structure and investigation of its thermal stability, J Geophys Res-Atmos, 103, 25587-25597, 1998.

Nussbaum, S., Vonballmoos, P., Gfeller, H., Schlunegger, U. P., Fuhrer, J., Rhodes, D., and Brunold, C.: Incorporation of Atmospheric $^{15}NO_2$-Nitrogen into Free Amino-Acids by Norway Spruce Picea-Abies (L) Karst, Oecologia, 94, 408-414, 1993.

Oka, E., Tagami, Y., Oohashi, T., and Kondo, N.: A physiological and morphological study on the injury caused by exposure to the air pollutant, peroxyacetyl nitrate (PAN), based on the quantitative assessment of the injury, J Plant Res, 117, 27-36, doi:10.1007/s10265-003-0127-1, 2004.

Okano, K., Fukuzawa, T., Tazaki, T., and Totsuka, T.: ^{15}N Dilution Method for Estimating the Absorption of Atmospheric NO_2 by Plants, New Phytol, 102, 73-84, 1986.

Okano, K., Tobe, K., and Furukawa, A.: Foliar Uptake of Peroxyacetyl Nitrate (PAN) by Herbaceous Species Varying in Susceptibility to this Pollutant, New. Phytol., 114, 139-145, 1990.

Ollinger, S. V., Aber, J. D., Reich, P. B., and Freuder, R. J.: Interactive effects of nitrogen deposition, tropospheric ozone, elevated CO_2 and land use history on the carbon dynamics of northern hardwood forests, Global Change Biol, 8, 545-562, 2002a.

Ollinger, S. V., Smith, M. L., Martin, M. E., Hallett, R. A., Goodale, C. L., and Aber, J. D.: Regional variation in foliar chemistry and N cycling among forests of diverse history and composition, Ecology, 83, 339-355, 2002b.

Ordin, L., Garber, M. J., Kindinge.Ji, Whitmore, S. A., Greve, L. C., and Taylor, O. C.: Effect of Peroxyacetyl Nitrate (PAN) in-Vivo on Tobacco Leaf Polysaccharide Synthetic Pathways Enzymes, Environ. Sci. Technol., 5, 621-626, 1971.

Pang, X. B., Mu, Y. J., Lee, X. Q., Fang, S. X., Yuan, J., and Huang, D. K.: Nitric oxides and nitrous oxide fluxes from typical vegetables cropland in China: Effects of canopy, soil properties and field management, Atmos Environ, 43, 2571-2578, doi:10.1016/j.atmosenv.2009.02.016, 2009.

Part, J. -H., Fares, S., Weber, R. and Goldstein, A. H.: Estimating BVOC (Biogenic Volatile Organic Compound) Emission by Flux-Gradient Relationship during BEARPEX 2009, in preparation, 2012.

Park, J. Y., and Lee, Y. N.: Solubility and Decomposition Kinetics of Nitrous-Acid in Aqueous-Solution, J Phys Chem-Us, 92, 6294-6302, 1988.

Parrish, D. D., Millet, D. B., and Goldstein, A. H.: Increasing ozone in marine boundary layer inflow at the west coasts of North America and Europe, Atmos. Chem. Phys., 9, 1303-1323, 2009.

Pawlowski, L.: Acidification: its impact on the environment and mitigation strategies, Ecol Eng, 8, 271-288, 1997.

Raivonen, M., Keronen, P., Vesala, T., Kulmala, M., and Hari, P.: Measuring shoot-level NO_X flux in field conditions: the role of blank chambers, Boreal Environ Res, 8, 445-455, 2003.

Raivonen, M., Bonn, B., Sanz, M. J., Vesala, T., Kulmala, M., and Hari, P.: UV-induced NOy emissions from Scots pine: Could they originate from photolysis of deposited HNO_3?, Atmos Environ, 40, 6201-6213, doi:10.1016/j.atmosenv.2006.03.063, 2006.

Raivonen, M., Vesala, T., Pirjola, L., Altimir, N., Keronen, P., Kulmala, M., and Hari, P.: Compensation point of NO_X exchange: Net result of NO_X consumption and production, Agr Forest Meteorol, 149, 1073-1081, doi:10.1016/j.agrformet.2009.01.003, 2009.

Raupach, M. R., and Legg, B. J.: The Uses and Limitations of Flux-Gradient Relationships in Micrometeorology, Agr Water Manage, 8, 119-131, 1984.

Raupach, M. R.: A Practical Lagrangian Method for Relating Scalar Concentrations to Source Distributions in Vegetation Canopies, Q J Roy Meteor Soc, 115, 609-632, 1989.

Rogers, H. H., Jeffries, H. E., and Witherspoon, A. M.: Measuring Air Pollutant Uptake by Plants - Nitrogen-Dioxide, J Environ Qual, 8, 551-557, 1979.

Rondon, A., and Granat, L.: Studies on the Dry Deposition of NO_2 to Coniferous Species at Low No2 Concentrations, Tellus B, 46, 339-352, 1994.

Rosen, R. S., Wood, E. C., Wooldridge, P. J., Thornton, J. A., Day, D. A., Kuster, W., Williams, E. J., Jobson, B. T., and Cohen, R. C.: Observations of total alkyl nitrates during Texas Air Quality Study 2000: Implications for O_3 and alkyl nitrate photochemistry, J Geophys Res-Atmos, 109, Artn D07303, doi:10.1029/2003jd004227, 2004.

Rummel, U., Ammann, C., Gut, A., Meixner, F. X., and Andreae, M. O.: Eddy covariance measurements of nitric oxide flux within an Amazonian rain forest, J Geophys Res-Atmos, 107, Artn 8050, doi:10.1029/2001jd000520, 2002.

Russell, A. R., Valin, L. C., Bucsela, E. J., Wenig, M. O., and Cohen, R. C.: Space-based Constraints on Spatial and Temporal Patterns of NO_X Emissions in California, 2005-2008, Environ Sci Technol, 44, 3608-3615, doi:10.1021/Es903451j, 2010.

Schade, G. W., Goldstein, A. H., Gray, D. W., and Lerdau, M. T.: Canopy and leaf level 2-methyl-3-buten-2-ol fluxes from a ponderosa pine plantation, Atmos Environ, 34, 3535-3544, 2000.

Schade, G. W., and Goldstein, A. H.: Fluxes of oxygenated volatile organic compounds from a ponderosa pine plantation, J. Geophys. Res., 106, 3111-3123, 2001.

Shu, Y. G., and Atkinson, R.: Rate Constants for the Gas-Phase Reactions of O_3 with a Series of Terpenes and OH Radical Formation from the O_3 Reactions with Sesquiterpenes at 296±2K, Int. J. Chem. Kinet., 26, 1193-1205, 1994.

Shu, Y. H., and Atkinson, R.: Atmospheric Lifetimes and Fates of a Series of Sesquiterpenes, J. Geophys. Res., 100, 7275-7281, 1995.

Sparks, J. P., Monson, R. K., Sparks, K. L., and Lerdau, M.: Leaf uptake of nitrogen dioxide (NO_2) in a tropical wet forest: implications for tropospheric chemistry, Oecologia, 127, 214-221, 2001.

Sparks, J. P., Roberts, J. M., and Monson, R. K.: The uptake of gaseous organic nitrogen by leaves: A significant global nitrogen transfer process, Geophys. Res. Lett., 30, 2003.

Sparks, J. P.: Ecological ramifications of the direct foliar uptake of nitrogen, Oecologia, 159, 1-13, doi:10.1007/s00442-008-1188-6, 2009.

Takahashi, M., Nakagawa, M., Konaka, D., Sakamoto, A., Matsubara, T., Ohsumi, C., Suzuki, H., and Morikawa, H.: Urban NO_X "pollution" is a plant vitalization signal, Plant Cell Physiol, 45, S125-S125, 2004.

Takahashi, M., Nakagawa, M., Sakamoto, A., Ohsumi, C., Matsubara, T., and Morikawa, H.: Atmospheric nitrogen dioxide gas is a plant vitalization signal to increase plant size and the contents of cell constituents, New Phytol, 168, 149-153, doi:10.1111/j.1469-8137.2005.01493.x, 2005a.

Takahashi, M., Nakayama, N., and Arihara, J.: Plant nitrogen levels and photosynthesis in the supernodulating soybean (Glycine max L. Merr.) cultivar 'Sakukei 4', Plant Prod Sci, 8, 412-418, 2005b.

Taylor, O. C.: Importance of peroxyacetylnitrate (PAN) as a phytotoxic air pollutant, J. Air Pollut., 19, 347-351, 1969.

Teklemariam, T. A., and Sparks, J. P.: Gaseous fluxes of peroxyacetyl nitrate (PAN) into plant leaves, Plant Cell Environ, 27, 1149-1158, 2004.

Teklemariam, T. A., and Sparks, J. P.: Leaf fluxes of NO and NO_2 in four herbaceous plant species: The role of ascorbic acid, Atmos Environ, 40, 2235-2244, doi:10.1016/j.atmosenv.2005.12.010, 2006.

Thornton, J. A., Wooldridge, P. J., and Cohen, R. C.: Atmospheric NO_2: In situ laser-induced fluorescence detection at parts per trillion mixing ratios, Anal. Chem., 72, 528-539, 2000.

Townsend, A. R., Braswell, B. H., Holland, E. A., and Penner, J. E.: Spatial and temporal patterns in terrestrial carbon storage due to deposition of fossil fuel nitrogen, Ecol Appl, 6, 806-814, 1996.

Turnipseed, A. A., Huey, L. G., Nemitz, E., Stickel, R., Higgs, J., Tanner, D. J., Slusher, D. L., Sparks, J. P., Flocke, F., and Guenther, A.: Eddy covariance fluxes of peroxyacetyl nitrates (PANs) and NOy to a coniferous forest, J Geophys Res-Atmos, 111, Artn D09304, doi:10.1029/2005jd006631, 2006.

Tyndall, G. S., Cox, R. A., Granier, C., Lesclaux, R., Moortgat, G. K., Pilling, M. J., Ravishankara, A. R., and Wallington, T. J.: Atmospheric chemistry of small organic peroxy radicals, J. Geophys. Res., 106, 12157-12182, 2001.

van Dijk, S. M., Gut, A., Kirkman, G. A., Meixner, F. X., Andreae, M. O., and Gomes, B. M.: Biogenic NO emissions from forest and pasture soils: Relating laboratory studies to field measurements, J Geophys Res-Atmos, 107, Artn 8058, doi:10.1029/2001jd000358, 2002.

Vandenhurk, B. J. J. M., and Mcnaughton, K. G.: Implementation of near-Field Dispersion in a Simple 2-Layer Surface-Resistance Model, J Hydrol, 166, 293-311, 1995.

Vila-Guerau de Arellano, J., Duynkerke, P. G., and Builtjes, P. J. H.: The Divergence of the Turbulent-Diffusion Flux in the Surface-Layer Due to Chemical-Reactions - the NO-O_3-NO_2 System, Tellus B, 45, 23-33, 1993.

Vitousek, P. M., Aber, J. D., Howarth, R. W., Likens, G. E., Matson, P. A., Schindler, D. W., Schlesinger, W. H., and Tilman, D.: Human alteration of the global nitrogen cycle: Sources and consequences, Ecol Appl, 7, 737-750, 1997a.

Vitousek, P. M., and Farrington, H.: Nutrient limitation and soil development: Experimental test of a biogeochemical theory, Biogeochemistry, 37, 63-75, 1997b.

Wang, Y. P., and Leuning, R.: A two-leaf model for canopy conductance, photosynthesis and partitioning of available energy I: Model description and comparison with a multi-layered model, Agr Forest Meteorol, 91, 89-111, 1998.

Weber, P., Nussbaum, S., Fuhrer, J., Gfeller, H., Schlunegger, U. P., Brunold, C., and Rennenberg, H.: Uptake of Atmospheric $^{15}NO_2$ and Its Incorporation into Free Amino-Acids in Wheat (Triticum-Aestivum), Physiol Plantarum, 94, 71-77, 1995.

Wesely, M. L., Eastman, J. A., Stedman, D. H., and Yalvac, E. D.: An Eddy-Correlation Measurement of No2 Flux to Vegetation and Comparison to O_3 Flux, Atmos Environ, 16, 815-820, 1982.

Wildt, J., Kley, D., Rockel, A., Rockel, P., and Segschneider, H. J.: Emission of NO from several higher plant species, J Geophys Res-Atmos, 102, 5919-5927, 1997.

Wolfe, G. M., Thornton, J. A., Yatavelli, R. L. N., Mckay, M., Goldstein, A. H., LaFranchi, B., Min, K. E., and Cohen, R. C.: Eddy covariance fluxes of acyl peroxy nitrates (PAN, PPN and MPAN) above a Ponderosa pine forest, Atmos Chem Phys, 9, 615-634, 2009.

Wolfe, G. M., Thornton, J. A., Bouvier-Brown, N. C., Goldstein, A. H., Park, J. H., Mckay, M., Matross, D. M., Mao, J., Brune, W. H., LaFranchi, B. W., Browne, E. C., Min, K. E., Wooldridge, P. J., Cohen, R. C., Crounse, J. D., Faloona, I. C., Gilman, J. B., Kuster, W. C., de Gouw, J. A., Huisman, A., and Keutsch, F. N.: The Chemistry of Atmosphere-Forest Exchange (CAFE) Model - Part 2: Application to BEARPEX-2007 observations, Atmos. Chem. Phys., 11, 1269-1294, doi:10.5194/acp-11-1269-2011, 2011.

Wooldridge, P. J., Perring, A. E., Bertram, T. H., Flocke, F. M., Roberts, J. M., Singh, H. B., Huey, L. G., Thornton, J. A., Wolfe, G. M., Murphy, J. G., Fry, J. L., Rollins, A. W., LaFranchi, B. W., and Cohen, R. C.: Total Peroxy Nitrates (ΣPNs) in the atmosphere: the Thermal Dissociation-Laser Induced Fluorescence (TD-LIF) technique and comparisons to speciated PAN measurements, Atmos. Meas. Tech., 3, 593-607, doi:10.5194/amt-3-593-2010, 2010.

Yienger, J. J., and Levy, H.: Empirical-Model of Global Soil-Biogenic NO_X Emissions, J Geophys Res-Atmos, 100, 11447-11464, 1995.

Zhang, L., Jacob, D. J., Boersma, K. F., Jaffe, D. A., Olson, J. R., Bowman, K. W., Worden, J. R., Thompson, A. M., Avery, M. A., Cohen, R. C., Dibb, J. E., Flock, F. M., Fuelberg, H. E., Huey, L. G., McMillan, W. W., Singh, H. B., and Weinheimer, A. J.: Transpacific transport of ozone pollution and the effect of recent Asian emission increases on air quality in North America: an integrated analysis using satellite, aircraft, ozonesonde, and surface observations, Atmos. Chem. Phys., 8, 6117-6136, 2008.

Zhou, X. L., Gao, H. L., He, Y., Huang, G., Bertman, S. B., Civerolo, K., and Schwab, J.: Nitric acid photolysis on surfaces in low-NO_X environments: Significant atmospheric implications, Geophys Res Lett, 30, Artn 2217, doi:10.1029/2003gl018620, 2003.

Zhou, X. L., Zhang, N., TerAvest, M., Tang, D., Hou, J., Bertman, S., Alaghmand, M., Shepson, P. B., Carroll, M. A., Griffith, S., Dusanter, S., and Stevens, P. S.: Nitric acid photolysis on forest canopy surface as a source for tropospheric nitrous acid, Nat Geosci, 4, 440-443, doi:10.1038/Ngeo1164, 2011.

Appendix A

The normalized exchange velocity of species C, nV_C are estimated from the ratio of exchange velocity and maximum exchange velocity of C as AE1. Here C refers NO, NO_2, CO_2 and O_3.

$$nV_c = \frac{V_c}{V\max_c} \quad \textbf{(AE1)}$$

$$V_c = \frac{1}{R_a} + \frac{1}{R_b} + \frac{1}{R_c} = \frac{Flux_c}{[C]} \quad \textbf{(AE2)}$$

$$V\max_c = \frac{1}{R_a} + \frac{1}{R_b} \quad \textbf{(AE3)}$$

The $Vmax_C$ is defined from resistance analogy (Wesley et al., 1989) by assuming canopy resistance, R_c, is 0 as AE3 to describe the vigorousness of turbulent mixing. Here, R_a stands for aerodynamic resistance to describe the turbulent transport from the mixed layer to the surface and defined as AE4. The laminar sublayer resisteance, R_b, parameterized as AE5, describe the molecular diffusion through the thin viscouse layer on surface.

$$R_a = \frac{\overline{U}(z-d)}{u_*^{\,2}} - \frac{\Psi_H\left(\frac{z-d}{L}\right) - \Psi_M\left(\frac{z-d}{L}\right)}{ku_*} \quad \textbf{(AE4)}$$

Here $\overline{U}(z-d)$ is the average wind speed at height z-d (the top of the surface layer), u_* is the friction velocity, κ is von Karman's constant (0.4), L is the Obukhov length, and Ψ_H, Ψ_M are the integrated stability corrections for sensible heat and momentum, respectively

(Dyer, 1974; Arya, 1988).

$$Rb = \frac{\nu}{D_c u_*}\left[\frac{100 \cdot l \cdot u_*}{(LAI)^2 \nu}\right]^{1/3} \quad \textbf{(AE5)}$$

Here ν is the pressure corrected kinematic viscosity of air (1.7×10^{-5} m^2 s^{-1}), D_c is the diffusion coefficient for species c (Massman, 1998), LAI stands for leaf area index (3.7 m^2 m^{-2}) and l=0.001m is the "characteristic length scale" of the canopy surface elements,

roughly the thickness of a pine needle (Jensen andHummelshøj, 1995, 1997).